

# **Hydrogen storage in Metal Organic Frameworks**

PROEFSCHRIEFT

Ter verkrijging van de graad van doctor  
Aan de Technische Universiteit Delft,  
Op gezag van de Rector Magnificus Prof. XXX  
Voorzitter van het College voor Promoties,  
In het openbaar te verdedigen op 16 Oktober 2012 om 12:30 uur

door

**Jie Yang**

Master of Science in Chemistry, Xiaan Normal University,  
Xi'an, China  
Geboren te Tianjin, China

Dit proefschrift is goedgekeurd door de promotor:

Prof. dr. T. J. Dingemans

Prof. dr. F. M. Mulder

Samenstelling promotiecommissie:

|                                 |   |
|---------------------------------|---|
| Rector Magnificus,              | voorzitter                                |
| Prof. dr. T. J. Dingemans,      | Technische Universiteit Delft, promotor   |
| Prof. dr. F. M. Mulder,         | Technische Universiteit Delft, copromotor |
| Prof. dr. ir. S. van der Zwaag, | Technische Universiteit Delft             |
| Prof. dr. F. Kapteijn,          | Technische Universiteit Delft             |
| Prof. dr. B. Dam,               | Technische Universiteit Delft             |
| Dr. P. de Jongh,                | Universiteit Utrecht                      |
| Dr. ir. K. Nijmeijer,           | Universiteit Twente                       |

Copyright©2012 Jie Yang

All rights reserved. No part of the material protected by this copyright notice may be reproduced or utilized in any form or by any means, electronic or mechanical, including photocopying, recording or by any information storage and retrieval system, without written permission from the author.

The research presented in this Ph.D thesis has been financed by NWO ACTS Sustainable Hydrogen Programme (Project No. 05361017).

# Contents

---

|          |   |           |
|----------|---|-----------|
| <b>1</b> | <b>Introduction</b>   | <b>1</b>  |
| 1.1      | Hydrogen storage: the state of the art  | 2         |
| 1.2      | Hydrogen storage in metal-organic frameworks (MOFs)                                   | 5         |
| 1.2.1    | Introduction of MOFs  | 5         |
| 1.2.2    | Relationships between structural nature and hydrogen storage capability of MOFs       | 7         |
| 1.3      | Synthetic considerations  | 12        |
| 1.4      | Scope and outline of the thesis.  | 13        |
| 1.5      | References  | 14        |
| <b>2</b> | <b>Mono-substituted MOF-5 derivatives: An Experimental and computational approach</b> | <b>19</b> |
| 2.1      | Introduction  | 20        |
| 2.2      | Experimental  | 22        |
| 2.2.1    | Materials   | 22        |
| 2.2.2    | Synthesis of mono-substituted terephthalic acid                                       | 22        |
| 2.2.3    | Synthesis of MOF-5 and the modified MOF-5s  | 23        |
| 2.2.4    | Activation by heat-treatment <i>in vacuo</i> .  | 24        |
| 2.2.5    | Characterization.   | 24        |
| 2.3      | Results and discussion  | 25        |
| 2.3.1    | Structure characterization of modified MOF-5s.  | 25        |
| 2.3.2    | Thermogravimetric analysis of modified MOF-5s.  | 27        |
| 2.3.3    | Thermogravimetric analysis of modified MOF-5s after heat-treatment                    | 28        |
| 2.3.4    | Structure characterization of modified MOF-5s after heat-treatment                    | 32        |
| 2.3.5    | Nitrogen sorption   | 35        |
| 2.2.6    | Hydrogen storage property   | 37        |

|          |   |           |
|----------|---|-----------|
| 2.3.7    | Computational studies on the diffusion coefficient of hydrogen for mono-substituted MOF-5s..... | 42        |
| 2.4      | Conclusions .....   | 43        |
| 2.5      | References .....  | 44        |
| <b>3</b> | <b>Methoxy-modified of MOF-5: a new MOF-5 framework prepared via a mixed ligand approach</b>    | <b>47</b> |
| 3.1      | Introduction .....  | 48        |
| 3.2      | Experimental .....  | 49        |
| 3.2.1    | Materials.....  | 49        |
| 3.2.2    | Synthesis of (OCH <sub>3</sub> ) <sub>x</sub> -MOF-5.....                                       | 49        |
| 3.2.3    | Characterization .....  | 51        |
| 3.3      | Results and discussion.....   | 52        |
| 3.3.1    | Structures of (OCH <sub>3</sub> ) <sub>x</sub> -MOF-5.....                                      | 52        |
| 3.3.2    | FT-IR analysis .....  | 53        |
| 3.3.3    | Thermogravimetric analysis.....   | 55        |
| 3.3.4    | Specific surface area and pore volume .....   | 56        |
| 3.3.5    | Hydrogen storage property .....   | 57        |
| 3.4      | Conclusions .....   | 60        |
| 3.5      | References .....  | 61        |
| <b>4</b> | <b>Methyl-modified MOF-5: a water-stable hydrogen storage material</b>                          | <b>63</b> |
| 4.1      | Introduction.....   | 64        |
| 4.2      | Experimental .....  | 65        |
| 4.2.1    | Materials.....  | 65        |
| 4.2.2    | Synthesis of methyl modified MOF-5 .....  | 65        |
| 4.2.3    | Characterization .....  | 66        |
| 4.3      | Results and discussion .....  | 67        |
| 4.3.1    | Structures of methyl modified MOF-5.....  | 67        |
| 4.3.2    | Thermogravimetric analysis .....  | 70        |
| 4.3.3    | Hydrogen storage property .....   | 72        |
| 4.4      | Conclusions .....   | 74        |
| 4.5      | References .....  | 75        |



|          |   |            |
|----------|---|------------|
| <b>5</b> | <b>Effect of metal salt-to-ligand ratio on structure and hydrogen storage capability of MOF-5</b>         | <b>77</b>  |
| 5.1      | Introduction .....  | 78         |
| 5.2      | Experimental .....  | 80         |
| 5.2.1    | Materials .....   | 80         |
| 5.2.2    | Synthesis of MOF-5 by varying the zinc nitrate-to-terephthalic acid ratio .....                           | 80         |
| 5.2.3    | Characterization .....  | 81         |
| 5.3      | Results and discussion .....  | 82         |
| 5.3.1    | Structural and compositional characterization .....   | 82         |
| 5.3.2    | Hydrogen storage property .....   | 89         |
| 5.4      | Conclusions .....   | 91         |
| 5.5      | References .....  | 91         |
| <b>6</b> | <b>Synthesis and characterization of MOFs containing short linkers</b>                                    | <b>93</b>  |
| 6.1      | Introduction .....  | 94         |
| 6.2      | Experimental .....  | 95         |
| 6.2.1    | Materials .....   | 95         |
| 6.2.2    | Synthesis of MOFs using short ligands .....   | 95         |
| 6.2.3    | Characterization .....  | 97         |
| 6.3      | Results and discussion .....  | 98         |
| 6.3.1    | Characterization of MOF-Ac .....  | 98         |
| 6.3.2    | Characterization of MOF-Fum .....   | 101        |
| 6.3.3    | Characterization of MOF-Oxa .....   | 104        |
| 6.3.4    | Hydrogen storage property .....   | 107        |
| 6.4      | Conclusions .....   | 108        |
| 6.5      | References .....  | 109        |
| <b>7</b> | <b>Cu(II) coordination polymers comprised of thiophene-2,5-dicarboxylate and furan- 2,5-dicarboxylate</b> | <b>111</b> |
| 7.1      | Introduction .....  | 112        |
| 7.2      | Experimental .....  | 113        |

## *Contents*

---

|       |  |     |
|-------|--|-----|
| 7.2.1 | Materials .....  | 113 |
| 7.2.2 | Synthesis of Cu-TDC and Cu-FDC .....                       | 114 |
| 7.2.3 | Characterization .....                                     | 114 |
| 7.3   | Results and discussion .....                               | 116 |
| 7.3.1 | Structures of Cu-TDC and Cu-FDC .....                      | 116 |
| 7.3.2 | Thermogravimetric analysis .....                           | 124 |
| 7.3.3 | Structural stability of Cu-TDC and Cu-FDC .....            | 125 |
| 7.3.4 | Structure and composition of Cu-TDC-A and Cu-FDC-A .....   | 127 |
| 7.3.5 | Hydrogen storage properties of Cu-TDC-A and Cu-FDC-A ..... | 130 |
| 7.4   | Conclusions .....  | 131 |
| 7.5   | References .....   | 132 |

## **Appendix**

### **Summary**

### **Samenvatting**

### **Acknowledgments**

### **List of publications**

# CHAPTER 1

## Introduction

---

In this chapter the importance and different approaches towards hydrogen storage materials will be reviewed. The emphasis will be on the synthesis, structure and hydrogen storage capability of a new and promising class of hydrogen storage materials, namely, metal organic frameworks (MOFs). The scientific challenges around the design and synthesis of high storage capacity MOFs will be discussed and the chapter will be concluded with the aim and outline of the thesis.

## **1.1 Hydrogen storage: state of the art**

With the continuous growth of economies and increasing demand for replacing fossil fuels, clean energy has become one of the main challenges for the 21<sup>st</sup> century.[1,2] Hydrogen is an ideal clean energy carrier because of its abundant availability, clean-burning qualities, and its potential for domestic production from e.g. renewably produced electricity and water. Moreover, its high energy density, which is nearly triple that of gasoline per mass unit, makes it an attractive energy carrier. However, the extremely low volumetric storage density of hydrogen presents a barrier that limits its practical usage as a fuel for vehicles.[3-5]

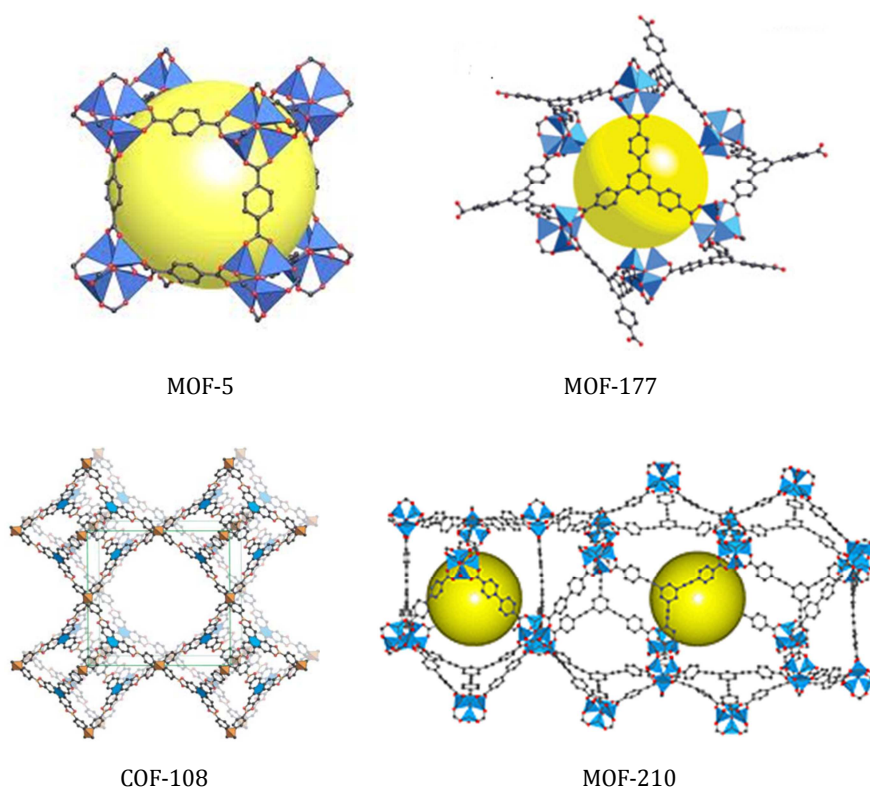
For on-board use, hydrogen can be compressed to very high pressures or stored cryogenically. Both technologies are energy intensive and substantially increase vehicle weight. Additionally, storage of hydrogen in liquid or gaseous form poses important safety concerns for on-board transport applications. Therefore, it is desirable to design safe, light-weight and low-cost materials that can reversibly and rapidly store hydrogen near ambient conditions at a density equal to or greater than that of liquid hydrogen.[6] In 2003, the U.S. Department of Energy (DOE) set a target for on-board hydrogen storage systems: 6 wt% or 45 g L<sup>-1</sup> by 2010, and 9 wt% or 81 g L<sup>-1</sup> by 2015. In 2009, DOE revised the targets: 4.5 wt% or 28 g L<sup>-1</sup> by 2010, 5.5 wt% or 40 g L<sup>-1</sup> by 2015, and 7.5 wt% or 70 g L<sup>-1</sup> as the ultimate value. Meanwhile, moderate conditions at near-ambient temperature and accessible pressures (<100 bar) for hydrogen storage are also considered prerequisites for future practical applications.[5]

Table 1.1 summarizes several hydrogen storage technologies and their operating conditions. In terms of safety, global yield and long-term storage, hydrogen binds via strong chemical association in metal hydrides or complex hydrides (chemical storage) and to adsorbents surfaces by weak dispersion interactions (physical storage).[7-12] Moreover, the hydrogen volumetric/gravimetric capacities for some of these materials have met the DOE target of 2015 under certain conditions. Materials storing hydrogen by chemisorption, such as Mg-based metal hydrides, complex hydrides, and metal nitrides, show high thermodynamic stability (300 °C) and slow hydrogen release kinetics and this will make them less attractive for practical hydrogen storage applications. Much effort has been devoted towards reducing their thermodynamic stability and improving the adsorption/desorption kinetics by changing the microstructure of the hydride, e.g. by mechanical alloying with elements or using proper catalysts. In comparison with chemical storage, storing hydrogen by physisorption has attracted more attention due to the fast kinetics and complete reversibility of the storage

process.[13-16] To date, many porous materials, such as nanostructured carbons, metal organic frameworks (MOFs) and covalent organic frameworks (COFs) have shown impressive hydrogen storage performance at cryogenic temperatures.[17-22] For instance, MOF-5 shows an excess hydrogen uptake of 7.1 wt% at 77 K and 40 bar. At 100 bar, a total uptake of 10.0 wt% can be achieved. MOF-177 gives a total gravimetric uptake of 11.2 wt% at 77 K and 78 bar. An extraordinary gravimetric capacity (18.9 wt%) has been predicted for COF-108.[23] MOF-210 exhibits an excess hydrogen uptake of 8.6 wt% and a predicted total hydrogen uptake of 17.6 wt%.[22c] The structures of MOF-5, MOF-177, COF-108 and MOF-210 are shown in Figure 1.1. The excellent hydrogen storage capabilities are related to their structural characteristics, such as a high specific surface area and high porosity. It would be more practical, however, if these porous materials show such high hydrogen uptake capacities at more accessible, non-cryogenic temperatures. To meet this target, the interaction between hydrogen molecules and the MOF needs to be enhanced by optimizing their structures. For example, by adjusting the pore size, framework geometry and by introducing strong surface dipoles. The modular nature of MOFs makes it possible to control the composition of the metal cluster and the (chemical) nature of the organic linker unit. Although the variation in metal centers is limited, the diversity of organic linkers on the other hand makes it possible to explore a large variety of metal organic frameworks.[13] Because the metal/organic-linker combination is almost endless, the role of molecular modeling becomes an important tool. Some important breakthroughs have been reported to date and it is clear that modeling efforts could guide the design of MOFs with high hydrogen storage capacities.[24]

**Table 1.1** DOE goal, several hydrogen storage technologies and their operation conditions. [7-12]

| Storage approach<br>Storage parameters         | DOE goal (2015) | Conventional techniques   |   | Physical storage   | Chemical storage  |  |
|--|-----------------|---|---|--|---|--|
|  |                 | Compressed hydrogen   | Liquid hydrogen   | Nanoporous materials (Activated carbon, MOFs, COFs)...                             | Complex hydrides, Metal hydride ( $\text{MgH}_2$ , $\text{NaAlH}_4$ , $\text{LiAlH}_4$ )... | Amine-borane, Amides/imides ( $\text{NH}_3\text{B}_3\text{H}_7$ , $\text{LiNH}_2$ )... |
|  |                 |  |  |  |            |  |
| Gravimetric Capacity (wt%)                     | >5.5            | 100   | 100   | Max. 11.4  | Max. 11.4   | Max. 7.5   |
| Volumetric Capacity (vol%)                     | 40              | n/a   | n/a   | Max. 66  | Max. 30   | n/a  |
| Pressure (bar)                                 | <100            | 350-700   | 1-10  | 30-100   | ~1  | ~1   |
| Temperature ( $^{\circ}\text{C}$ )             | -40-85          | 25  | -253  | >-200  | 70-400  | 25-350   |
| Reversibility (cycle)                          | 1500            | n/a   | n/a   | Reversible   | Limited reversible  | Limited reversible   |
| System fill time (for 5 Kg $\text{H}_2$ )(min) | 3.3             | Fast  | Fast  | Fast (in mins)   | Too slow  | Slow   |



**Figure 1.1.** The structures of MOF-5, MOF-177, COF-108 and MOF-210 (Yellow sphere represents the largest sphere that can occupy the pores without compromising the Van der Waals size of the framework). Reproduced from ref. [28,22c,22b,35]. Copyright 2003, 2007 and 2010, American Association for the Advancement of Science. Copyright 2004, American Chemical Society.

## 1.2 Hydrogen storage in metal organic frameworks

### 1.2.1 Introduction of Metal organic frameworks (MOFs)

Metal organic frameworks (MOFs) are a unique class of crystalline porous solids that have been studied extensively for a number of applications, including gas storage, gas separation, heterogeneous catalysis, and so on.[25-26] Generally, metal-organic frameworks are constructed by assembling metal atoms or small metal-containing clusters, referred to as the secondary building unit or SBU, with multidentate organic ligands via coordination bonds.[27] Figure 1.2 shows examples of metal carboxylate clusters and organic units. As already mentioned, the great variety of organic ligands and metal ions or metal clusters offers the opportunity to design a range of networks with

desired structures and properties. Most MOFs have three-dimensional structures incorporating uniform pores and a network of channels, which can be filled with guest species such as solvents that are trapped during synthesis. The porosity can be generated by proper removal of the trapped guest molecules. Unlike other porous materials, MOFs have exceptionally high specific surface areas because they are open scaffolds that have pores without walls. Moreover, since the topology of the scaffold is defined by molecular building blocks, the pore or aperture size of the framework is very small, typically less than 20 Å, resulting in strong interactions between guest molecules and the frameworks.

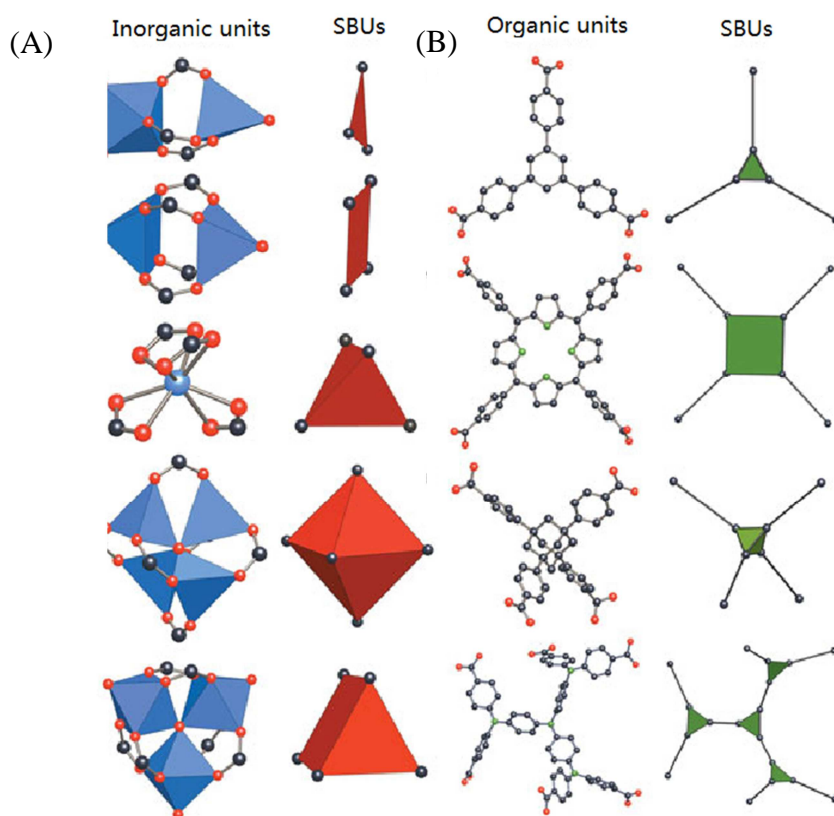


**Figure 1.2.** Examples of inorganic metal carboxylate clusters and their corresponding secondary building unit (SBU) geometry (A) and organic units and their corresponding secondary building unit (SBU) geometry. Reproduced from ref. [28b]. Copyright 2003, with permission from the Nature owner society.



In 2003, the first results on hydrogen storage in MOF-5 (IRMOF-1) and two types of MIL-53 (Al or Cr) were reported.[28,29] From then on, MOFs have become a burgeoning research field and a promising family for hydrogen storage materials due to their exceptionally high porosity, uniform but adjustable pore size and well-defined hydrogen-framework interacting sites. Some exciting results have shown that in principle the DOE targets (2015) can be achieved at 77 K using MOFs for hydrogen storage. For instance, MOF-5 gives an absolute hydrogen uptake capacity of 10 wt% when the pressure reaches up to 100 bar at 77 K; MOF-177 adsorbs reversibly up to 11.2 wt% of H<sub>2</sub> at 77 K and 78 bar.[30,31] Moreover, the reproducibility of these MOFs demonstrates that 100% hydrogen uptake and release can be achieved in several minutes without compromising the MOF structure.

Although results so far seem to indicate that MOFs are serious candidates for future hydrogen storage devices, achieving on-board hydrogen storage for automotive transportation is still a big challenge. Issues such as moisture sensitivity and the ability to storage hydrogen at near ambient temperatures need to be resolved prior to exploring commercial applications.

### **1.2.2 Relationships between MOF structure and hydrogen storage capability**

Coupled with measurements on the hydrogen uptake capacities of MOFs, much effort has been under taken towards understanding the factors that determine the hydrogen adsorption capability for developing new, safe and convenient hydrogen storage materials. Factors include specific surface area (SSA), pore volume, pore size, and hydrogen binding sites (metal clusters and/or ligands), etc. Recent studies have revealed that excess hydrogen uptake at 77 K generally scale up with specific surface area.[32-34] One of the highest excess gravimetric capacities at saturation is held by MOF-177, which displays an absolute value of 0.112 kg kg<sup>-1</sup> of hydrogen adsorption. This is attributed to its exceptionally high surface area of 5600 m<sup>2</sup> g<sup>-1</sup>. [35] Furukawa and co-workers reported that MOF-210 with a record BET surface area of 6240 m<sup>2</sup> g<sup>-1</sup>, shows an excess hydrogen uptake of 8.6 wt% and a calculated total hydrogen uptake of 0.176 kg kg<sup>-1</sup>. [22c] Generally, the higher the surface area, the lower the crystal density. In most cases, low volumetric hydrogen uptake capacities of MOFs are obtained because of their low density. A compromise between specific surface area and crystal density should be achieved in the search of porous MOFs with both high gravimetric and volumetric hydrogen uptake capacities.

To date, some MOFs have met the DOE criteria at 77 K, but these materials have very low hydrogen uptake capacities at room temperature due to the weak interaction between hydrogen molecules and the framework of porous MOFs. High specific surface area alone is insufficient to reach high hydrogen storage capacity for ambient-temperature storage. The heats of hydrogen adsorption for most MOFs are usually in the range of 4-7 kJ mol<sup>-1</sup>. [36,37] It was reported that the heat of adsorption of hydrogen on an “ideal” adsorbent should be ca. 20 kJ mol<sup>-1</sup> over the entire hydrogen loading range, if both the delivery and storage is to take place at room temperature. [38] Therefore, enhancing the hydrogen adsorption energy is key towards increasing the hydrogen uptake capacities of MOFs under non-cryogenic conditions. Both experimental and computational studies have demonstrated that the hydrogen adsorption energy can be significantly improved by introducing unsaturated metal sites, by reducing the pore size, or by selecting the appropriate organic linkers.

It has been claimed that MOFs containing coordinative unsaturated metal sites provide the most attractive binding sites where open metal sites directly bind to hydrogen molecules, giving rise to an enhanced heat of hydrogen adsorption. Yaghi et al. have found that MOF-74, MOF-199 and MOF-505 possessing open metal sites (Zn or Cu) show higher hydrogen uptake capacities than MOFs without open metal sites. [39, 40] The highest values of approximately 10 kJ mol<sup>-1</sup> at low hydrogen coverage have been found for Mn-BTT (btt = 1,3,5-benzenetristetrazolate) and MIL-101 (Figure 1.3) and they show high hydrogen uptake capacities of around 2 wt% at 77 K and 1 atm. [41,42] Zhou and co-workers investigated the role of different open metal ions in hydrogen adsorption of an isostructural MOF system, M<sub>2</sub>(dhtp) series (M = Mg, Co, Ni and Zn; dhtp = 2,5-hydroxyterephthalate). In this series, the authors found that the heats of hydrogen adsorption are inversely proportional to the metal ion radius. By combining experimental and theoretical results, they propose that the relative M<sup>2+</sup>-H<sub>2</sub> interaction strength may be empirically predicted by the ionic radius of cations in the same coordination environment. [43]

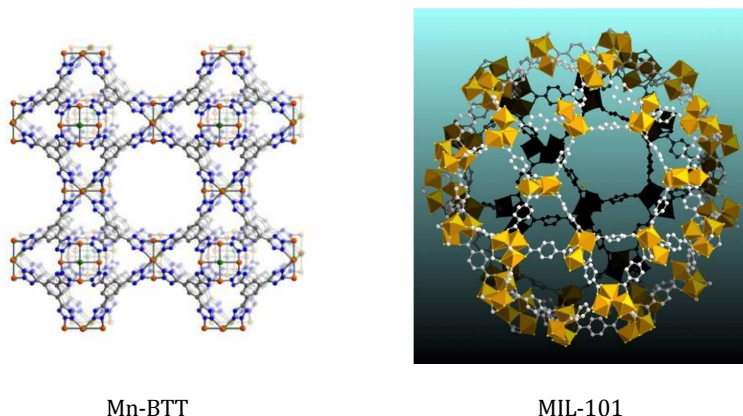


**Figure 1.3.** The structures of Mn-BTT and MIL-101. Reproduced from ref. [41, 42b]. Copyright 2006, American Chemical Society. Copyright 2008, The Royal Society of Chemistry.

Reducing the pore size makes it possible for hydrogen molecules to interact with multiple portions of the MOF framework, increasing hydrogen-framework interactions. Some studies have indicated that an ideal pore size of  $\sim 6$  Å may allow for the formation of a monolayer of hydrogen molecules with a kinetic diameter of 2.89 Å on opposite pore walls. This should result in an optimal interaction between the hydrogen molecules and the framework by maximizing the total Van der Waals force acting on the hydrogen molecules.[44] A smaller pore size may be achieved by introducing short organic linkers, the incidence of interpenetration, or the modification of organic linkers.[45-48] MOF-324, constructed from  $\text{Zn}_3\text{OH}$  clusters where the Zn ion is fully coordinated and 4-pyrazolecarboxylate, for example, shows a good performance on hydrogen adsorption (2.1 wt% at 77 K and 760 torr). The effective hydrogen uptake was attributed to the small pore diameter (7.6 Å), which is roughly three times larger than the kinetic diameter of hydrogen. Additionally, the two nitrogen atoms in the organic linker may help with the polarization of adsorbent, leading to an improvement in the adsorption enthalpy.[39] The typical effect of interpenetration on porosity is to subdivide the large single pore into several smaller ones. One example of an increased hydrogen uptake capacity of MOFs resulting from interpenetrated structures has been reported by Ma and co-workers.[49] Compared to the non-interpenetrated PCN-6' ( $\text{Cu}_6(\text{H}_2\text{O})_6(\text{TATB})_4\text{DMA-12H}_2\text{O}$ ), the interpenetrated counterpart PCN-6 exhibits an increase by 41% in specific surface area, and increases in the gravimetric and volumetric hydrogen uptake capacities by 29% and 133% at 77 K and 1 bar, respectively. The structures of PCN-6' and PCN-6 are shown in Figure 1.4.

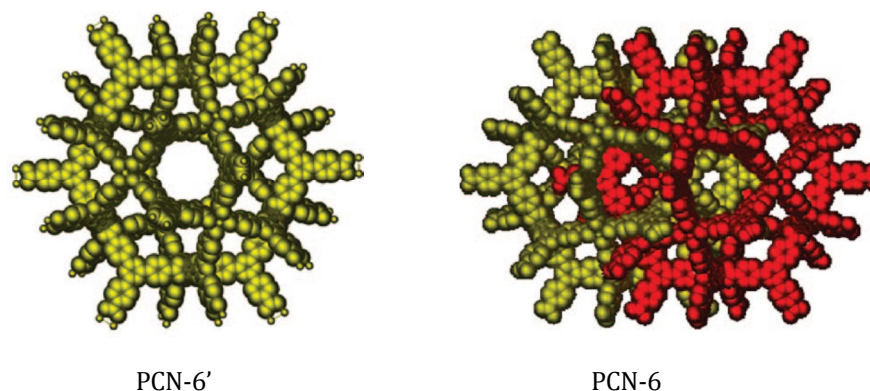


**Figure 1.4.** The structures of non-interpenetrated PCN-6' and interpenetrated PCN-6. Reproduced from ref. [49]. Copy right 2008, American Chemical Society.

The metal sites are the preferential adsorption sites for hydrogen molecules. The organic linker plays an important secondary role in increasing the adsorption strength further. Both theory and experiments have shown that increasing the aromaticity of the organic ligands results in an enhanced hydrogen adsorption capacity.[24a,50,35] A typical example is the iso-reticular MOF series (IRMOFs), *i.e.* MOFs with the same cubic symmetry but different pore sizes, show an increased hydrogen adsorption per formula unit with an increasing number of aromatic rings in the organic linker units at 77 K and 1 bar.[35] In addition, simply adorning the organic linkers with pendant functional groups is also a possible route towards improving the average interaction potential and is the result of the reduced interaction distance and the presence of (often) polar functional groups. For example, IRMOF-2, IRMOF-3, IRMOF-6 and IRMOF-20 show higher hydrogen uptake capacities than IRMOF-1 on a molar basis.[51] The hydrogen uptake capacity as a function of pressure for this series is shown in Figure 1.5. The same effect has also been found for the NOTT-series.[52]

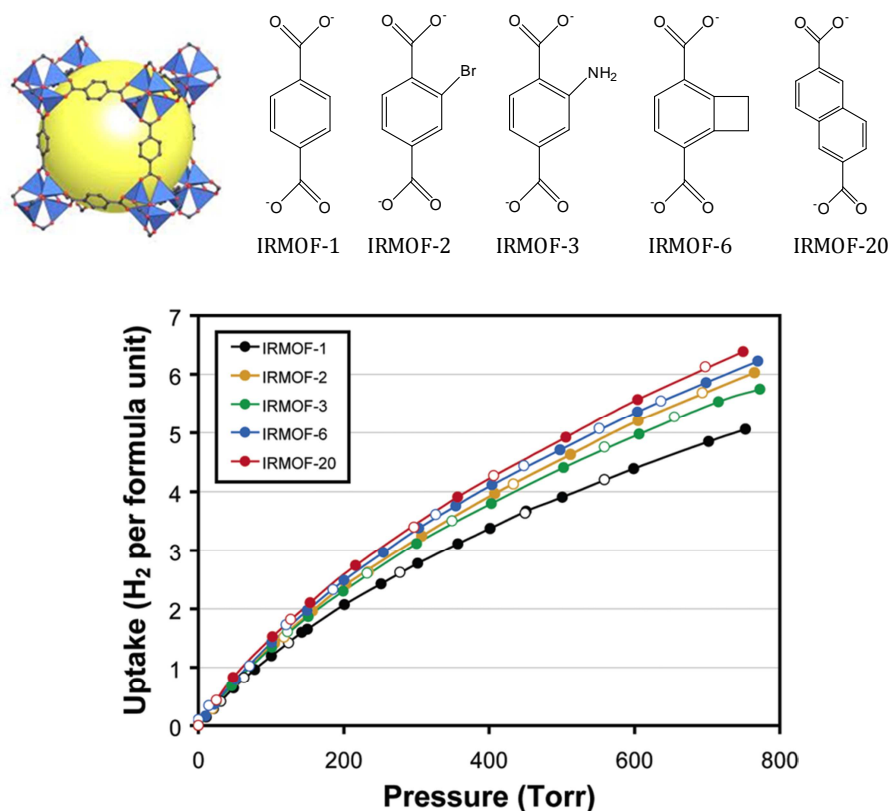


**Figure 1.5.** Examples of IRMOFs and their hydrogen uptake as a function of pressure. Reproduced from ref. [51]. Copyright 2006, American Chemical Society.

It is clear that the variability in organic ligands provides more possibilities to enhance the isosteric heat of hydrogen adsorption in MOFs by employing short linkers, achieving interpenetrated structures, or functionalizing the interior of the pores by simple chemical modifications. However, the diverse coordination modes and ability of both metal ions and organic ligands give rise to the formation of uncontrollable structures, for instance, the uncontrolled degree of interpenetration.[53] Therefore, the synthesis of a MOF with a specific targeted structure is a challenge. On the other hand, the final MOF structure is strongly affected by synthetic parameters and small changes in synthetic parameters may result in totally different framework structures or a lack of structure.[54-55] Simply modifying organic linkers by a one-pot or post synthetic procedure is attractive because a variety of functionalities can be introduced to MOFs using controlled conditions without damaging the host structures, making it possible to explore the role of functional groups in the hydrogen adsorption process. Both

computational and experimental studies in this field have been carried out.[37,52,56] However, the effect of functional groups *i.e.* their size, electronic effect on the hydrogen storage capability of MOFs is still not fully understood. For example, it has been found that the same functional group may play a different role in the hydrogen adsorption capability of MOFs with different structures.[57]

### **1.3 Synthetic considerations**

MOFs can be synthesized via many methods: solvothermal, hydrothermal, vapour diffusion, direct mixing, sonochemical, microwave heating, etc. The solvothermal method is frequently used and involves heating a mixture of organic ligands and metal salt in a solvent system. The solvents include, for example, ethanol, water, dioxane, dimethylformamide and diethylformamide. Among these solvents, formamides are popular because they not only dissolve the reactants but also deprotonate the carboxylic acids. In addition, variables in the reaction conditions including reagent concentration, time, temperature and fractional volume filling of the vessel are important parameters as well. Due to the disadvantages of the solvothermal method, such as long reaction time, high temperature, and high cost of solvents, alternative synthetic methods towards the synthesis of MOFs have been developed, and include solvent-free syntheses, microwave heating and electrochemical methods.[58-61].

In hydrogen uptake studies of MOFs, sample activation has been recognized as the key factor toward obtaining reproducible and reliable hydrogen uptake data. Traditionally, MOF samples are soaked in low boiling solvents (such as dichloromethane, chloroform, methanol, etc.) to exchange and remove high boiling solvents (*N,N*-dimethylformamide, *N,N*-diethylformamide, dioxane, dimethylsulfoxide, etc.), which typically occupy pores and channels of as-synthesized MOFs. The lower boiling point guest solvent is removed by evacuating under vacuum or by mild heating. However, this process may lead to poor porosity or even collapse of a MOF structure because of the surface tension. Recently, activation via supercritical drying and freeze-drying was demonstrated and this has resulted in a significant improvement in pore quality. Both techniques have provided a route towards MOFs that were previously inaccessible.[62-63] When using one of these activation methods, the solvent is replaced under mild conditions and the problem of surface tension is eliminated. Improved gas-accessible specific surface areas of four MOFs via a supercritical carbon dioxide (sc-CO<sub>2</sub>) drying procedure have been reported by Nelson and co-workers. For example, IRMOF-16 shows a 400% increase in the specific surface area compared to the conventional

solvent-exchanged sample.[62] Ma and co-workers reported that by applying a freeze-drying activation procedure, the Langmuir surface area of a Cu-based MOF comprised of methanetetra (*p*-benzoate) is triple that of the sample activated by conventional solvent-exchange techniques, moreover, the hydrogen uptake capacity at 77 K and 1 atm was improved by 82%.[63]

## 1.4 Scope and outline of the thesis

The main aim of the work presented in this thesis is to better understand the role of the organic linkers on structure formation of IRMOFs and how they affect the hydrogen storage capability. The MOFs synthesized by us and reported herein are selected such that they can be used as model systems for molecular modelling efforts.

In *Chapter 2* we present the synthesis and characterization of a series of mono-substituted (-OCH<sub>3</sub>, -CH<sub>3</sub>, -Br and -Cl) MOF-5s prepared under similar reaction conditions. The structure, thermal stability, and hydrogen storage capability of these MOF-5s were investigated and the experimentally obtained heats of hydrogen adsorption and hydrogen diffusion coefficients were contrasted with computational results.

In *Chapter 3* the synthesis and hydrogen uptake capacity of a homologous series methoxy-modified MOF-5s will be presented. The methoxy functionality has electron donating capability and will restrict the pores, and hence, a high hydrogen storage capacity exceeding that of MOF-5 is expected. Since high quality MOF-5 solely built from methoxyterephthalic acid cannot be synthesized, we prepared this MOF series via a mixed-ligand (terephthalic acid/methoxyterephthalic acid) method. The impact of the methoxy group on the hydrogen storage capacity of MOF-5 will be discussed.

In *Chapter 4* the synthesis, structural stability and hydrogen adsorption characteristics of methyl- (-CH<sub>3</sub>) and di-methyl substituted MOF-5s will be discussed. The methyl groups are per definition *ortho* with respect to the carboxylate functionality and it was anticipated that the hydrophobic nature of -CH<sub>3</sub> could aid in reducing the moisture sensitive nature of this MOF.

In order to understand whether the metal salt-to-organic ligand ratio (Zn(NO<sub>3</sub>)<sub>2</sub>·6H<sub>2</sub>O-to-terephthalic acid) is critical during the synthesis of MOF-5 we prepared eight MOF-5s using a variable stoichiometric offset (in the range of 1:1 and 1:7). In *Chapter 5* the effects on structure, thermal stability and hydrogen uptake capacity will be discussed.

Based on our current understanding, increasing the density of Zn<sub>4</sub>O clusters should result in an increase in hydrogen uptake capacity of MOFs. In *Chapter 6* we will present the synthetic challenges and hydrogen storage properties of a series ‘short linker’ IRMOFs, *i.e.* IRMOFs based on acetylenedicarboxylate, fumarate and oxalate.

Finally, in *Chapter 7* we will present the synthesis of two novel Cu(II) coordination polymers constructed from polar 5-membered heterocycles, *i.e.* 2,5-thiophene-dicarboxylate and 2,5-furan-dicarboxylate. We will discuss how the heterocycles affect the structural stability, specific surface area, heat of hydrogen adsorption and the hydrogen storage capability of this class of materials.

## 1.5 References

- [1] (a) Sandrock, G. *J. Alloys Compd.* **1999**, 293-295, 877. (b) Energy and Transportation: Challenges for the Chemical Sciences in the 21<sup>st</sup> Century, Organizing Committee for the Workshop on Energy and Transportation, The National Academies Press, Washington, D.C. 2003.
- [2] Grochala, W.; Edwards, P.P. *Chem. Rev.* **2004**, 104, 1283.
- [3] Schuth, F.; Bogdanov, B.; Felderhoff, M. *Chem. Commun.* **2004**, 2249.
- [4] Becher, M.; Haluska, M.; Hirscher, M.; Quintel, A.; Skakalova, V.; Dettlaff-Weglikovska, U.; Chen, X.; Hulman, M.; Choi, Y.; Roth, S.; Meregallo, V.; Parrinello, M.; Strübel, R.; Jürissen, L.; Kappes, M. M.; Fink, J.; Züttel, A.; Stepanek, I.; Bernier, P. *C. R. Phys.* **2003**, 4, 1055.
- [5] (a) Ogden, J.M. *Int. J. Hydrogen Energy* **1999**, 24, 709. (b) <http://www1.eere.energy.gov/hydrogenandfuelcells/mypp/pdfs/storage.pdf>.
- [6] (a) Nijkamp, M.G.; Raaymakers, J.; van Dillen, A. J.; de Jong, K.P. *Appl. Phys. A: Mater. Sci. Process.* **2001**, 72, 619. (b) Fichtner, M. *Adv. Eng. Mater.* **2005**, 7, 443.
- [7] Everett, D.H. *Pure Appl. Chem.* **1972**, 31, 577.
- [8] Yang, J.; Sudik, A.; Wolverton, C.; Siegel, D.J. *Chem. Soc. Rev.* **2010**, 39, 656.
- [9] Seayad, A.M.; Antonelli, D.M. *Adv. Mater.* **2004**, 16, 765.
- [10] (a) Graetz, J. *Chem. Soc. Rev.* **2009**, 38, 73. (b) Eberle, U.; Felderhoff, M.; Schuth, F. *Angew. Chem. Int. Ed.* **2009**, 48, 2.
- [11] Chen, P.; Wu, X.; Lin, J.; Tan, K.L. *Science* **1999**, 285, 91.
- [12] Sculley, J.; Yuan, D.; Zhou, H.-C. *Energy Environ. Sci.* **2011**, 4, 2721.
- [13] (a) Zhao, D.; Timmons, D.; Yuan, D.; Zhou, H.-C. *Accounts of Chemical Research* **2011**, 44, 123. (b) Hu, Y.; Zhang, L. *Adv. Mater.* **2010**, 22, 117.



- [14] (a) Froudakis, G.E. *Materials today* **2011**, *14*, 324. (b) Benard, P.; Chahine, R. *Scripta Materials* **2007**, *56*, 803.
- [15] Liu, C.; Fan, Y.Y.; Liu, M.; Cong, H.T.; Cheng, H.M.; Dresselhaus, M.S. *Science*, **1999**, *286*, 1127.
- [16] (a) Yang, R.T. *Carbon* **2000**, *38*, 623. (b) Kajiura, H.; Tsutsui, S.; Kadono, K.; Kakuta, M.; Ata, M.; Murakami, Y. *Appl. Phys. Lett.* **2003**, *82*, 1105.
- [17] Ströbel, R.; Garche, J.; Moseley, P.T.; Jörisen, L.; Wolf, G. *J. Power Source* **2006**, *159*, 781.
- [18] Zecchina, A.; Bordiga, S.; Vitillo, J.G.; Ricchiardi, G.; Lamberti, C.; Spoto, G. *J. Am. Chem. Soc.* **2005**, *127*, 6361.
- [19] (a) Florusse, L.J.; Peters, C.J.; Schoonman, J.; Hester, K.C.; Koh, C.A.; Dec, S.F.; Marsh, K.N.; Sloan, E.D. *Science* **2004**, *306*, 469. (b) Rowsell, J.L.C.; Yaghi, O. M. *Angew. Chem. Int. Ed.* **2005**, *44*, 4670.
- [20] Furukawa, H.; Yaghi, O.M. *J. Am. Chem. Soc.* **2009**, *131*, 8875.
- [21] Kubota, Y.; Takata, M.; Matsuda, R.; Kitaura, R.; Kitagawa, S.; Kato, K.; Sakata, M.; Kobayashi, T.C. *Angew. Chem. Int. Ed.* **2005**, *44*, 920.
- [22] (a) Côté, A.P.; Benin, A.I.; Ockwig, N.W.; O’Keeffe, M.; Matzger, A.J.; Yaghi, O.M. *Science* **2005**, *310*, 1166. (b) El-Kaderi, H.M.; Hunt, J.R.; Mendoza-Cortés, J.L.; Côté, A.P.; Taylor, R.E.; O’Keeffe, M.; Yaghi, O.M. *Science* **2007**, *316*, 268. (c) Furukawa, H.; Ko, N.; Go, Y. B.; Aratani, N.; Choi, S. B.; Choi, E.; Yazaydin, A.Ö.; Snurr, R.Q.; O’Keeffe, M.; Kim, J. Yaghi, O.M. *Science* **2010**, *329*, 424.
- [23] Han, S.S.; Furukawa, H.; Yaghi, O.M.; Goddard, W.A. *J. Am. Chem. Soc.* **2008**, *130*, 11580.
- [24] (a) Duren, T.; Bae, Y.-S.; Snurr, R.Q. *Chem. Soc. Rev.* **2009**, *38*, 1237. (b) Han, S.S.; Goddard III, W.A. *J. Am. Chem. Soc.* **2007**, *129*, 8422.
- [25] (a) Czaja, A. U.; Trukhan, N.; Muller, U. *Chem. Soc. Rev.* **2009**, *38*, 1284. (b) Halder, G.J.; Kepert, C.J.; Moubaraki, B.; Murray, K.S.; Cashion, J.D. *Science* **2002**, *298*, 1762. (c) Mines, G.A.; Tzeng, B.-C.; Stevenson, K.J.; Li, J.; Hupp, J.T. *Angew. Chem. Int. Ed.* **2002**, *41*, 154. (d) Li, J.-R.; Kuppler, R.J.; Zhou, H.-C. *Chem. Soc. Rev.* **2009**, *38*, 1477. (e) Wu, C.D.; Hu, A.; Zhang, L.; Lin, W. *J. Am. Chem. Soc.* **2005**, *127*, 8940.
- [26] (a) Lee, E.Y.; Farha, O.M.; Roberts, J.; Scjeodt, K.A.; Nguyen, S.; Hupp, J.T. *Chem. Soc. Rev.* **2009**, *38*, 1450. (b) Dinca, M.; Long, J.R. *J. Am. Chem. Soc.* **2005**, *127*, 9376. (c) Farha, O.K.; Mulfort, K.L.; Thorsness, A.M.; Hupp, J.T. *J. Am. Chem. Soc.* **2008**, *130*, 8598.
- [27] (a) Kitagawa, S.; Kitaura, R.; Noro, S. *Angew. Chem. Int. Ed.* **2004**, *43*, 2334. (b) Vagin, S.I.; Ott, A.K.; Rieger, B. *Chemie Ingenieur Technik* **2007**, *79*, 767.
- [28] (a) Rosi, N.L.; Eckert, J.; Eddaoudi, M.; Vodak, D.T.; Kim, J.; O’Keeffe, M.;

- Yaghi, O.M. *Science* **2003**, *300*, 1127. (b) Yaghi, O. M.; O'Keeffe, M.; Ockwig, N. W.; Chae, H. K.; Eddaoudi, M.; Kim, J. *Nature*, **2003**, *423*, 705.
- [29] Férey, G.; Latroche, M.; Serre, C.; Millange, F.; Loiseau, T.; Percheron-Guégan, A. *Chem. Commun.* **2003**, 2976.
- [30] Kafye, S.S.; Dailly, A.; Yaghi, O.M.; Long, J.R. *J. Am. Chem. Soc.* **2007**, *129*, 14176.
- [31] Chae, H.K.; Siberio-Pérez, D.Y.; Kim, J.; Go, Y.B.; Eddaoudi, M.; Matzger, A.J.; O'Keeffe, M.; Yaghi, O.M. *Nature* **2004**, *427*, 523.
- [32] Wong-Foy, A.G.; Matzger, A.J.; Yaghi, O.M. *J. Am. Chem. Soc.* **2006**, *128*, 3494.
- [33] Panella, B.; Hönes, K.; Müller, U.; Trukhan, N.; Schubert, M.; Pütter, H.; Hirscher, M. *Angew. Chem. Int. Ed.* **2008**, *47*, 2138.
- [34] Bae, Y.-S.; Yazaydm, A.O.; Snurr, R.Q. *Langmuir* **2010**, *26*, 5475.
- [35] Rowsell, J.L.C.; Millward, A.R.; Park, K.S.; Yaghi, O.M. *J. Am. Chem. Soc.* **2004**, *126*, 5666.
- [36] (a) Panella, B.; Hirscher, M.; Pitter, H.; Miller, U. *Adv. Funct. Mater.* **2006**, *16*, 520. (b) Kaye, S.S.; Long, J.R. *J. Am. Chem. Soc.* **2005**, *127*, 6506.
- [37] Murray, L.J.; Dinca, M.; Long, J.R. *Chem. Soc. Rev.* **2009**, *38*, 1294.
- [38] Bathia, S.K.; Myers, A.L. *Langmuir* **2006**, *22*, 1688.
- [39] Yaghi, O.M. *DOE hydrogen program. Annual progress report* **2007**, 593.
- [40] Chen, B.; Ockwig, N.W.; Millward, A.R.; Contreras, D.S.; Yaghi, O.M. *Angew. Chem. Int. Ed.* **2005**, *44*, 4745.
- [41] Dincă, M.; Dailly, A.; Liu, Y.; Brown, C.M.; Neumann, D.A.J.; Long, R. *J. Am. Chem. Soc.* **2006**, *128*, 16876.
- [42] Latroche, M.; Surble, S.; Serre, C.; Mellot-Draznieks, C.; Llewellyn, P.L.; Lee, J. H.; Chang, J.S.; Jhung, S.H.; Férey, G. *Angew. Chem. Int. Ed.* **2006**, *45*, 8227. (b) Férey, G. *Chem. Soc. Rev.* **2008**, *37*, 191.
- [43] Zhou, W.; Wu, H.; Yildirim, T. *J. Am. Chem. Soc.* **2008**, *130*, 15268.
- [44] De la Casa-Lillo, M.A.; Lamari-Darkrim, F.; Cazorla-Amorós, D.; Linares-Solano, A. *J. Phys. Chem. B* **2002**, *106*, 10930.
- [45] Dybtsev, D.N.; Chun, H.; Yoon, S.H.; Kim, D.; Kim, K. *J. Am. Chem. Soc.* **2004**, *126*, 32.
- [46] Ma, S.Q.; Sun, D.F.; Ambrogio, M.; Fillinger, J.A.; Parkin, S.; Zhou, H.-C. *J. Am. Chem. Soc.* **2007**, *129*, 1858.
- [47] Mulfort, K.L.; Hupp, J.T. *Inorg. Chem.* **2008**, *47*, 7936. (b) Mulfort, K.L.; Hupp, J.T. *J. Am. Chem. Soc.* **2007**, *129*, 9604.
- [48] Rood, J.A.; Noll, B.C.; Henderson, K.W. *Inorg. Chem.* **2006**, *45*, 5521.
- [49] Ma, S.; Eckert, J.; Forster, P.M.; Yoon, J.W.; Hwang, Y.K.; Chang, J.-S.; Collier, C. D.; Parise, J.B.; Zhou, H.-C. *J. Am. Chem. Soc.* **2008**, *130*, 15896.
- [50] Han, S.S.; Deng, W.-Q.; Goddard III, W.A. *Angew. Chem. Int. Ed.* **2007**, *46*, 6289.

- [51] Rowsell, J.L.C.; Yaghi, O.M. *J. Am. Chem. Soc.* **2006**, *128*, 1304.
- [52] Lin, X.; Telepeni, I.; Blake, A.J. Dailly, A.; Brown, C.M.; Simmons, J.M.; Zoppi, M.; Walker, G.S.; Thomas, K.M.; Mays, T.J.; Hubberstey, P.; Champness, N.R.; Schroder, M. *J. Am. Chem. Soc.* **2009**, *131*, 2159.
- [53] Gadzikwa, T.; Zhang, B.-S.; Hupp, J.T. Nguyen, J.G. *Chem. Commun.* **2008**, 3672.
- [54] Li, J.; Cheng, S.; Zhao, Q.; Long, Q.; Dong J. *Int. J. Hydrogen Energy* **2009**, *34*, 1377.
- [55] Chen, B.; Wang, X.; Zhang, Q.; Xi, X.; Cai, J.; Qi, H.; Shi, S.; Wang, J.; Yuan, D.; Fang, M. *J. Mater. Chem.* **2010**, *20*, 3758.
- [56] Mulder, F.M.; Dingemans, T.J.; Wagemaker, M.; Kearley, G.J. *Chem. Phys.* **2005**, *317*, 113.
- [57] Zlotea, C.; Phanon, D.; Mazaj, M.; Heurtaux, D.; Guillern, V.; Serre, C.; Horcajada, P.; Devic, T.; Magnier, E.; Cuevas, F.; Férey, G.; Llewellyn, P.L.; Latroche, M. *Dalton Transactions* **2011**, *40*, 4879.
- [58] Pichon, A.; Lazuen-Garay, A.; James, S.L. *CrystEngComm* **2006**, *8*, 211.
- [59] (a) Ni, Z.; Maesl, R.I. *J. Am. Chem. Soc.* **2006**, *128*, 12394. (b) Jhung, S.H.; Lee, J. H.; Yoon, J.W.; Serre, C.; Férey, G.; Chang, J.S. *Adv. Mater.* **2007**, *19*, 121. (c) Choi, J.S.; Son, W.J.; Kim, J.; Ahn, W.S. *Microporous Mesoporous Mater.* **2008**, *166*, 727.
- [60] Qiu, L.-G.; Li, Z.-Q.; Wu, Y.; Wang, W.; Xu, T.; Jiang, X. *Chem. Commun.* **2008**, 3642.
- [61] Son, W.-J.; Kim, J.; Kim, J.; Ahn, W.-S. *Chem. Commun.* **2008**, 6336.
- [62] Nelson, A.P.; Farha, O.K.; Mulfort, K.L.; Hupp, J.T. *J. Am. Chem. Soc.* **2008**, *131*, 458.
- [63] Ma, L.; Jin, A.; Xie, Z.; Lin, W. *Angew. Chem. Int. Ed.* **2009**, *48*, 9905.



## CHAPTER 2

### **Mono-substituted MOF-5 derivatives: an experimental and computational approach**

---

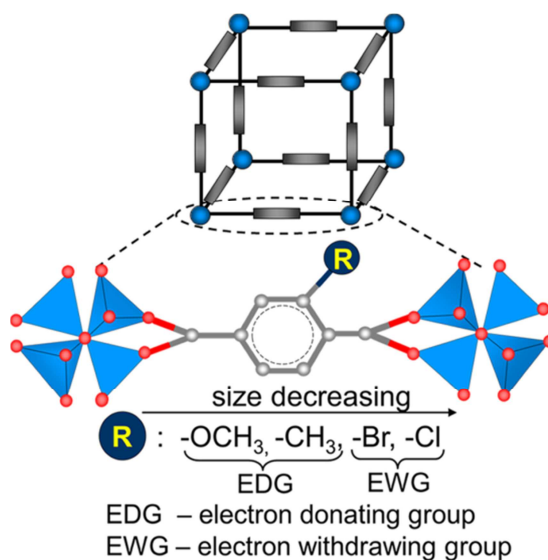
In this chapter, we will discuss how simple functional groups on the benzene linker of MOF-5 affect the crystal structure, thermal stability and hydrogen uptake capacity of MOF-5. Four functional groups *i.e.* methyl (-CH<sub>3</sub>), methoxy (-OCH<sub>3</sub>), bromine (-Br) and chlorine (-Cl), were introduced into the MOF-5 structure. All MOF modifications, except for OCH<sub>3</sub>-MOF-5, show the same topology as MOF-5. The thermal stability of MOF-5 is not affected by introducing a -CH<sub>3</sub> group, but is reduced by introducing -Br and -Cl functionalities. Experimental and computational results reveal that the introduction of -CH<sub>3</sub>, -Br and -Cl plays only a minor role in the isosteric heat of hydrogen adsorption for MOF-5 and the experimental values are in the range of 2.83 – 3.03 kJ mol<sup>-1</sup> for all derivatives. This explains the similar hydrogen adsorption capacities of MOF-5 and CH<sub>3</sub>-MOF-5. The poor porous structures of Br-MOF-5 and Cl-MOF-5, however, result in a lower hydrogen adsorption capacity (77 K and 1 bar) compared to MOF-5 despite their similar isosteric heats of hydrogen adsorption. At high pressures (> 20 bar), the excess hydrogen capacity appears to be a strong function of the specific surface area.

## 2.1 Introduction

Metal organic frameworks (MOFs) have emerged as a class of promising materials for a wide range of applications due to their exceptionally high surface area, low density and adjustable pore size and functionality.[1-4] Among these advantages, functionality is attractive because it can be used to tune the chemistry and physical dimensions of the pores and by doing so make MOFs attractive for specific applications such as catalysis, luminescent materials, gas sorption and gas separation.[5-9] Both one-pot and post-synthetic approaches are used to introduce functional groups into MOFs while keeping the parent framework structure intact.[10,11] For example, amino-modified MOFs have been reported and shown to perform as excellent solid base catalysts and sorbents for selective CO<sub>2</sub> capture and storage.[12]

Over the last decade, more and more MOFs have been reported as hydrogen storage materials.[3,4] However, the current generation MOFs has only limited applicability for on-board hydrogen storage because of their low hydrogen storage capacities under mild conditions. Considerable efforts have been made to improve the hydrogen storage capacities of MOFs.[8,9] Functionalization of organic linkers is one route that is currently being explored by several groups.[10,13-16] Rowsell and co-workers have shown that tuning the organic linker of MOF-5 without changing the basic cubic topology can affect the hydrogen storage capability of MOF-5. Functionalized MOF-5s prepared from amino (-NH<sub>2</sub>), bromine (-Br) or 1,2-dihydrocyclobutabenzene dicarboxylic acid (-C<sub>2</sub>H<sub>4</sub>-) do display larger hydrogen uptake capacities than that of unsubstituted MOF-5 at 77 K and below 1 bar on a molar basis, which is explained by the constriction of the pores by the pendant groups.[14a] The same group also reported allyloxy- and benzyloxy-functionalized MOF-5 analogs and these modifications also show a pronounced improvement in hydrogen uptake capacity.[14b] The same effect was found for Zn-MOFs built from (non)-substituted 4,4'-ethynylene dibenzoate and a 4,4'-dipyridyl co-ligand, as explored by Gadzikwa *et al.* Zn-MOF constructed with 4,4'-ethynylene dibenzoate does not adsorb hydrogen whereas the introduction of bromine (-Br) or methyl (-CH<sub>3</sub>) substituents results in hydrogen uptake capacities of 0.3 wt% and 1 wt% at 77 K and 1 bar, respectively.[13c] Recently we demonstrated that the moisture stability of MOF-5 can be improved significantly without compromising the hydrogen uptake capacity by introducing hydrophobic methyl groups on the phenylene linker.[16] In conclusion, the effect of functional groups, i.e. their size, the number of substituents and electronic effect on the hydrogen storage capability of MOFs is still not fully understood.

Herein we selected MOF-5 as a basic model compound because MOF-5 exhibits a simple cubic crystal structure and high thermal stability and is one of the most promising MOFs for future cryogenic hydrogen storage applications.[8b] Four functional groups, i.e.  $-\text{CH}_3$ ,  $-\text{OCH}_3$ ,  $-\text{Br}$  and  $-\text{Cl}$ , as shown in Scheme 2.1, were introduced at the 2-position of the phenylene unit in the MOF-5 framework. These substituents were selected because they vary in size and electronic make-up, which makes them ideal candidates for our computational studies. The structural characteristics and thermal stability of MOF-5 alter when introducing these functional groups. Although previous reports have indicated that the effect of functional groups on the hydrogen adsorption capacity of MOF-5 is rather small,[17-19] conclusive evidence has not been reported as of yet. Herein, the hydrogen adsorption properties of four modified MOF-5s, i.e. the isosteric heats of hydrogen adsorption and hydrogen uptake capacities, were investigated experimentally. Furthermore, the heat of hydrogen adsorption and the hydrogen diffusion coefficient for the four MOFs were determined using computational methods and contrasted with our experimental results.



**Scheme 2.1.** Modified MOF-5s with different functional groups on the central benzene linker unit.

## 2.2 Experimental

### 2.2.1 Materials

Zn(NO<sub>3</sub>)<sub>2</sub>·6H<sub>2</sub>O (98%, Aldrich), terephthalic acid (>99%, BP Chembel) were used as received. Bromoterephthalic acid (95%, Aldrich) was recrystallized from THF/hexane (1:1). *N,N*-diethylformamide (DEF, 99%, Acros) and CHCl<sub>3</sub> were dried over and distilled from CaH<sub>2</sub> and P<sub>2</sub>O<sub>5</sub>, respectively, before use. 2-chloro-1,4-dimethylbenzene (98%, Aldrich), diethylene glycol (99%, Acros), methylterephthalonitrile (98%, Acros), and 2,5-dimethylanisole (>99%, Acros) were used as received.

### 2.2.2 Synthesis of mono-substituted terephthalic acid

**Synthesis of chloroterephthalic acid.**[20] A 100 mL autoclave charged with 2.50 g (17.8 mmol) of 2-chloro-1,4-dimethylbenzene, 5 mL of 65% HNO<sub>3</sub> and 12 mL of distilled water was placed into an oven at 170 °C for 20 h. After cooling, the product was collected and dried at 80 °C under vacuum. The light yellow crude (1.93 g, 54% yield) was recrystallized from THF/hexane (1:1). <sup>1</sup>H-NMR (DMSO-*d*<sub>6</sub>, 400 MHz): δ (ppm) 7.71-8.06 (m, 3H, ArH), 5.8 (s, 2H, COOH). <sup>13</sup>C-NMR (DMSO-*d*<sub>6</sub>, 100 MHz): δ (ppm) 166.8, 166.0, 135.8, 134.7, 132.0, 131.3, 131.2, 128.3. FT-IR (cm<sup>-1</sup>): 3060, 2960, 2813, 2650, 2514, 1686, 1558, 1487, 1407, 1382, 1283, 1251, 1147, 1129, 1051, 906, 885, 856, 780, 745, 714, 680, 660. MS (EI), *m/z* (rel.): 200 (91) (M<sup>+</sup>), 183 (100), 157 (17), 99 (40), 75 (35), 28 (19).

**Synthesis of methylterephthalic acid.**[21] Methylterephthalonitrile (35.2 mmol, 5.00 g.) was added to a solution of NaOH (141 mmol, 5.63 g) and 0.1 mL water in 100 mL of diethylene glycol (DEG). The reaction mixture was heated to 200 °C with a heating rate of 1 °C min<sup>-1</sup> and kept at 200 °C for 42 h. During this time, 60 mL of DEG was added to the reaction mixture. After cooling, the reaction mixture was adjusted to pH≈1 by adding a 37% HCl solution. The precipitate was collected by filtration, and the crude product was washed with cold ethanol and dried at 80 °C under vacuum. Crude methylterephthalic acid (5.24 g, 83% yield) was recrystallized from acetone/hexane (10:1). <sup>1</sup>H-NMR (DMSO-*d*<sub>6</sub>, 400 MHz): δ (ppm) 12.17 (s, 2H, COOH), 7.80-7.88 (3H, ArH), 2.54 (s, 3H, CH<sub>3</sub>). <sup>13</sup>C-NMR (DMSO-*d*<sub>6</sub>, 100 MHz): δ(ppm) 168.7, 167.2, 139.4, 134.9, 133.6, 132.5, 130.6, 127.1, 21.4. FT-IR (cm<sup>-1</sup>): 3058, 2935, 2812, 2650, 2531, 1673, 1567, 1497, 1450, 1411, 1386, 1291, 1250, 1200, 1132, 1085, 952, 900, 857, 781, 746, 676. MS (EI), *m/z* (rel.): 180 (61) (M<sup>+</sup>), 162 (100), 134 (64), 89 (25), 77 (44), 28 (63).



**Synthesis of methoxyterephthalic acid.**[22] A mixture of 2,5-dimethylanisole (6.03 g, 44.3 mmol) and potassium permanganate (30 g, 152.2 mmol) in 200 mL of distilled water was refluxed for 5 h. The reaction mixture was cooled to room temperature and filtered. The filtrate was acidified with HCl (37%). The white precipitate was collected, washed with distilled water and recrystallized from distilled water.  $^1\text{H-NMR}$  ( $\text{DMSO-}d_6$ , 400 MHz):  $\delta$  (ppm) 13.14 (s, 2H,  $\text{COOH}$ ), 7.54-7.70 (3H,  $\text{ArH}$ ), 3.87 (s, 3H,  $\text{OCH}_3$ ).  $^{13}\text{C-NMR}$  ( $\text{DMSO-}d_6$ , 100 MHz):  $\delta$  (ppm) 167.7, 167.3, 158.2, 135.2, 131.0, 126.4, 121.7, 113.2, 55.5. FT-IR ( $\text{cm}^{-1}$ ): 3068, 2972, 2821, 3642, 2529, 1676, 1611, 1571, 1499, 1400, 1295, 1233, 1186, 1149, 1088, 1029, 926, 875, 791, 755, 690. MS (EI),  $m/z$  (rel.): 196 (37) ( $\text{M}^+$ ), 149 (100), 119 (30), 79 (25), 77 (34), 28 (5).

### 2.2.3 Synthesis of MOF-5 and modified MOF-5s

MOF-5 has been synthesized according to a literature procedure.[23] The synthetic procedures of the substituted MOF-5s are similar to that of MOF-5. The modified MOF-5s were labeled as  $\text{CH}_3\text{-MOF-5}$ ,  $\text{OCH}_3\text{-MOF-5}$ ,  $\text{Br-MOF-5}$  and  $\text{Cl-MOF-5}$ , respectively.

**$\text{CH}_3\text{-MOF-5}$ .** 5.11 g (17.2 mmol) of  $\text{Zn}(\text{NO}_3)_2 \cdot 6\text{H}_2\text{O}$ , 1.00 g (5.6 mmol) of methylterephthalic acid and 120 mL of DEF were heated at 125 °C for 6 h. The product was collected, washed with DEF (3×20 mL) and followed by immersing the crystals in  $\text{CHCl}_3$  (40 mL) for 24 h (3×). The solvent exchanged product was vacuum dried overnight at 100 °C and stored in a glove box (0.83 g, 55% yield). FT-IR ( $\text{cm}^{-1}$ ): 2982, 1605, 1565, 1497, 1405, 1380, 1293, 1209, 1099, 911, 828, 788, 763.

**$\text{OCH}_3\text{-MOF-5}$ .** 4.06 g (13.6 mmol) of  $\text{Zn}(\text{NO}_3)_2 \cdot 6\text{H}_2\text{O}$ , 0.80 g (4.1 mmol) of methoxyterephthalic acid and 98 mL of DEF were heated at 125 °C for 8 h. After  $\text{CHCl}_3$ -exchange and solvent removal, the product was stored in a glove box (0.62 g, 53% yield). FT-IR ( $\text{cm}^{-1}$ ): 2973, 2932, 1650, 1573, 1504, 1457, 1412, 1381, 1303, 1250, 1104, 1026, 926, 886, 835, 773.

**$\text{Br-MOF-5}$ .** 4.49 g (15.1 mmol) of  $\text{Zn}(\text{NO}_3)_2 \cdot 6\text{H}_2\text{O}$ , 1.23 g (5.0 mmol) of bromoterephthalic acid and 150 mL of DEF were heated at 125 °C for 9 h. After  $\text{CHCl}_3$ -exchange and solvent removal, the product was stored in a glove box (1.20 g, 71% yield). FT-IR ( $\text{cm}^{-1}$ ): 2979, 1583, 1487, 1388, 1259, 1209, 1151, 1039, 910, 887, 829, 767, 734, 662.

**$\text{Cl-MOF-5}$ .** 5.58 g (18.8 mmol) of  $\text{Zn}(\text{NO}_3)_2 \cdot 6\text{H}_2\text{O}$ , 1.24 g (6.2 mmol) of chloroterephthalic acid and 140 mL of DEF were heated at 125 °C for 11 h. After  $\text{CHCl}_3$ -

exchange and solvent removal, the product was stored in a glove box (1.31 g, 72% yield). FT-IR (cm<sup>-1</sup>): 2979, 1575, 1490, 1391, 1258, 1210, 1156, 1049, 900, 830, 769, 748, 671.

#### **2.3.4 Activation by heat-treatment *in vacuo***

MOF-5, CH<sub>3</sub>-MOF-5, and Br-MOF-5 were heated at 200 °C *in vacuo* for 40 h. OCH<sub>3</sub>-MOF-5 was vacuum heated at 200 °C for 24 h. Cl-MOF-5 was also heated *in vacuo* at 200 °C for 24 h or 40 h, respectively. Samples were labeled as MOF-5-40h, CH<sub>3</sub>-MOF-5-40h, Br-MOF-5-40h, OCH<sub>3</sub>-MOF-5-24h, Cl-MOF-5-24h, and Cl-MOF-5-40h.

#### **2.3.5 Characterization**

XRD patterns of all samples were recorded on an X'Pert X-ray diffractometer operated at 45 kV and 40 mA with monochromatic Cu K $\alpha$  radiation within a 2-theta range of 5-60°. For each XRD measurement, a sample was placed into an air-tight sample holder in order to avoid exposure to air and moisture using an Ar glovebox. IR spectra were collected on a PerkinElmer Spectrum 100 FT-IR Spectrometer. TGA curves were obtained on a PerkinElmer Pyris Diamond Thermogravimetric Differential Thermal/Analyzer. Samples were heated from room temperature to 600 °C with a heating rate of 10 °C min<sup>-1</sup> under a dry nitrogen or air flow. Elemental Analyses were performed on a Thermo Scientific InterScience Flash 2000 Organic Elemental Analyzer. The pore textural properties, including BET surface area and pore volume, were recorded on a Micromeritics ASAP 2010 adsorption analyzer at 77 K. Prior to the adsorption measurements, the samples were *in-situ* degassed in vacuum at 135 °C. The dead volume of the sample cell was determined in a separate experiment. *In-situ* pretreatment coupled to a separate dead volume measurement after the analysis was employed in order to avoid the helium entrapment phenomenon. The weight of a sample obtained after the pretreatment was used in the various calculations. BET surface areas were calculated in the adapted pressure range of  $P/P_0=0.01-0.1$ . Hydrogen storage measurements at different pressures were performed on a Sievert's setup at 77 K and room temperature. Each sample was pretreated under high vacuum (10<sup>-6</sup> mbar) prior to the measurement as follows: samples without heat-treatment were heated at 150 °C for 3 days; samples with heat-treatment were heated at 120 °C overnight. Hydrogen (ultra-high-purity grade, 99.999%) was additionally purified by leading it over a bed of zeolite spheres at 77 K before being loaded in the samples. The pressure change was monitored and recorded after the hydrogen reservoir was connected to the sample holder. The samples were weighed in a glove box after each measurement for calculating hydrogen uptake capacity. The amount of hydrogen stored in the dead volume was examined at

low pressure (<1.5 bar) with sea sand as a reference. For all high-pressure measurements, the dead volume was determined with helium in the presence of a sample. This procedure of determining the dead volume was also performed for the measurements at 64 K and 100 K below 2 bar. The hydrogen uptake capacities of all samples were obtained by subtracting the amount of hydrogen in the dead volume from the total amount of hydrogen released from the reservoir.

The istosteric heat of hydrogen adsorption can be calculated according to the Clausius-Clapeyron equation (1)

$$\left( \frac{\partial \ln P}{\partial T} \right)_{\vartheta} = \frac{Q_{st}}{RT^2} \quad (1)$$

Where  $R$  is the universal gas constant and  $\vartheta$  is the fractional surface coverage at pressure  $P$  and temperature  $T$ . For a certain surface coverage  $\vartheta$ , if  $P_1$  and  $P_2$  are the pressures at two temperatures  $T_1$  and  $T_2$ , equation (1) has the form:

$$\ln\left(\frac{P_2}{P_1}\right) = \frac{Q_{st}}{R} \left( \frac{1}{T_1} - \frac{1}{T_2} \right) \quad (2)$$

We used the hydrogen adsorption isotherms at 64 K, 77 K, and 100 K to calculate  $Q_{st}$  from equation (2).

The computational studies on the heats of hydrogen adsorption and diffusion coefficients of hydrogen on MOF-5 and modified MOF-5s were carried out by another project.

## 2.3 Results and discussion

### 2.3.1 Structure characterization of modified MOF-5s

The structures of all modified MOF-5s were characterized by powder X-ray diffraction (PXRD). MOF-5 has been synthesized as a reference and its PXRD pattern (Figure 2.1) closely matches the MOF-5 data reported in literature.[20] Figure 2.2 shows the PXRD patterns of CH<sub>3</sub>-MOF-5, OCH<sub>3</sub>-MOF-5, Br-MOF-5 and Cl-MOF-5, which were synthesized under similar conditions as MOF-5. We have also simulated the PXRD patterns of the modified MOF-5s and the results are shown in Figure 2.2 as well. All peak positions in the PXRD pattern of CH<sub>3</sub>-MOF-5 are identical to the simulated results, implying that CH<sub>3</sub>-MOF-5 has the same cubic topology as MOF-5. Meanwhile, some differences exist between both structures as revealed by the intensity of some peaks.

Compared to simulated results (Figure 2.2A), a higher  $13.8^\circ$  to  $6.9^\circ$  peak intensity ratio, as indicated by  $R_2$ , was found for  $\text{CH}_3\text{-MOF-5}$ . A similar result was obtained for our MOF-5 (Figure 2.1) and can be explained by the presence of an interpenetrated structure.[24,25] A detailed Rietveld refinement for these types of structures does not give conclusive results, which is thought to be due to the presence of inhomogeneities in the structure. The  $\text{CH}_3\text{-MOF-5}$  may also partly contain an interpenetrated structure.  $\text{OCH}_3\text{-MOF-5}$  showed a very poor diffraction pattern. The diffraction peaks at  $6.9^\circ$  and  $9.7^\circ$  are not pronounced, indicating that  $\text{OCH}_3\text{-MOF-5}$  hardly exhibits a MOF-5-type structure. The halogenated MOFs, i.e.  $\text{Br-MOF-5}$  and  $\text{Cl-MOF-5}$  gave similar PXRD patterns. Sharp peaks appeared at  $6.9^\circ$  and  $9.7^\circ$  in their PXRD patterns but some peaks do not fit well with their simulated PXRD patterns, suggesting  $\text{Br-MOF-5}$  and  $\text{Cl-MOF-5}$  have the same topology as MOF-5, but some impurities may still be present. The PXRD results indicate that the mono-substituted MOF-5s can be prepared under similar reaction conditions as used for preparing MOF-5. The frameworks showed the same cubic topology as that of MOF-5 but the crystal quality and overall yield vary.

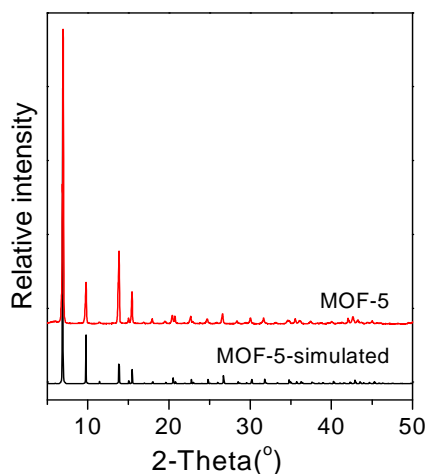


**Figure 2.1.** Simulated and experimental PXRD patterns of MOF-5.

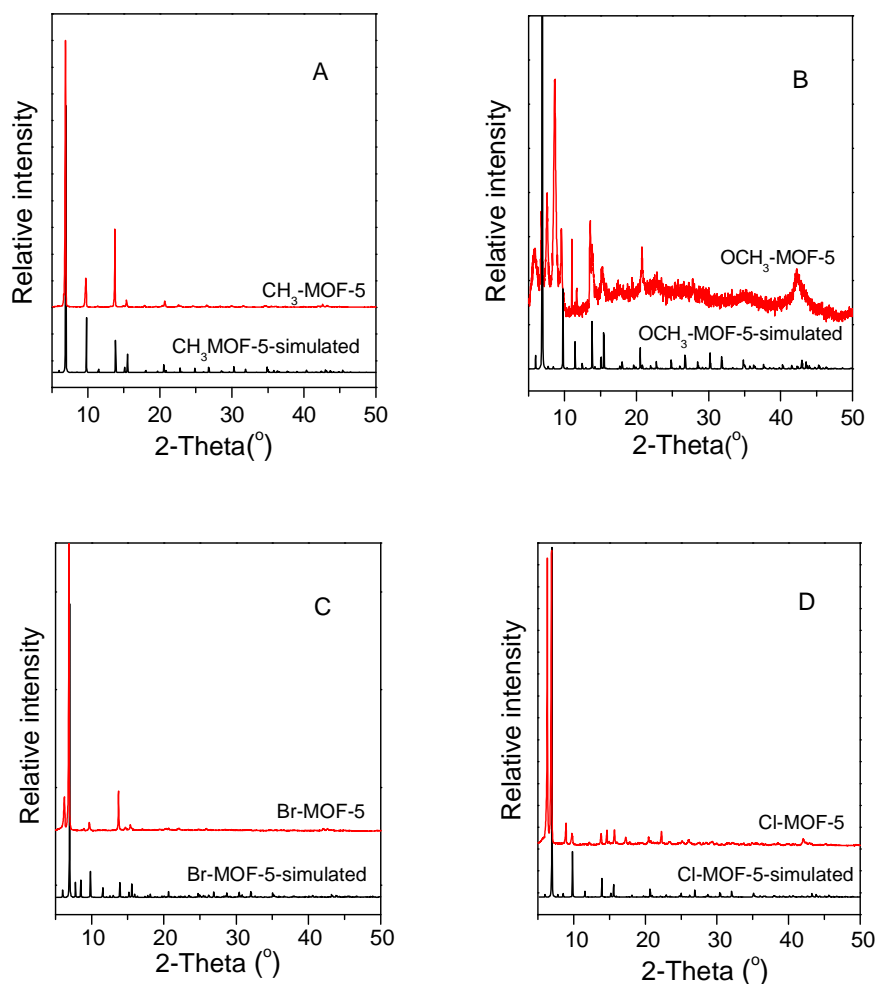


**Figure 2.2.** Simulated and experimental PXRD patterns of CH<sub>3</sub>-MOF-5 (A), OCH<sub>3</sub>-MOF-5(B), Br-MOF-5 (C) and Cl-MOF-5(D).

### 2.3.2 Thermogravimetric analysis of modified MOF-5s

Figure 2.3 shows the TGA curves of CH<sub>3</sub>-MOF-5, OCH<sub>3</sub>-MOF-5, Br-MOF-5 and Cl-MOF-5 (under N<sub>2</sub> flow). Two weight loss events were observed in the thermogram of CH<sub>3</sub>-MOF-5 (Figure 2.3). The first weight loss (140 °C – 300 °C) is 3.4 wt% and is due to the removal of solvent (DEF). The second weight loss event started at about 440 °C and can be attributed to the decomposition of the organic linker. A similar result was found

for MOF-5. For OCH<sub>3</sub>-MOF-5, Br-MOF-5 and Cl-MOF-5, the weight loss below 140 °C is due to the removal of water and the values are 1.7 wt%, 4.7 wt% and 5.5 wt%, respectively. Water loss was not observed for MOF-5 and CH<sub>3</sub>-MOF-5. A continuous weight loss from 140 °C to 600 °C was observed for Br-MOF-5 and Cl-MOF-5, and can be assigned to the removal of DEF and decomposition of the organic linkers. The results are a strong indication that guest molecules, i.e. water and DEF, cannot be removed efficiently by conventional activation methods, e.g. CHCl<sub>3</sub>-exchange, from Br-MOF-5 and Cl-MOF-5.

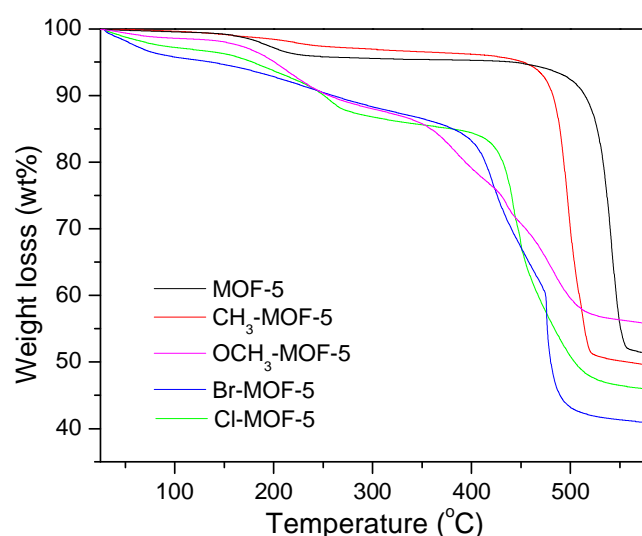


**Figure 2.3.** TGA curves of MOF-5, CH<sub>3</sub>-MOF-5, OCH<sub>3</sub>-MOF-5, Br-MOF-5 and Cl-MOF-5. All thermograms were recorded at 10 °C min<sup>-1</sup> under a nitrogen atmosphere.

### 2.3.3 Thermogravimetric analysis of modified MOF-5s after heat-treatment

In order to remove all residual water and DEF, all samples were activated by heat-treatment at 200 °C under vacuum for either 24 or 40 hours. Due to the poor structure of OCH<sub>3</sub>-MOF-5, this sample was vacuum dried at 200 °C for 24 h. Weight loss was followed by TGA under a N<sub>2</sub> atmosphere. This thermal treatment method appears effective since the weight loss below 350 °C for MOF-5-40h and CH<sub>3</sub>-MOF-5-40h were effectively reduced to less than 1.5% (Figure 2.4), which was also corroborated by the negligible N content (0.04-0.1%) found by elemental analysis (Table 2.1). However, a weight loss of about 2-5 wt% was still observed below 140 °C for OCH<sub>3</sub>-MOF-5-24h, Br-

MOF-5-40h and Cl-MOF-5-40h. The weight loss in the range of 140 °C-350 °C was significantly reduced for Cl-MOF-5-40h and OCH<sub>3</sub>-MOF-5-24h, implying that DEF removal has been successful. For Br-MOF-5-40h, on the other hand, we found a weight loss of ~5 wt% in the same temperature range. The general observation is that the thermal stability of MOF-5 is unchanged when a methyl-functionality is introduced but the thermal stability becomes compromised in the presence of -OCH<sub>3</sub>, -Br and -Cl substituents.

Samples were also examined by TGA using an air atmosphere to determine the chemical composition based on the metal oxide residue. According to the TGA thermograms (Figure 2.5), 58.5 wt% and 61.1 wt% of the observed weight loss is related to the organic linkers of MOF-5-40h and CH<sub>3</sub>-MOF-5-40h, and these values are consistent with values calculated on the basis of ZnO from formulas Zn<sub>4</sub>O(C<sub>8</sub>H<sub>4</sub>O<sub>4</sub>)<sub>3</sub> (57.8%) and Zn<sub>4</sub>O(C<sub>9</sub>H<sub>6</sub>O<sub>4</sub>)<sub>3</sub> (60.1%). However, the weight loss for Br-MOF-5-40h (78.7%) and Cl-MOF-5-40h (68.9%) are 10.9 % and 6.1 % higher than the values calculated from formulas Zn<sub>4</sub>O(C<sub>8</sub>H<sub>3</sub>O<sub>4</sub>Br)<sub>3</sub> (67.8%) and Zn<sub>4</sub>O(C<sub>8</sub>H<sub>3</sub>O<sub>4</sub>Cl)<sub>3</sub> (62.8%). We have followed the decomposition process by mass spectroscopy and found that release of DEF was observed at temperatures below 150 °C and at temperatures between 200 °C and 350 °C for both Br-MOF-5-40h and Cl-MOF-5-40h. Based on a nitrogen content of ~ 1%, we conclude that about 7 wt% DEF is still present in Br-MOF-5-40h and Cl-MOF-5-40h (Table 2.1). Since 5.5 wt% and 3.5 wt% of DEF were released below 350 °C, this implies that ~1.5 wt% and ~3.5 wt% of DEF contributes to the weight loss for Br-MOF-5-40h and Cl-MOF-5-40h at thermal decomposition. The remainder may be due to uncoordinated or partially coordinated ligands, as evidenced by the presence of a broad band at ~1650 cm<sup>-1</sup> in their respective IR spectra (Figure 2.6). We propose that some uncoordinated ligands are confined within the pores of the MOF structure during synthesis. The other possibility is that one oxygen atom of the carboxyl group coordinates to Zn<sup>2+</sup> whereas the other oxygen atom interacts with DEF. The partially coordinated ligands can still hold the structure together but the final MOF structure has a lower degree of crystal perfection. The weight loss for OCH<sub>3</sub>-MOF-5 (63.2 %) is in agreement with the formula Zn<sub>4</sub>O(C<sub>9</sub>H<sub>6</sub>O<sub>5</sub>)<sub>3</sub> (62.2%). However, the inconsistency in C and H contents between the experimental and theoretical values infers that OCH<sub>3</sub>-MOF-5 does not form a structure which is in agreement with Zn<sub>4</sub>O(C<sub>9</sub>H<sub>6</sub>O<sub>5</sub>)<sub>3</sub>.

**Table 2.1.** C, H and N contents of MOF-5 and three modified MOF-5s with heat-treatment (vacuum dried at 200 °C for 40 h) obtained by element analysis (theoretical values are in *italics*).

| Sample                      | C (%)      | H (%)      | N (%)   |
|-----------------------------|------------|------------|---------|
| MOF-5-40h                   | 37.6(37.5) | 1.66(1.56) | 0.10(0) |
| CH <sub>3</sub> -MOF-5-40h  | 39.3(40.0) | 2.60(2.20) | 0.04(0) |
| Br-MOF-5-40h                | 28.7(28.6) | 2.06(0.90) | 0.90(0) |
| Cl-MOF-5-40h                | 32.8(33.0) | 2.19(1.00) | 1.00(0) |
| OCH <sub>3</sub> -MOF-5-24h | 33.3(37.8) | 2.78(2.10) | 0.21(0) |

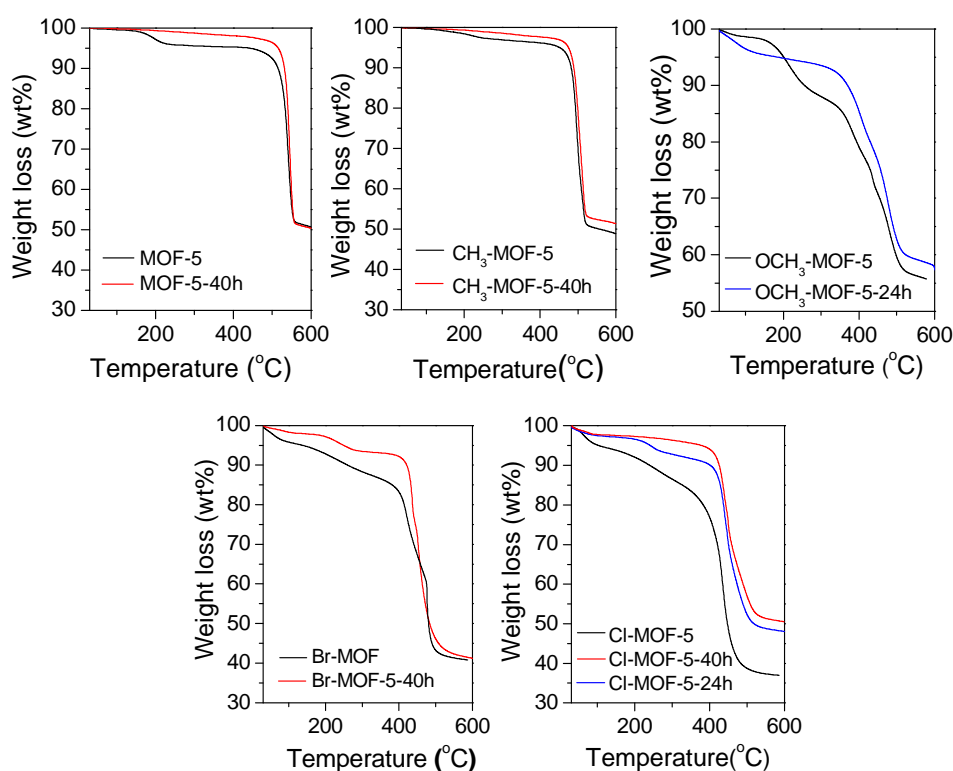


**Figure 2.4.** TGA curves of MOF-5, CH<sub>3</sub>-MOF-5, OCH<sub>3</sub>-MOF-5, Br-MOF-5 and Cl-MOF-5 without heat-treatment and with heat-treatment (24h or 40h) using a heating rate of 10 °C min<sup>-1</sup> and a nitrogen atmosphere.



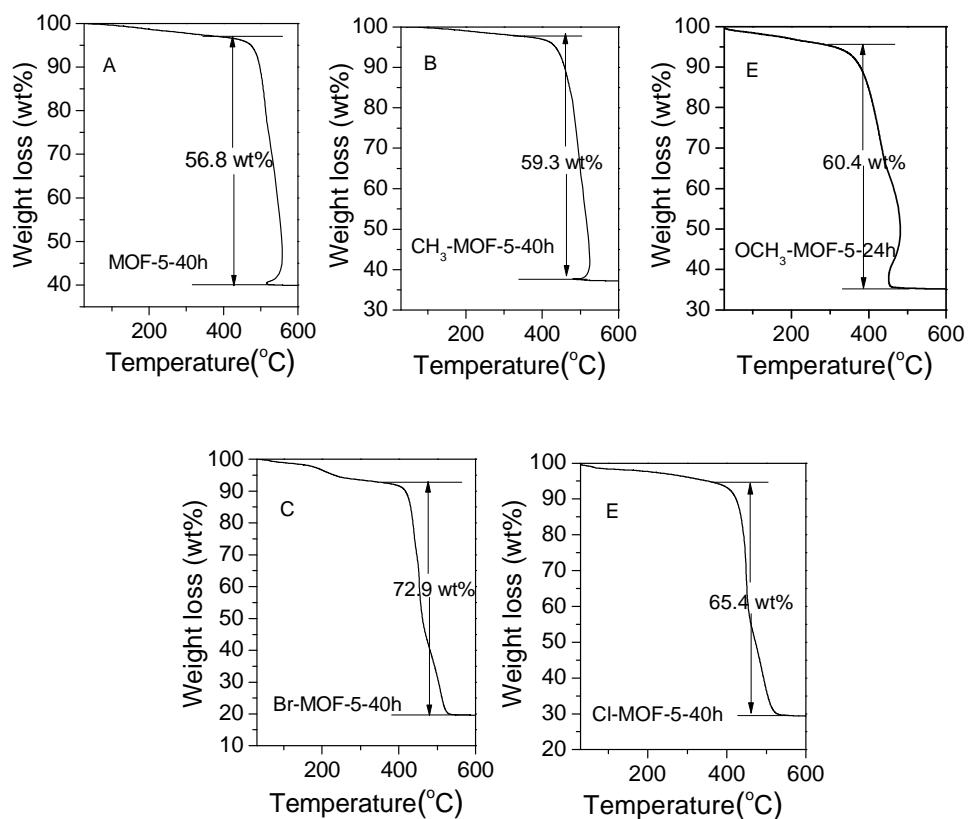


**Figure 2.5.** TGA curves of MOF-5 (A) and CH<sub>3</sub>-, OCH<sub>3</sub>-, Br- and Cl- modified MOF-5s (B, C, D and E, respectively) measured under a dry air-flow at 10 °C min<sup>-1</sup>. MOF-5, CH<sub>3</sub>-, Br- and Cl- modified MOF-5 were vacuum dried at 200 °C for 40 h, and OCH<sub>3</sub>-modified MOF-5 was vacuum dried at 200 °C for 24 h prior to the TGA measurement.

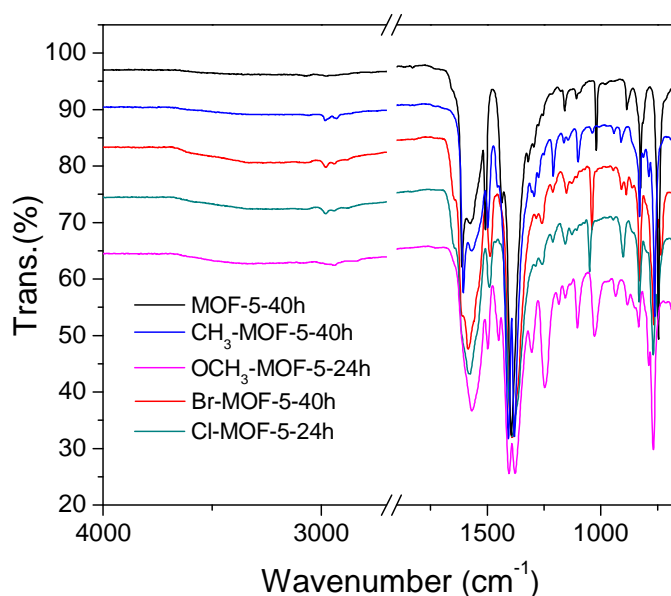


**Figure 2.6.** FT-IR spectra of MOF-5-40h, CH<sub>3</sub>-MOF-5-40h, OCH<sub>3</sub>-MOF-5-24h, Br-MOF-5-40h and Cl-MOF-5-40h.

### 2.3.4 Structure characterization of modified MOF-5s after heat-treatment

The structures of the samples after the heat-treatment were examined by PXRD (Figure 2.7). The intensity of the peak at 6.9° increased significantly as shown in the PXRD pattern of CH<sub>3</sub>-MOF-5-40h. A similar result was found for MOF-5-40h. The decreased peak intensity ratio ( $R_1$ ) of 9.7°/6.9° can be attributed to the highly porous structure obtained after removal of DEF via the heat-treatment.[24] This indicates that the structures of MOF-5 and CH<sub>3</sub>-MOF-5 are not compromised by DEF removal via heat-treatment. OCH<sub>3</sub>-MOF-5 displayed a similar PXRD pattern after thermal treatment, which suggests that the framework remains largely intact. The PXRD pattern of Br-MOF-5 showed unchanged peak positions but a decrease in the peak intensities suggests that the structure of Br-MOF-5 is retained during the thermal treatment. A broad peak at 6.9° with low intensity is present in the PXRD pattern of Cl-MOF-5-40h but most other peaks have disappeared, which means that a large fraction of the Cl-MOF-5 structure has collapsed. The presence of -Cl, an electron-withdrawing functionality, may weaken the

coordination bond between  $\text{Zn}^{2+}$  and the coordinating carboxyl functionality.[26] In an attempt to preserve the crystal structure we reduced the thermal activation time to 24 h. The diffraction peaks of Cl-MOF-5-24h below  $20^\circ$  remain albeit with a low intensity, which indicates that the structure can survive the heat-treatment for 24 h. Cl-MOF-5-24h showed a weight loss of  $\sim 5$  wt% in the temperature range of  $140^\circ\text{C}$  to  $350^\circ\text{C}$ , which is similar to what has been observed for Br-MOF-5-40h. These findings strongly suggest that the introduction of -Br or -Cl compromises the structural stability of MOFs whereas -CH<sub>3</sub> does not.

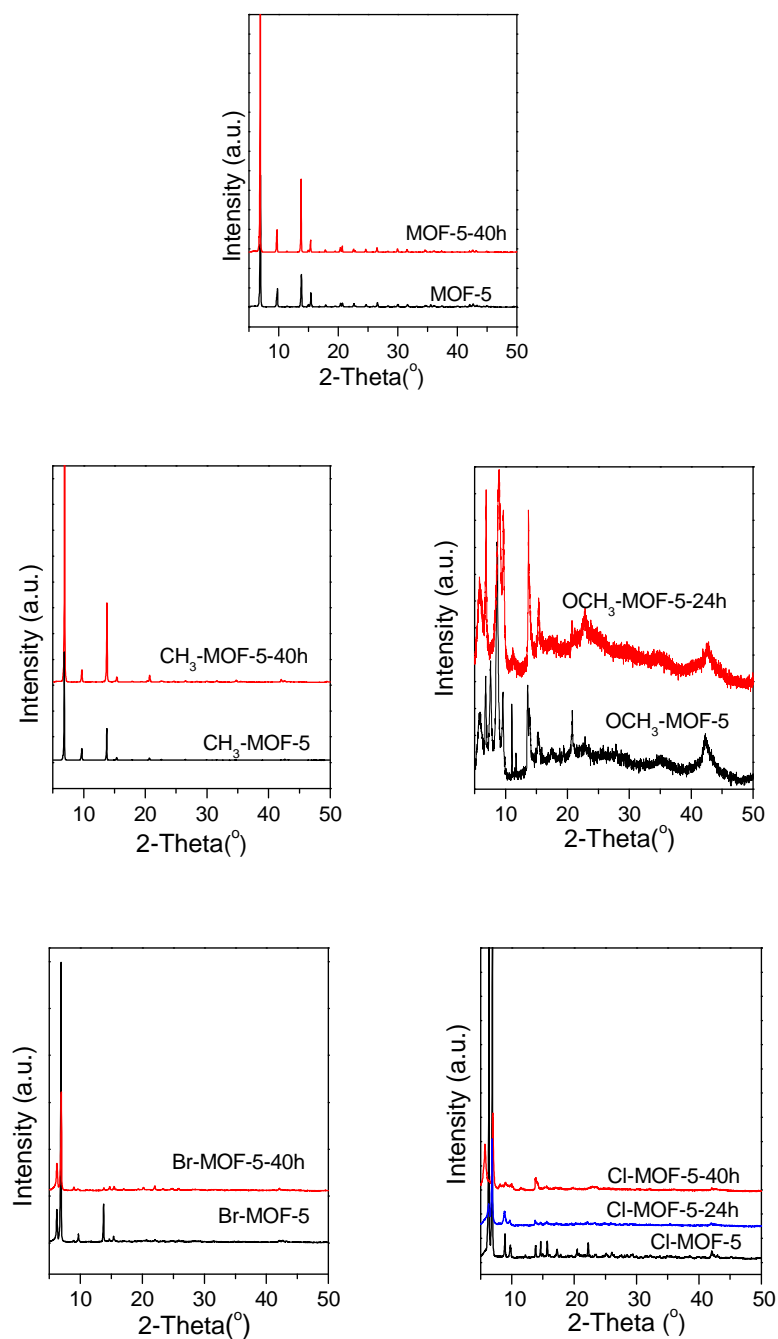


**Figure 2.7.** PXRD patterns of MOF-5, CH<sub>3</sub>-MOF-5, OCH<sub>3</sub>-MOF-5, Br-MOF-5 and Cl-MOF-5 with(out) heat-treatment (24h or 40h).

### 2.3.5 N<sub>2</sub> sorption

Both MOF-5-40h and CH<sub>3</sub>-MOF-5-40h gave type-I N<sub>2</sub> adsorption isotherms as observed for microporous solids (Figure 2.8). The specific surface area and pore volume of MOF-5-40h are 2750 m<sup>2</sup> g<sup>-1</sup> and 1.15 cm<sup>3</sup> g<sup>-1</sup>. These results are in close agreement with the literature[4b] and computational methods such as PLATON (Table 2.2). CH<sub>3</sub>-MOF-5-40h gave a BET specific surface area of 1685 m<sup>2</sup> g<sup>-1</sup> and a pore volume of 0.69 cm<sup>3</sup> g<sup>-1</sup>. As expected, OCH<sub>3</sub>-MOF-5 showed the lowest measured surface area and pore volume due to its poor structure. Br-MOF-5 and Cl-MOF-5 also showed type-I isotherms. However, the specific surface areas and pore volumes of Br-MOF-5 (840 m<sup>2</sup> g<sup>-1</sup> and 0.36 cm<sup>3</sup> g<sup>-1</sup>) and Cl-MOF-5 (675 m<sup>2</sup> g<sup>-1</sup> and 0.28 cm<sup>3</sup> g<sup>-1</sup>) are significant lower than that of CH<sub>3</sub>-MOF-5-40h and MOF-5-40h. Note that their pore volumes are much lower than the calculated values (Table 2.2), we consider the possibility that organic species such as DEF and uncoordinated ligands, reside in the pores and block the galleries.

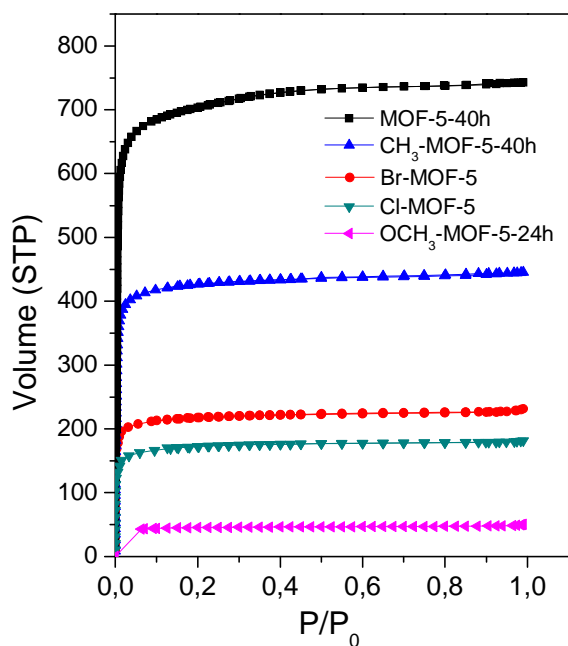


**Figure 2.8.** N<sub>2</sub> adsorption isotherms of MOF-5-40h, CH<sub>3</sub>-MOF-5-40h, Br-MOF-5, Cl-MOF-5 and OCH<sub>3</sub>-MOF-5-24h.

**Table 2.2.** Summary of the physical properties and hydrogen uptake capacities of MOF-5 and mono-substituted MOF-5s.

| Sample                           | SSA <sub>Langmuir</sub><br>(m <sup>2</sup> g <sup>-1</sup> ) | SSA <sub>bet</sub><br>(m <sup>2</sup> g <sup>-1</sup> ) | V <sub>ptotal</sub><br>(cm <sup>3</sup> g <sup>-1</sup> ) | V <sub>ptotal</sub> <sup>a</sup><br>(cm <sup>3</sup> g <sup>-1</sup> ) | N <sub>H2</sub> <sup>b,c</sup><br>(wt%) | N <sub>H2</sub> <sup>d</sup><br>(wt%) | Polar effect<br>of substituent <sup>e</sup> |
|----------------------------------|--|---|---|--|---|---------------------------------------|---|
| <b>MOF-5-40h</b>                 | 3058   | 2750  | 1.15  | 1.22   | 1.33(1.44)                              | 4.4                                   | n/a   |
| <b>CH<sub>3</sub>-MOF-5-40h</b>  | 1855   | 1685  | 0.69  | 1.09   | 1.42(1.47)                              | 3.3                                   | ED  |
| <b>OCH<sub>3</sub>-MOF-5-24h</b> | 203  | 182   | 0.08  | n/a  | 0.20(0.17)                              | n/a                                   | ED  |
| <b>Br-MOF-5</b>                  | 947  | 840   | 0.36  | 1.00   | 1.08(0.96)                              | 1.8                                   | EW  |
| <b>Cl-MOF-5</b>                  | 751  | 675   | 0.28  | 0.86   | 0.99(0.69)                              | 1.6                                   | EW  |

<sup>a</sup> Calculated by PLATON, <sup>b</sup> at 77 K and 1 bar, <sup>c</sup> values in brackets are for MOF-5s with heat-treatment, <sup>d</sup> at 77 K and 60 bar,

<sup>e</sup> ED: electron-donating, EW: electron-withdrawing.

### 2.3.6 Hydrogen storage property

The hydrogen uptake capacities of the MOFs below 1.3 bar and 77 K are shown in Figure 2.9. Hydrogen uptake capacities of 1.33 wt% and 1.42 wt% were found for MOF-5 and CH<sub>3</sub>-MOF-5 at 77 K and 1 bar, respectively. Under the given conditions, the hydrogen uptake capacity of CH<sub>3</sub>-MOF-5 is higher than that of MOF-5. Br-MOF-5, Cl-MOF-5 and OCH<sub>3</sub>-MOF-5 exhibited 1.08 wt%, 0.99 wt% and 0.20 wt% of hydrogen uptake capacities at 77 K and 1 bar, respectively, and their hydrogen uptake capacities are lower than that of MOF-5 and CH<sub>3</sub>-MOF-5. Heat treatment results in a measurable improvement in hydrogen uptake capacities for CH<sub>3</sub>-MOF-5 and MOF-5 due to a more efficient DEF removal. The hydrogen uptake capacities of MOF-5-40h and CH<sub>3</sub>-MOF-5-40h are 1.44 wt% and 1.47 wt%, respectively, which constitutes an 8% and 4% improvement in hydrogen uptake capacity. The hydrogen uptake capacity of MOF-5-40h is slightly lower than that of CH<sub>3</sub>-MOF-5 below 1.2 bar and surpasses that of CH<sub>3</sub>-MOF-5-40h at 1.2 bar. In contrast, Br-MOF-5-40h and Cl-MOF-5-24h displayed reduced hydrogen uptake capacities as compared to their untreated analogs. Additionally, MOF-5 and the modified MOF-5s all showed very poor hydrogen uptake capacities at room temperature and 1 bar (less than 0.04 wt%, Figure 2.10). No hydrogen uptake was observed for OCH<sub>3</sub>-MOF-5-24h at room temperature. The order for the hydrogen uptake capacities at 77 K and 1 bar: CH<sub>3</sub>-MOF-5-40h≈MOF-5-40h>Br-MOF-5>Cl-MOF-5>>OCH<sub>3</sub>-MOF-5-24h.

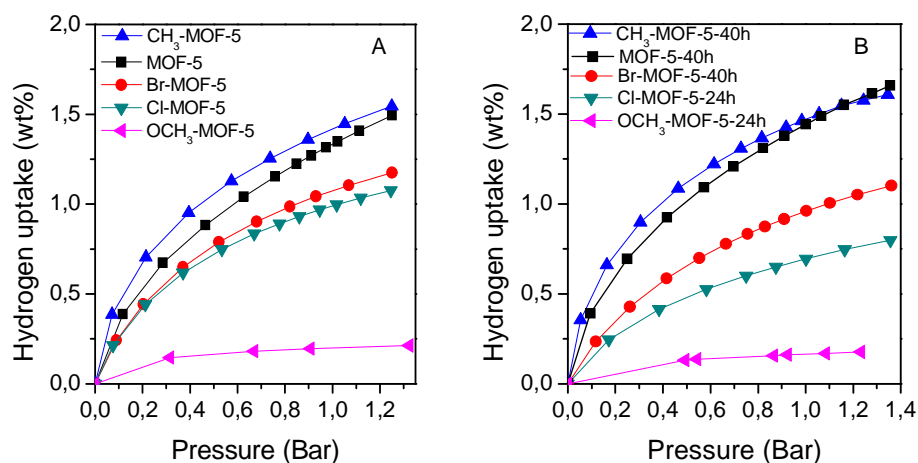


**Figure 2.9.** Low-pressure hydrogen adsorption isotherms of activated MOF-5 and mono-substituted MOF-5s at 77 K. Activated but before additional heat-treatment (A), after additional heat-treatment (vacuum/200 °C) (B).

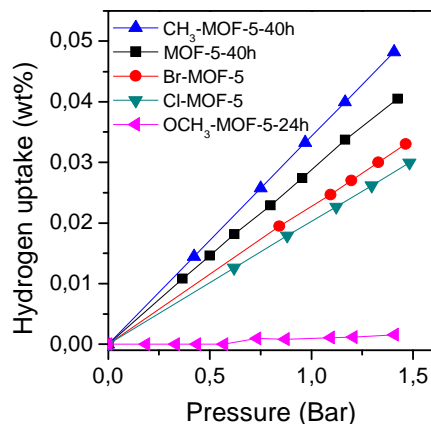


**Figure 2.10.** Low-pressure hydrogen adsorption isotherms of MOF-5-40h, CH<sub>3</sub>-MOF-5-40h, Br-MOF-5, Cl-MOF-5 and OCH<sub>3</sub>-MOF-5-24h at room temperature.

It is well documented that the isosteric heat of hydrogen adsorption relates directly to the hydrogen adsorption capability of MOFs at low pressures (<1 bar) and near room temperature.[10,13c,27] Introducing functional groups may reduce pore sizes and tune the chemical or electronic environment of the pore surface. As a result,



the heats of hydrogen adsorption for MOFs become affected as well. In order to investigate whether functional groups have an impact on how hydrogen molecules interact with the MOF-5 framework, we determined the isosteric heat of hydrogen adsorption ( $Q_{st}$ ) for MOF-5 and the four mono-substituted MOF-5 analogs. We employed the Clausius-Clapeyron equation at a hydrogen uptake capacity of 1 mol mol<sup>-1</sup> obtained from the respective adsorption isotherms at 64 K and 100 K (Figure 2.11). OCH<sub>3</sub>-MOF-5-24h gave a low heat of hydrogen adsorption (1.29 kJ mol<sup>-1</sup>) and is not discussed further due to its non-MOF-5 structure. Isosteric heats of hydrogen adsorption were obtained for MOF-5-40h, CH<sub>3</sub>-MOF-5-40h, Br-MOF-5 and Cl-MOF-5 and they are 2.83, 2.83, 3.03 and 2.96 kJ mol<sup>-1</sup>, respectively. It appears that introducing -CH<sub>3</sub>, -Br or -Cl functionalities does not have a pronounced effect on the isosteric heat of hydrogen adsorption for MOF-5. We also investigated the heat of hydrogen adsorption of MOF-5, CH<sub>3</sub>-MOF-5, Br-MOF-5 and Cl-MOF-5 using computational methods and the results are summarized in Table 2.3. The adsorption energies of the four sites on MOF-5 are comparable to our previous results.[19] The energies of Cup, ZnO<sub>3</sub> and ZnO<sub>2</sub> sites are in the range of 6-8 kJ mol<sup>-1</sup> for the three MOF-5 modifications. The adsorption energy of the C6 site related to benzene is the lowest for each sample, which is in agreement with previous studies.[28] Apparently, the adsorption energy for each site in MOF-5 is only moderately affected when benzene -H was replaced with -CH<sub>3</sub>, -Br or -Cl. This is consistent with our experimental and computational results.[17,18] In comparison to the heats of hydrogen adsorption obtained experimentally, the calculated energies are higher. This may be explained by the very low coverage of hydrogen (only one hydrogen molecule) that was taken into account in our calculations, while the experimental coverage is higher. Combining the experimental and computational results, we may conclude that functional groups such as -CH<sub>3</sub>, -Br and -Cl, have only a marginal impact on the heat of hydrogen adsorption of MOF-5.

**Table 2.3.** Calculated heats of hydrogen adsorption of four adsorption sites in MOF-5 and modified MOF-5s (Unit: kJ mol<sup>-1</sup>).

| Sample                 | Cup  | ZnO <sub>3</sub> | ZnO <sub>2</sub> | C6   |
|------------------------|------|------------------|------------------|------|
| MOF-5                  | -6.6 | -7.6             | -7.0             | -4.4 |
| CH <sub>3</sub> -MOF-5 | -6.7 | -7.7             | -6.3             | -3.9 |
| Br-MOF-5               | -6.9 | -8.5             | -6.8             | -5.1 |
| Cl-MOF-5               | -7.0 | -9.5             | -7.6             | -6.0 |

Although the isosteric heats of hydrogen adsorption in MOF-5 and CH<sub>3</sub>-MOF-5 are similar, CH<sub>3</sub>-MOF-5 in fact, showed a 10% higher hydrogen uptake capacity over that of MOF-5 at 77 K below 1 bar. This may be explained by the constriction of the pores by the presence of bulky CH<sub>3</sub>- groups or by the presence of an interpenetrated structure. The hydrogen adsorption capacities of Br-MOF-5 and Cl-MOF-5 are 33% and 45% lower than that of MOF-5 at 77 K and 1 bar despite their similar heats of hydrogen adsorption, which can be attributed to their poor porous structures. In addition, electron-withdrawing groups, i.e. -Br and -Cl, destabilize the coordination bond between the carboxyl group and the zinc ion in MOF-5. Consequently, the structural integrity of Br-MOF-5 and Cl-MOF-5 became compromised upon heat-treatment, resulting in reduced hydrogen uptake capacities, especially for Cl-MOF-5.

The excess hydrogen uptake capacities of all MOFs are shown in Figure 2.12. MOF-5-40h nearly reached its saturated uptake capacity of 4.4 wt% at about 40 bar and 77 K. CH<sub>3</sub>-MOF-5-40h exhibited 3.3 wt% of hydrogen uptake capacity at 60 bar but has not reached the saturated uptake capacity. The excess hydrogen uptake capacities of Br-MOF-5 and Cl-MOF-5 are 1.8 wt% and 1.6 wt%, respectively, which are much lower than that of CH<sub>3</sub>-MOF-5-40h and MOF-5-40h. The excess hydrogen uptake capacities of these four samples are well related to their surface areas, which is in agreement with previous results.[29,30]

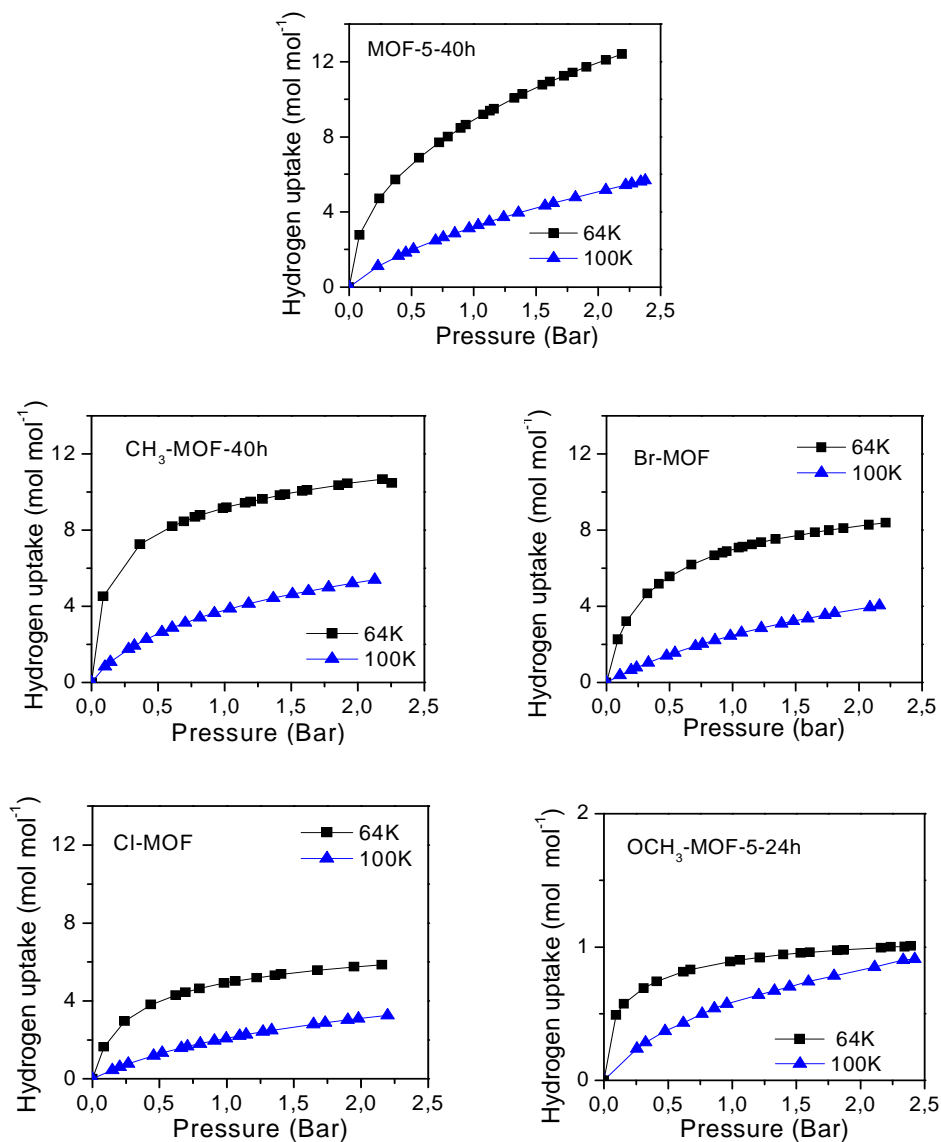


**Figure 2.11.** Low-pressure H<sub>2</sub> adsorption isotherms of MOF-5-40h, CH<sub>3</sub>-MOF-5-40h, Br-MOF-5, Cl-MOF-5 and OCH<sub>3</sub>-MOF-5-24h at 64 K and 100 K (Note that the Y-axis scale in graph of OCH<sub>3</sub>-MOF-5-24h was adjusted accordingly because of the very low hydrogen uptake capacity of OCH<sub>3</sub>-MOF-5-24h).

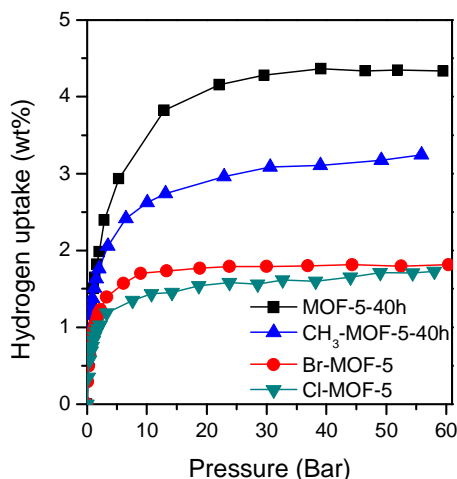


**Figure 2.12.** High-pressure excess hydrogen adsorption isotherms of MOF-5-40h, CH<sub>3</sub>-MOF-5-40h, Br-MOF-5 and Cl-MOF-5 at 77 K.

### 2.3.7 Computational studies on the diffusion coefficient of hydrogen for mono-substituted MOF-5s.

Studies on hydrogen adsorption and desorption kinetics have clearly shown that adsorption of hydrogen is fast enough for refilling and releasing hydrogen from the porous MOF-5 framework.[31] We have also investigated how functional groups affect the adsorption kinetics by calculating the diffusion coefficients of hydrogen for MOF-5 and the mono-substituted MOF-5 analogs. The diffusion coefficients of the MOFs at three different temperatures are shown in Table 2.4. The diffusion coefficients of MOF-5 at 38 K and 77 K are  $6.0 \times 10^{-8} \text{ m}^2 \text{ s}^{-1}$  and  $9.1 \times 10^{-8} \text{ m}^2 \text{ s}^{-1}$ , respectively. These results are similar to what was reported in one of our previous papers, with the only difference that we used shorter simulation time scales.[19] It is clear that the diffusion coefficients for all modified MOF-5s are smaller than that for MOF-5 at each given temperature. It appears that the diffusion coefficient for MOF-5 decreases with increasing size of the functional group. Cl-MOF-5, with the smallest pendant group, has the highest diffusion coefficient among the modified MOF-5s at three temperatures. OCH<sub>3</sub>-MOF-5, which contains the largest group (-OCH<sub>3</sub>), showed the lowest diffusion coefficient at each given temperature. These results demonstrate that the size of the functional group affects the hydrogen diffusion coefficient for MOF-5, but the difference is less than an order of magnitude. However, the experimental hydrogen uptake kinetics does not match the calculated

results. For instance, the equilibrium of hydrogen adsorption was obtained within 3 min for MOF-5-40h and CH<sub>3</sub>-MOF-5-40h, whereas Br-MOF-5 and Cl-MOF-5 took about 6 min to reach the adsorption equilibrium pressure. Although a longer time was needed to reach equilibrium for Br-MOF-5 and Cl-MOF-5 as compared to MOF-5, the equilibrium was obtained within minutes.

**Table 2.4.** Calculated diffusion coefficients of hydrogen on MOF-5 and mono-substituted MOF-5s at different temperatures.

| Sample                  | 38 K<br>(10 <sup>-8</sup> m <sup>2</sup> s <sup>-1</sup> ) | 77 K<br>(10 <sup>-8</sup> m <sup>2</sup> s <sup>-1</sup> ) | 298 K<br>(10 <sup>-7</sup> m <sup>2</sup> s <sup>-1</sup> ) |
|-------------------------|--|--|---|
| MOF-5                   | 6.0  | 9.1  | 2.5   |
| OCH <sub>3</sub> -MOF-5 | 2.8  | 4.8  | 1.3   |
| CH <sub>3</sub> -MOF-5  | 4.6  | 6.8  | 1.3   |
| Br-MOF-5                | 5.3  | 6.2  | 1.5   |
| Cl-MOF-5                | 5.4  | 7.1  | 2.2   |

## 2.4 Conclusions

In order to investigate whether the presence of functional groups has an effect on the hydrogen uptake capability of metal organic frameworks, -CH<sub>3</sub>, -OCH<sub>3</sub>, -Br, and -Cl were introduced in MOF-5 using a solvothermal method. Except for OCH<sub>3</sub>-MOF-5, the CH<sub>3</sub>-, Br- and Cl- modified MOF-5s show the typical topology of MOF-5 but with different degrees of crystal perfection. CH<sub>3</sub>-MOF-5 displays a high quality crystal structure and good thermal stability, which is comparable to MOF-5. However, introducing -Br or -Cl in MOF-5 destabilizes the MOF-5 structure and compromises the thermal stability. This may be explained in terms of a reduced interaction between the Zn<sup>2+</sup> metal center and the carboxyl group due to the electron-withdrawing nature of -Br or -Cl. The experimental and computational results suggest that -CH<sub>3</sub>, -Br or -Cl modifications have only a minor effect on the heat of hydrogen adsorption for MOF-5 in spite of their size, chemical and electronic nature. CH<sub>3</sub>-MOF-5 shows a hydrogen uptake capacity comparable to that of MOF-5 at 77 K and 1 bar (1.44 wt% for MOF-5 and 1.47 wt% for CH<sub>3</sub>-MOF-5) due to similar heat of hydrogen adsorption. Although similar heats of hydrogen adsorption were found for MOF-5 and the halogenated MOF-5s, i.e. Br-MOF-5 and Cl-MOF-5, the poor porous structures of Br-MOF-5 and Cl-MOF-5 result in lower hydrogen uptake capacities (1.08 wt% and 0.99 wt%) than that of MOF-5 at 77 K and 1

bar. Computational results predict a moderate reduction in the hydrogen diffusion coefficient for MOF-5 when -CH<sub>3</sub>, -OCH<sub>3</sub>, -Br or -Cl is introduced.

## 2.5 References

- [1] Czaja, A.U.; Trukhan, N.; Muller, U. *Chem. Soc. Rev.* **2009**, *38*, 1284.
- [2] Li, J.-R.; Kuppler, R.J.; Zhou, H.-C. *Chem. Soc. Rev.* **2009**, *38*, 1477.
- [3] Ma, L.; Abney, C.; Lin, W. *Chem. Soc. Rev.* **2009**, *38*, 1248.
- [4] (a) Horcajada, P.; Serre, C.; Maurin, G.; Ramsahye, N.A.; Balas, F.; Vallet-Reg, M.; Sebban, M.; Taulelle, F.; Ferey, G. *J. Am. Chem. Soc.* **2008**, *130*, 6774. (b) Sabo, M.; Henschel, A.; Frode, H.; Klemm, E.; Kaskel, S. *J. Mater. Chem.* **2007**, *17*, 3827. (c) Farha, O.K.; Hupp, J.T. *Acc. Chem. Res.* **2010**, *43*, 1166. (d) Murray, L.J.; Dinca, M.; Long, J.R. *Chem. Soc. Rev.* **2009**, *38*, 1294.
- [5] Wu, C.-D.; Hu, A.; Zhang, L.; Lin, W. *J. Am. Chem. Soc.* **2005**, *127*, 8940.
- [6] (a) Zhang, X.; Llabres i Xamena, F.X.; Corma, A. *J. Catal.* **2009**, *265*, 155. (b) Jiang, H.-L.; Xu, Q. *Chem. Commun.* **2011**, *47*, 3351.
- [7] Park, Y.K.; Chio, S.B.; Kim, H.; Kim, K.; Won, B.-H.; Chio, K.; Chio, J.-S.; Ahn, W.-S.; Won, N.; Kim, S.; Jung, D.H.; Chio, S.-H.; Kim, G.-H.; Cha, S.-S.; Jhon, Y.H.; Yang, J.K.; Kim, J. *Angew. Chem. Int. Ed.* **2007**, *46*, 8230.
- [8] (a) Kaye, S.S.; Dailly, A.; Yaghi, O.M.; Long, J.R. *J. Am. Chem. Soc.* **2007**, *129*, 14176. (b) Yang, S.J.; Choi, J.Y.; Chae, H.K.; Cho, J.H.; Nahm, K.S.; Park, C.R. *Chem. Mater.* **2009**, *21*, 1893.
- [9] (a) Li, Y.; Yang R.T. *J. Am. Chem. Soc.* **2006**, *128*, 8136. (b) Zhao, D.; Timmons, D.J.; Yuan, D.; Zhou, H. *Acc. Chem. Res.* **2011**, *44*, 123. (c) Wang, X.-S.; Ma, S.; Rauch, K.; Simmons, J.M.; Yuan, D.; Wang, X.; Yildirim, T.; Cole, W.C.; López, J.J.; Meijere, A.; Zhou, H.-C. *Chem. Mater.* **2008**, *20*, 3145.
- [10] (a) Lin, X.; Telepeni, I.; Blake, A.J.; Dailly, A.; Brown, C.M.; Simmons, J.M.; Zoppi, M.; Walker, G.S.; Thomas, K.M.; Mays, T.J.; Hubberstey, P.; Champness, N.R.; Schroder, M. *J. Am. Chem. Soc.* **2009**, *131*, 2159. (b) Neofotistou, E.; Malliakas, C.D.; Trikalitis, P.N. *Chem. Eur. J.* **2009**, *15*, 4523. (c) Zlotea, C.; Phanon, D.; Mazaj, M.; Heurtaux, D.; Guillern, V.; Serre, C.; Horcajada, P.; Devic, T.; Magnier, E.; Cuevas, F.; Ferey, G.; Llewellyn, P.L.; Latroche, M. *Dalton Transactions* **2011**, *40*, 4879. (d) Pachfule, P.; Chen, Y.; Sahoo, S.C.; Jiang, J.; Banerjee, R. *Chem. Mater.* **2011**, *23*, 2908.
- [11] (a) Yang, S. J.; Choi, J. Y.; Chae, H. K.; Cho, J. H.; Nahm, K. S.; Park, C. R. *Chem. Mater.* **2009**, *21*, 1893. (b) Proch, S.; Herrmannsdorfer, J.; Kempe, R.; Kern, C.; Jess, A.; Seyfarth, L.; Senker, J. *Chem. Eur. J.* **2008**, *14*, 8204. (c) Chen, B.; Xiang, S.; Qian, G.

- Acc. Chem. Res.* **2010**, *43*, 1115. (d) Falcaro, P.; Hill, A. J.; Nairn, K. M.; Jasieniak, J.; Mardel, J. I.; Bastow, T. J.; Mayo, S. C.; Gimona, M.; Gomez, D.; Whitfield, H. J.; Riccò, R.; Patelli, A.; Marmiroli, B.; Amenitsch, H.; Colson, T.; Villanova, L.; Buso, D. *Nature Communications* **2011**, *2*, 1.
- [12] (a) Gascon, J.; Aktay U.; Hernandez-Alonso, M. D.; van Klink, G. P. M.; Kapteijn, F. J. *Catal.* **2009**, *261*, 75. (b) Hwang, Y. K.; Hong, D. -Y.; Chang, J. -S.; Jhung, S. H.; Seo, Y. -K.; Kim, J.; Vimont, A.; Daturi, M.; Serre, C.; Feray, G. *Angew. Chem. Int. Ed.* **2008**, *47*, 4144. (c) Arstad, B.; Fjellvag, H.; Kongshaug, K. O.; Swang, O.; Blom, R. *Adsorption* **2008**, *14*, 755.
- [13] (a) Mulfort, K.L.; Hupp, J.T. *J. Am. Chem. Soc.* **2007**, *129*, 9604. (b) Mulfort, K.L.; Farha, O.K.; Stern, C.L.; Sarjeant, A.A.; Hupp, J.T. *J. Am. Chem. Soc.* **2009**, *131*, 3866. (c) Gadzikwa, T.; Zhang, B.-S.; Hupp, J.T. Nguyen, J.G. *Chem. Commun.* **2008**, 3672.
- [14] (a) Rowsell, J.L.C.; Yaghi, O.M. *J. Am. Chem. Soc.* **2006**, *128*, 1304. (b) Deng, H.; Doonan, C.J.; Furukawa, H.; Ferreira, R.B. Towne, J.; Knobler, C.B.; Wang, B. Yaghi, O.M. *Science* **2010**, *327*, 846.
- [15] Yuan, D.; Lu, W.; Zhao, D.; Zhou, H.-C. *Adv. Mater.* **2011**, *23*, 3723.
- [16] Yang, J.; Grzech, A.; Mulder, F.M.; Dingemans, T.J. *Chem. Commun.* **2011**, 47, 5244.
- [17] Lochan, R.C.; Head-Gordon, M. *Phys. Chem. Chem. Phys.* **2006**, *8*, 1357.
- [18] Sagara, T.; Klassen, J.; Ortony, J.; Ganz, E. *J. Chem. Phys.* **2005**, *123*, 14701.
- [19] Mulder, F.M.; Dingemans, T.J.; Wagemaker, M.; Kearley, G.J. *Chem. Phys.* **2005**, *317*, 113.
- [20] Li, X.; Cheng, F. Zhang, S.; Chen, J. *J. Power Sources*, **2006**, *160*, 542.
- [21] Anzalone, L.; Hirsch, J.A. *J. Org. Chem.* **1985**, *50*, 2131.
- [22] Chen, Y.W.; Chen, L.; Zhou, W.H.; Zha, D.J.; Zhou, D.; Bai, F.L.; Wan, M.X. *Synthetic Metals*. **2009**, *159*, 1649.
- [23] Panella, B.; Hirscher, M.; Putter, H.; Mueller, U. *Adv. Funct. Mater.* **2006**, *16*, 520.
- [24] Chen, B.; Wang, X.; Zhang, Q.; Xi, X.; Cai, J.; Qi, H.; Shi, S.; Wang, J.; Yuan, D.; Fang, M. *J. Mater. Chem.* **2010**, *20*, 3758.
- [25] Yang, S.J.; Cho, J.H.; Lee, K.; Kim, T.; Park, C.R. *Chem. Mater.* **2010**, *22*, 6138.
- [26] Polunin, R.A.; Kolotilov, S.V.; Kiskin, M.A.; Gavrilenko, K.S.; Ouahab, L.; Eremenko, I. L.; Novotortsev, V.M.; Pavlishchuk, V.V. *Russian Chemical Bulletin, International Edition* **2010**, *59*, 1217.
- [27] Chun, H.; Dybtsev, D.N.; Kim, H.; Kim, K. *Chem. Eur. J.* **2005**, *11*, 3521.
- [28] (a) Yildirim, T.; Hartman, M.R. *Phys. Rev. Lett.* **2005**, *95*, 215504. (b) Mulder, F.M.; Dingemans, T.J.; Schimmel, H.G.; Ramirez-Cuesta, A.J.; Kearley, G.J. *Chem. Phys.*

- 2008**, 351, 72. (c) Rosi, N.L.; Eckert, J.; Eddaoudi, M.; Vodak, D.T.; Kim, J.; O'Keeffe, M.; Yaghi, O.M. *Science* **2003**, 300, 1127. (d) Rowsell, J.L.C.; Eckert, J.; Yaghi, O.M. *J. Am. Chem. Soc.* **2005**, 127, 14904.
- [29] Duren, T.; Bae, Y.-S.; Snurr, R.Q. *Chem. Soc. Rev.* **2009**, 38, 1237.
- [30] Wong-Foy, A.G.; Matzger, A.J.; Yaghi, O.M. *J. Am. Chem. Soc.* **2006**, 128, 3494.
- [31] Rowsell, J.L.C.; Millward, A.R.; Park, K.S.; Yaghi, O.M. *J. Am. Chem. Soc.* **2004**, 126, 5666.



## CHAPTER 3

### **Methoxy-modified MOF-5: a new MOF-5 framework prepared via a mixed ligand approach**

---

In this chapter we present the synthesis, thermal properties and hydrogen storage capabilities of a series of MOF-5 frameworks based on a mixed diacid composition, *i.e.* 2-methoxyterephthalic acid and terephthalic acid. Using this mixed ligand approach, the MOF-5 structure remains intact when the 2-methoxyterephthalate concentration increases up to 75 mol%. Moreover, the hydrogen uptake capacity of MOF-5 at 77 K and 1 bar can be improved by 10% at a 2-methoxyterephthalate concentration of 75 mol% (1.32 wt% vs. 1.45 wt%) due to an enhanced isosteric heat of hydrogen adsorption. At higher concentrations, the structural integrity and hydrogen adsorption capability of the framework become compromised.

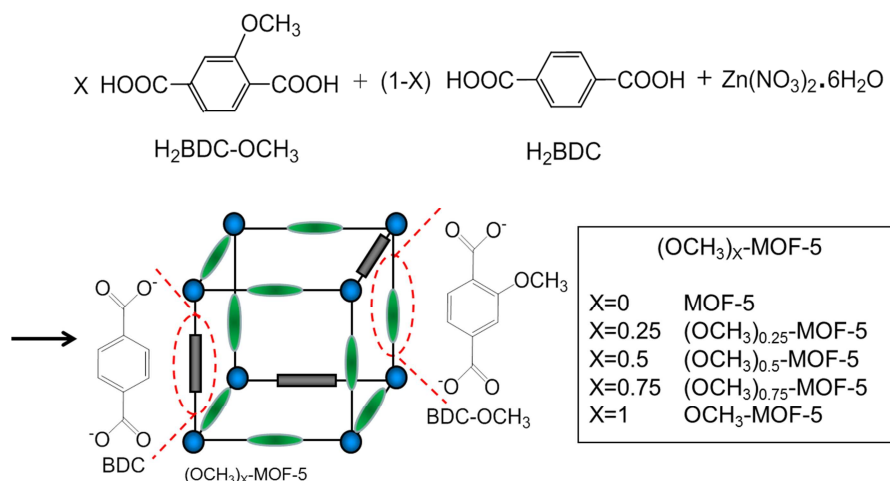
### 3.1 Introduction

Previous studies have revealed that the presence of functional groups may reduce the pore size of MOFs, leading to an improved hydrogen adsorption capability in the low pressure range (0-1 bar).[1,2] We also found this effect for a methyl-modified MOF-5 ( $\text{CH}_3\text{-MOF-5}$ ), as reported in *Chapter 2*. Moreover, the introduction of an electron-donating group (or groups) to the central portion of the ligand might have a favorable effect on the hydrogen uptake capability of MOFs.[2-5] A methoxy ( $-\text{OCH}_3$  or  $-\text{OMe}$ ) group is therefore an interesting group as it is electron -donating and somewhat larger in size than  $-\text{CH}_3$ . As described in *Chapter 2*, we attempted to synthesize a methoxy-modified MOF-5 but our approach appeared unsuccessful. Unexpectedly, a non-MOF-5 structure was obtained when all terephthalic acid was replaced by methoxyterephthalic acid ( $\text{H}_2\text{BDC-OCH}_3$ ). We used similar synthetic conditions as applied for the synthesis of MOF-5 and  $\text{CH}_3\text{-MOF-5}$ .

The formation of a good quality MOF strongly depends on the synthetic conditions, such as the reagent concentration, temperature, solvent type, reaction time, solution volume.[6-10] Obviously, the electronic nature of the ligand plays an important role as well. Although the ligands have similar exocyclic bond angles, they react differently when used for the synthesis of MOFs. A good example is the IRMOF series (iso-reticular metal organic frameworks), which share the same primitive cubic topology but are composed of different linear linkers. A variety of terephthalic acid derivatives have been employed as ligands for the synthesis of IRMOFs.[10-14] A MOF-5 type structure is formed when zinc(II) nitrate reacts with certain members of the terephthalic acid family, including aminoterephthalic acid ( $\text{H}_2\text{BDC-NH}_2$ ), bromoterephthalic acid ( $\text{Br-H}_2\text{BDC}$ ), and methylterephthalic acid ( $\text{H}_2\text{BDC-CH}_3$ ), but not with nitroterephthalic acid ( $\text{H}_2\text{BDC-NO}_2$ ) and 2,5-dichloroterephthalic acid ( $\text{H}_2\text{BDC-DiCl}$ ). In order to obtain IRMOFs,  $\text{Zn}_4\text{O}(\text{BDC-NO}_2)_3$  and  $\text{Zn}_4\text{O}(\text{BDC-DiCl})_3$ , Deng and co-workers have employed a mixed ligand approach in which  $\text{H}_2\text{BDC-NO}_2$  or  $\text{H}_2\text{BDC-DiCl}$  was mixed with  $\text{H}_2\text{BDC}$  in the starting reaction mixture. Via this approach, they have also synthesized a series of multi-functionalized MOF-5s. A functionalized MOF-5 containing both allyloxy- and benzyloxy- groups shows a volumetric hydrogen uptake capacity (77 K and 1 bar) twice as high as that of MOF-5.[15] Clearly, this approach is a viable route towards introducing a wide range of desirable functionalities into metal organic frameworks without compromising the integrity of the framework.

In order to explore whether methoxy functionality has a favorable effect on the hydrogen storage capability of MOF-5, we have explored the synthesis of a methoxy-

modified MOF-5 series via the mixed ligand approach. Three MOFs with different concentrations of methoxy groups were synthesized by varying the methoxyterephthalic acid/terephthalic acid ratio, *i.e.* 25, 50 and 75 mol%, in the initial reaction mixture (Scheme 3.1). In this chapter the effect of the methoxy concentration on the structure and hydrogen uptake capability of the resulting MOFs will be discussed.



**Scheme 3.1.** Synthesis of a series MOF-5 frameworks based on a mixed diacid composition, *i.e.* methoxyterephthalic acid ( $\text{H}_2\text{BDC-OCH}_3$ ) and terephthalic acid ( $\text{H}_2\text{BDC}$ ).

## 3.2 Experimental

### 3.2.1 Materials

Zinc nitrate hexahydrate ( $\text{Zn}(\text{NO}_3)_2 \cdot 6\text{H}_2\text{O}$ , 98 %, Aldrich) and terephthalic acid ( $\text{H}_2\text{BDC}$ ) (>99%, BP Chembel) were used as received. *N,N*-diethylformamide (DEF, 99 %, Acros) and chloroform ( $\text{CHCl}_3$ ) were dried over and distilled from calcium hydride ( $\text{CaH}_2$ ) and phosphorus pentoxide ( $\text{P}_2\text{O}_5$ ), respectively. The detailed synthetic procedure of methoxyterephthalic acid has been described in *Chapter 2*.

### 3.2.2 Synthesis of $(\text{OCH}_3)_x\text{-MOF-5}$

**Synthesis of  $(\text{OCH}_3)_{0.25}\text{-MOF-5}$ .** 1 mL of a 0.1 M methoxyterephthalic acid DEF solution, 3 mL of a 0.1 M terephthalic acid DEF solution and 4 mL of a 0.3 M  $\text{Zn}(\text{NO}_3)_2 \cdot 6\text{H}_2\text{O}$  DEF solution were mixed in a 20 mL vial. The vial was sealed and heated in an oven at 100 °C for 31 h. Cubic crystals were collected and immersed in DEF (3 mL)

for 24 h (2×), followed by immersing the crystals in CHCl<sub>3</sub> (4 mL) for 1 day (3×). The solvent exchanged product was vacuum dried at 160 °C for 24 h and stored in a glove box. (27 mg, 26% yield). Elemental analysis (EA): Calc. for Zn<sub>4</sub>O((C<sub>8</sub>H<sub>4</sub>O<sub>4</sub>)<sub>0.75</sub>(C<sub>9</sub>H<sub>6</sub>O<sub>5</sub>)<sub>0.25</sub>)<sub>3</sub>: C, 37.6%, H, 1.71%. Found C, 37.7%, H, 1.69%. FT-IR (cm<sup>-1</sup>): 3069, 2955, 1611, 1563, 1509, 1435, 1394, 1185, 1159, 1106, 1020, 884, 825, 791, 746, 711.

**Synthesis of (OCH<sub>3</sub>)<sub>0.5</sub>-MOF-5.** 2 mL of a 0.1 M methoxyterephthalic acid DEF solution, 2 mL of a 0.1 M terephthalic acid DEF solution and 4 mL of a 0.3 M Zn(NO<sub>3</sub>)<sub>2</sub>·6H<sub>2</sub>O DEF solution were mixed in a 20 mL vial. The vial was sealed and heated in an oven at 100 °C for 28 h. A similar solvent exchange procedure was used as described for (OCH<sub>3</sub>)<sub>0.25</sub>-MOF-5. The solvent exchanged product was vacuum dried at 160 °C for 24 h and stored in a glove box. (43 mg, 40% yield). Elemental analysis (EA): Calc. for Zn<sub>4</sub>O((C<sub>8</sub>H<sub>4</sub>O<sub>4</sub>)<sub>0.5</sub>(C<sub>9</sub>H<sub>6</sub>O<sub>5</sub>)<sub>0.5</sub>)<sub>3</sub>: C, 37.6%, H, 1.85%. Found C, 37.7%, H, 1.79%. FT-IR (cm<sup>-1</sup>): 3069, 2955, 1610, 1507, 1435, 1395, 1255, 1185, 1159, 1105, 1020, 937, 884, 825, 791, 746, 711, 689.

**Synthesis of (OCH<sub>3</sub>)<sub>0.75</sub>-MOF-5.** 3 mL of a 0.1 M methoxyterephthalic acid DEF solution, 1 mL of a 0.1 M terephthalic acid DEF solution and 4 mL of a 0.3 M Zn(NO<sub>3</sub>)<sub>2</sub>·6H<sub>2</sub>O DEF solution were mixed in a 20 mL vial. The vial was sealed and heated in an oven at 100 °C for 45 h. A similar solvent exchange procedure was used as described for (OCH<sub>3</sub>)<sub>0.25</sub>-MOF-5. The solvent exchanged product was vacuum dried at 160 °C for 24 h and stored in a glove box. (26 mg, 23% yield). Elemental analysis (EA): Calc. for Zn<sub>4</sub>O((C<sub>8</sub>H<sub>4</sub>O<sub>4</sub>)<sub>0.25</sub>(C<sub>9</sub>H<sub>6</sub>O<sub>5</sub>)<sub>0.75</sub>)<sub>3</sub>: C, 37.7%, H, 1.97%. Found C, 37.6%, H, 2.00%. FT-IR (cm<sup>-1</sup>): 2943, 2853, 1610, 1507, 1454, 1395, 1387, 1255, 1185, 1159, 1105, 1033, 1020, 937, 884, 833, 825, 790, 746, 710, 689.

**Synthesis of OCH<sub>3</sub>-MOF-5.** 4 mL of a 0.1 M methoxyterephthalic acid DEF solution and 4 mL of a 0.3 M Zn(NO<sub>3</sub>)<sub>2</sub>·6H<sub>2</sub>O DEF solution were mixed in a 20 mL vial. The vial was sealed and heated in an oven at 100 °C for 43 h. A similar solvent exchange procedure was used as described for (OCH<sub>3</sub>)<sub>0.25</sub>-MOF-5. The solvent exchanged product was vacuum dried at 160 °C for 24 h and stored in a glove box. (63 mg, 57% yield). Elemental analysis (EA): Calc. for Zn<sub>4</sub>O(C<sub>9</sub>H<sub>6</sub>O<sub>5</sub>)<sub>3</sub>: C, 37.8%, H, 2.10%. Found C, 36.6%, H, 2.53%, N, 0.30%. FT-IR (cm<sup>-1</sup>): 2945, 2846, 1569, 1497, 1451, 1404, 1381, 1156, 1247, 1103, 1030, 933, 884, 833, 788, 710, 689.

**Synthesis of MOF-5.** 0.12 g (4.04 mmol) of Zn(NO<sub>3</sub>)<sub>2</sub>·6H<sub>2</sub>O, 0.22 g (1.32 mmol) of terephthalic acid and 40 mL of DEF were heated at 100 °C for 48 h. Cubic crystals were collected and immersed in DEF (20 mL) for 24 h (2×), followed by immersing the

crystals in  $\text{CHCl}_3$  (40 mL) for 24 h (3 $\times$ ). The solvent exchanged product was vacuum dried at 160 °C for 24h and stored in a glove box (0.21 g, 62% yield). Elemental analysis (EA): Calc. for  $\text{Zn}_4\text{O}(\text{C}_8\text{H}_4\text{O}_4)_3 \cdot \text{C}$ , C, 37.5%, H, 1.56%. Found C, 37.0%, H, 1.51%, N, 0.01%. FT-IR ( $\text{cm}^{-1}$ ): 2960, 1610, 1508, 1435, 1394, 1159, 1181, 1106, 1020, 884, 824, 746.

### 3.2.3 Characterization

XRD patterns of all samples were recorded on an X'Pert X-ray diffractometer operated at 45 kV and 40 mA with monochromatic Cu  $K\alpha$  radiation within a 2-theta range of 5-60°. For each XRD measurement, a sample was placed into an air-tight sample holder in order to avoid exposure to air and moisture using an Argon filled glove box. IR spectra were collected on a PerkinElmer Spectrum 100 FT-IR Spectrometer. TGA curves were obtained on a PerkinElmer Pyris Diamond Thermogravimetric Differential Thermal/Analyzer. Samples were heated from room temperature to 600 °C with a heating rate of 10 °C  $\text{min}^{-1}$  under a dry nitrogen or air flow. Elemental analyses were performed on a Thermo Scientific InterScience Flash 2000 Organic Elemental Analyzer. The pore textural properties, including BET surface area and pore volume, were recorded on a Micromeritics ASAP 2010 adsorption analyzer at 77 K. Prior to the adsorption measurements, the samples were degassed *in situ* under vacuum at 135 °C. The dead volume of the sample cell was determined in a separate experiment. In-situ pretreatment coupled to a separate dead volume measurement after the analysis was employed in order to avoid the helium entrapment phenomenon. The weight of a sample obtained after the pretreatment was used in various calculations. BET surface areas were calculated in the adapted pressure range of  $P/P_0=0.01-0.1$ . Hydrogen storage measurements at different pressures were performed on a Sievert's setup at 77 K and 100 K. Each sample was pretreated under high vacuum ( $10^{-6}$  mbar) at 150 °C overnight prior to the hydrogen uptake measurement. Hydrogen (ultra-high-purity grade, 99.999%) was additionally purified by leading it over a bed of zeolite spheres at 77 K before being loaded onto the samples. The pressure change was monitored and recorded after the hydrogen reservoir was connected to the sample holder. The samples were weighed in a glove box after the measurement for calculating the hydrogen uptake capacity. The amount of hydrogen stored in the dead volume was examined at low pressures (<2 bar) with sea sand as a reference. For the high-pressure measurements, the dead volume was determined using helium in the presence of a sample. The hydrogen uptake capacities of all samples were obtained by subtracting the amount of hydrogen in the dead volume from the total amount of hydrogen released from the reservoir.

### 3.3 Result and discussion

#### 3.3.1 Structures of $(\text{OCH}_3)_x\text{-MOF-5}$

The structures of all methoxy-modified MOF-5s were characterized by powder X-ray diffraction (PXRD) and the PXRD patterns are shown in Figure 3.1. MOF-5 was synthesized as a reference under similar synthetic conditions. Its PXRD pattern closely matches that of MOF-5 data reported in literature [16] and is shown in Figure 3.1 as well.  $(\text{OCH}_3)_{0.25}\text{-MOF-5}$ ,  $(\text{OCH}_3)_{0.5}\text{-MOF-5}$  and  $(\text{OCH}_3)_{0.75}\text{-MOF-5}$  showed PXRD patterns similar to that of MOF-5, which suggests that the methoxy-modified MOF-5s exhibit the same topology as MOF-5. We have simulated the PXRD pattern of a methoxy-modified MOF-5 constructed from 100% methoxyterephthalate as linkers and the result is shown in Figure 3.2. Compared to the simulated PXRD pattern, the  $\text{OCH}_3\text{-MOF-5}$ , solely comprised of methoxyterephthalate, showed a similar PXRD pattern (Figure 3.2). However, the additional peaks at  $5.7^\circ$  and  $8.9^\circ$  are also present. This indicates that the methoxy-modified MOF-5 constructed only from methoxyterephthalate as linker units exhibits a MOF-5-type structure but the crystal is of poor quality. The results demonstrate that the structure of MOF-5 remains intact when methoxy groups were introduced, but the framework become compromised when all terephthalate was replaced by methoxyterephthalate.

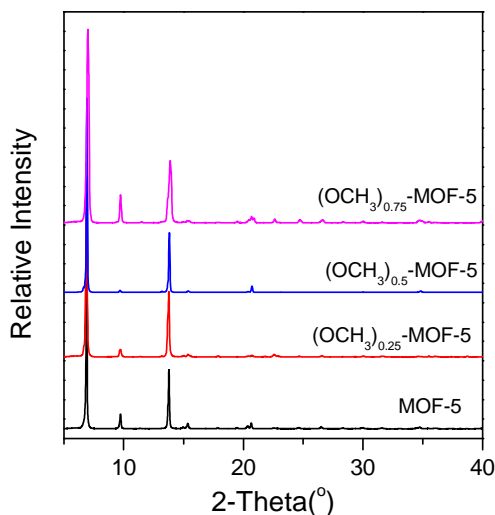


**Figure 3.1.** The PXRD patterns of MOF-5 and the  $(\text{OCH}_3)_x\text{-MOF-5}$  series ( $x=0.25, 0.5, 0.75$ ).

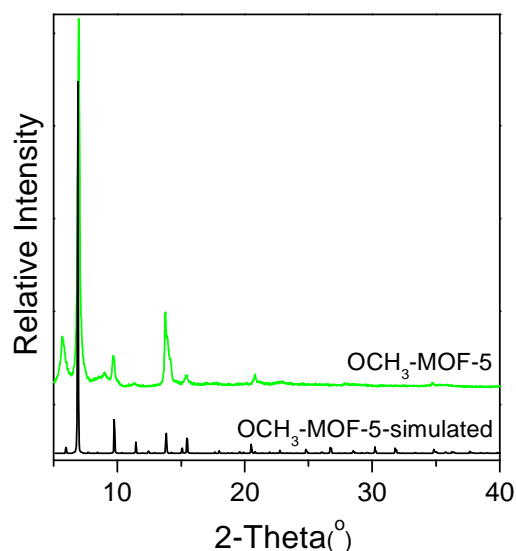


**Figure 3.2.** The experimental and simulated PXRD patterns of OCH<sub>3</sub>-MOF-5.

We have reported the attempt to synthesize methoxy-modified MOF-5, using methoxyterephthalic acid only, at 125 °C in *Chapter 2*, but a non-MOF-5 structure was obtained. In the present study we synthesized a methoxy-modified MOF-5 by lowering the reaction temperature to 100 °C, which resulted in a MOF with a significantly improved crystal structure. This demonstrates that the temperature is a crucial factor for the synthesis of methoxy-modified MOF-5.

### 3.3.2 FT-IR analysis

The FT-IR spectra of MOF-5 and the methoxy-modified MOF-5s are shown in Figure 3.3. In the spectrum of MOF-5, the bands at 1607 cm<sup>-1</sup> and 1391 cm<sup>-1</sup> are attributed to the carboxylate (COO<sup>-</sup>) asymmetric and symmetric stretching vibrations of BDC. With the increase in methoxy content, these two bands became weak and finally disappeared when all terephthalate was replaced by methoxyterephthalate (OCH<sub>3</sub>-MOF-5). Meanwhile, new bands appeared and became intensified. For example, the carboxylate (COO<sup>-</sup>) stretching vibrations of BDC-OCH<sub>3</sub> at 1572 and 1407 cm<sup>-1</sup>; the C-O-C stretching vibration at 1246 cm<sup>-1</sup> and the bands attributed to CH<sub>3</sub>O- groups, *i.e.* 2941, 2848, 1450, 1378, 1030, and 934 cm<sup>-1</sup>. The FT-IR results confirm the presence of methoxy groups in (OCH<sub>3</sub>)<sub>x</sub>-MOF-5 (X=0.25, 0.5, 0.75 and 1) and that the methoxy

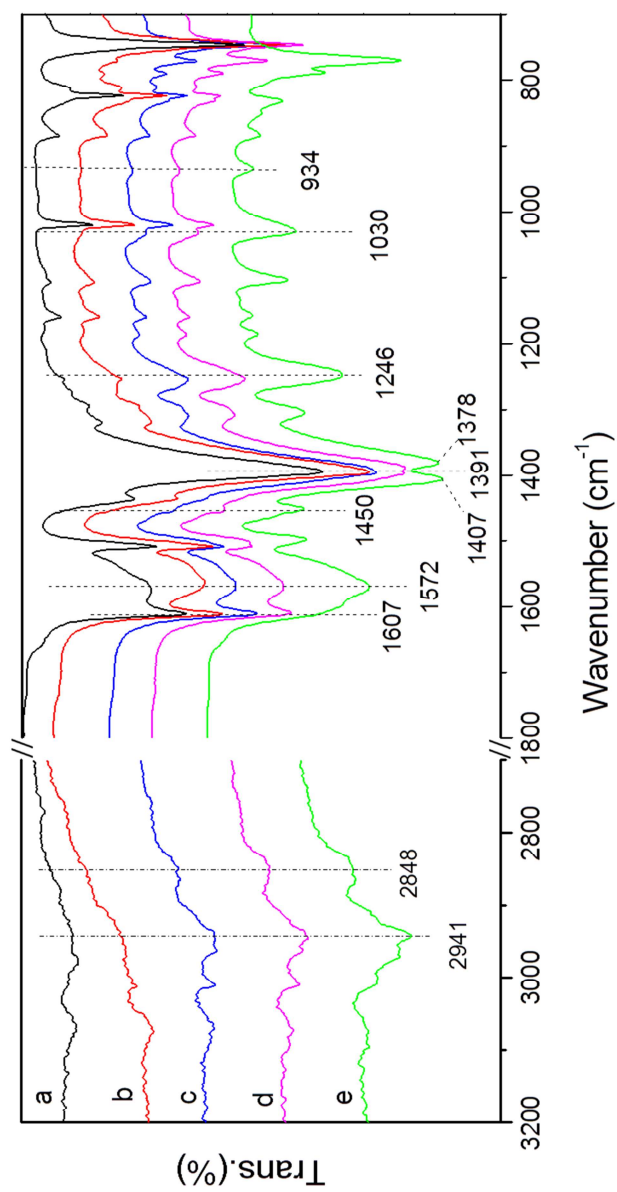


**Figure 3.3.** FT-IR spectra of MOF-5 and the methoxy-modified MOF-5s. MOF-5 (a), (OCH<sub>3</sub>)<sub>0.25</sub>-MOF-5 (b), (OCH<sub>3</sub>)<sub>0.5</sub>-MOF-5 (c), (OCH<sub>3</sub>)<sub>0.75</sub>-MOF-5 (d) and OCH<sub>3</sub>-MOF-5 (e).



content increases by increasing the concentration of methoxyterephthalic acid in the initial reaction solution.

### 3.3.3 Thermogravimetric analysis

The TGA curves of MOF-5 and the methoxy-modified MOF-5s are shown in Figure 3.4. No pronounced weight loss was found below 400 °C for MOF-5, (OCH<sub>3</sub>)<sub>0.25</sub>-MOF-5, (OCH<sub>3</sub>)<sub>0.5</sub>-MOF-5 and (OCH<sub>3</sub>)<sub>0.75</sub>-MOF-5, indicating a successful activation and that stable frameworks have been obtained. In contrast, a weight loss of ~1 wt% below 150 °C and weight loss of ~3 wt% in the range of 150-320 °C were observed in the thermogram of OCH<sub>3</sub>-MOF-5. The former can be assigned to the release of water; the latter is attributed to the removal of DEF, which is corroborated by a nitrogen content of 0.3% found by elemental analysis (Table 3.1). In comparison with MOF-5, the decomposition temperature is decreased by 30 °C for (OCH<sub>3</sub>)<sub>0.25</sub>-MOF-5 and (OCH<sub>3</sub>)<sub>0.5</sub>-MOF-5, 80 °C and 130 °C for (OCH<sub>3</sub>)<sub>0.75</sub>-MOF-5 and OCH<sub>3</sub>-MOF-5, respectively. From these results we may conclude that the incorporation of methoxy groups reduces the thermal stability of MOF-5. The higher the methoxy content, the poorer the thermal stability. Nevertheless, the methoxy-modified MOF-5s are stable enough (up to 350 °C) to be useful for hydrogen storage applications.

According to the TGA thermograms, the weight loss of 58%, 59%, 59% and 61% is related to the organic linkers of MOF-5, (OCH<sub>3</sub>)<sub>0.25</sub>-MOF-5, (OCH<sub>3</sub>)<sub>0.5</sub>-MOF-5 and (OCH<sub>3</sub>)<sub>0.75</sub>-MOF-5, respectively. These values are in good agreement with the theoretical values calculated on the basis of ZnO from formulas Zn<sub>4</sub>O(C<sub>8</sub>H<sub>4</sub>O<sub>4</sub>)<sub>3</sub> (57.8%), Zn<sub>4</sub>O((C<sub>8</sub>H<sub>4</sub>O<sub>4</sub>)<sub>0.75</sub>(C<sub>9</sub>H<sub>6</sub>O<sub>5</sub>)<sub>0.25</sub>)<sub>3</sub> (59.0%), Zn<sub>4</sub>O((C<sub>8</sub>H<sub>4</sub>O<sub>4</sub>)<sub>0.5</sub>(C<sub>9</sub>H<sub>6</sub>O<sub>5</sub>)<sub>0.5</sub>)<sub>3</sub> (60.1%) and Zn<sub>4</sub>O((C<sub>8</sub>H<sub>4</sub>O<sub>4</sub>)<sub>0.25</sub>(C<sub>9</sub>H<sub>6</sub>O<sub>5</sub>)<sub>0.75</sub>)<sub>3</sub> (61.2%). With respect to OCH<sub>3</sub>-MOF-5, the weight loss (61%) seems to be consistent with the theoretical value (62.2%). However, the inconsistency in the C and H contents between the experimental and theoretical values indicates the presence of impurities, which is in agreement with the PXRD results.

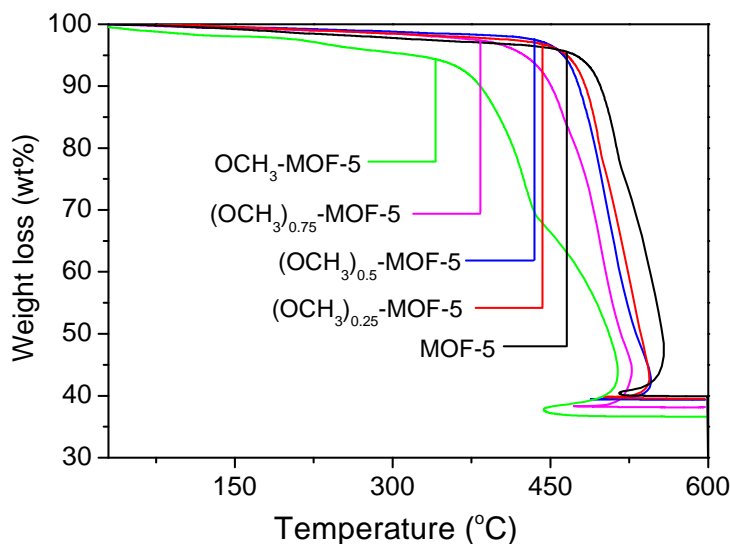


**Figure 3.4.** TGA curves of the methoxy-modified MOF-5s and MOF-5 measured with a heating rate of  $10\text{ }^{\circ}\text{C min}^{-1}$  under a dry air atmosphere.

**Table 3.1.** Elemental analysis results of the methoxy-modified MOF-5s (the theoretical values are listed in brackets and *italics*).

| Sample | $(\text{OCH}_3)_{0.25}\text{-MOF-5}$ | $(\text{OCH}_3)_{0.5}\text{-MOF-5}$ | $(\text{OCH}_3)_{0.75}\text{-MOF-5}$ | $\text{OCH}_3\text{-MOF-5}$ |
|--------|--------------------------------------|-------------------------------------|--------------------------------------|-----------------------------|
| C (%)  | 37.7(37.6)                           | 37.7(37.6)                          | 37.6(37.7)                           | 36.6(37.8)                  |
| H(%)   | 1.67(1.71)                           | 1.79(1.85)                          | 2.00(1.97)                           | 2.53(2.10)                  |
| N(%)   | 0(0)                                 | 0(0)                                | 0(0)                                 | 0.30(0)                     |

### 3.3.4 Specific surface area and pore volume

The BET surface area and pore volume of MOF-5 and the methoxy-modified MOF-5s were measured by  $\text{N}_2$  sorption. The specific surface areas/pore volumes of  $(\text{OCH}_3)_{0.25}\text{-MOF-5}$  and  $(\text{OCH}_3)_{0.5}\text{-MOF-5}$  are  $3264\text{ m}^2\text{ g}^{-1}/1.35\text{ cm}^3\text{ g}^{-1}$  and  $3045\text{ m}^2\text{ g}^{-1}/1.26\text{ cm}^3\text{ g}^{-1}$ , respectively, which is comparable to that of MOF-5 ( $3039\text{ m}^2\text{ g}^{-1}/1.29\text{ cm}^3\text{ g}^{-1}$ ) (Figure 3.5). In fact,  $(\text{OCH}_3)_{0.25}\text{-MOF-5}$  showed a modest increase in surface area and pore volume of 7% and 5%, respectively, over MOF-5.  $(\text{OCH}_3)_{0.75}\text{-MOF-5}$  showed a BET surface area of  $2263\text{ m}^2\text{ g}^{-1}$  and a pore volume of  $0.97\text{ cm}^3\text{ g}^{-1}$ . A significant drop in the

surface area ( $529 \text{ m}^2 \text{ g}^{-1}$ ) and pore volume ( $0.23 \text{ cm}^3 \text{ g}^{-1}$ ) was found for  $\text{OCH}_3$ -MOF-5 and is attributed to its poor structure. The results reveal that the surface area and pore volume of MOF-5 are retained when the methoxyterephthalate concentration does not exceed 75 mol%. Beyond this point the surface area and pore volume drop rapidly, which is due to the rapid destabilization of the framework.

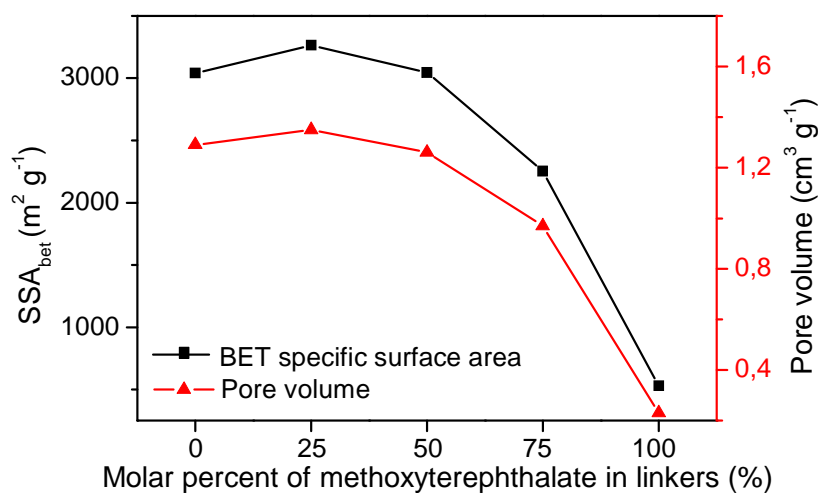


**Figure 3.5.** The surface areas and pore volumes of the  $(\text{OCH}_3)_x$ -MOF-5 series (the x-axis stands for molar percentage of methoxyterephthalate. 0(MOF-5), 25( $(\text{OCH}_3)_{0.25}$ -MOF-5), 50( $(\text{OCH}_3)_{0.5}$ -MOF-5), 75( $(\text{OCH}_3)_{0.75}$ -MOF-5) and 100( $\text{OCH}_3$ -MOF-5)).

### 3.3.5 Hydrogen storage property

The hydrogen uptake capacities of MOF-5 and the methoxy-modified MOF-5s at 77 K and below 1.2 bar are shown in Figure 3.6. MOF-5,  $(\text{OCH}_3)_{0.25}$ -MOF-5 and  $(\text{OCH}_3)_{0.5}$ -MOF-5 all adsorb 1.3 wt% at 77 K and 1 bar. Under the given conditions, the hydrogen uptake capacities of  $(\text{OCH}_3)_{0.25}$ -MOF-5 and  $(\text{OCH}_3)_{0.5}$ -MOF-5 are thus similar to that of MOF-5.  $(\text{OCH}_3)_{0.75}$ -MOF-5 displayed a hydrogen uptake capacity of 1.45 wt% at 77 K and 1 bar, which constitutes a 10% improvement over MOF-5. Moreover,  $(\text{OCH}_3)_{0.75}$ -MOF-5 showed the highest hydrogen uptake capacity over the whole pressure range studied (0–1.2 bar). The hydrogen uptake capacity of  $\text{OCH}_3$ -MOF-5 below 0.1 bar is superior to that of MOF-5,  $(\text{OCH}_3)_{0.25}$ -MOF-5 and  $(\text{OCH}_3)_{0.5}$ -MOF-5. However, it showed the lowest hydrogen uptake capacity above 0.1 bar.

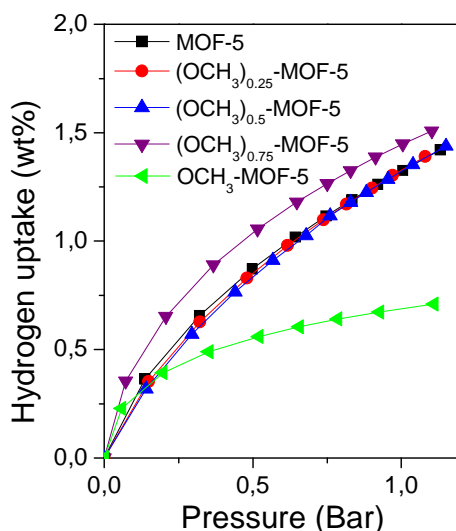


**Figure 3.6.** Low-pressure hydrogen adsorption isotherms of MOF-5 and the methoxy-modified MOF-5s at 77 K.

It is clear that the incorporation of methoxy groups ( $-\text{OCH}_3$ ) improves the hydrogen adsorption capacity of MOF-5 at low pressures. To understand the adsorption behavior in more detail, the isosteric heats of hydrogen adsorption for these materials were calculated from the Clausius-Clapeyron equation at a hydrogen uptake capacity of 0.5 wt% at 77 K and 100 K. The isosteric heats of hydrogen adsorption are 3.8, 3.6, 3.6, 4.4 and 4.5  $\text{kJ mol}^{-1}$  for MOF-5,  $(\text{OCH}_3)_{0.25}$ -MOF-5,  $(\text{OCH}_3)_{0.5}$ -MOF-5,  $(\text{OCH}_3)_{0.75}$ -MOF-5 and  $\text{OCH}_3$ -MOF-5, respectively (Figure 3.7). Compared to MOF-5, similar isosteric heats of hydrogen adsorption were found for  $(\text{OCH}_3)_{0.25}$ -MOF-5 and  $(\text{OCH}_3)_{0.5}$ -MOF-5. Interestingly,  $\text{OCH}_3$ -MOF-5 and  $(\text{OCH}_3)_{0.75}$ -MOF-5 showed  $\sim 18\%$  higher isosteric heats of hydrogen adsorption than that of MOF-5. This result suggests that methoxy groups indeed improve the interaction between hydrogen molecules and the MOF-5 structure when over 75 mol% methoxyterephthalate was incorporated as a linker unit. The increased isosteric heat of hydrogen adsorption may be partially attributed to a reduction in the pore size by the introduction of  $-\text{OCH}_3$  groups. In addition, it is believed that the introduction of an electron-donating group (or groups) to the central portion of the ligand enhance the affinity of the ligand towards hydrogen, which may be another reason of the improved isosteric heats of hydrogen adsorption for  $(\text{OCH}_3)_{0.75}$ -MOF-5 and  $\text{OCH}_3$ -MOF-5.

It has been documented that the heat of hydrogen adsorption plays a vital role in the hydrogen adsorption capacity at low pressures.[17,18] Apparently, the isosteric heat of hydrogen adsorption results are in close agreement with the hydrogen uptake capacity trend in the low-pressure range (not including OCH<sub>3</sub>-MOF-5), *i.e.* MOF-5 $\approx$ (OCH<sub>3</sub>)<sub>0.25</sub>-MOF-5 $\approx$ (OCH<sub>3</sub>)<sub>0.5</sub>-MOF-5<(OCH<sub>3</sub>)<sub>0.75</sub>-MOF-5. The isosteric heat of hydrogen adsorption for MOF-5 is not affected by incorporating up to 50 mol% methoxyterephthalate as linkers, while 75 mol% does result in an increase. As a result, (OCH<sub>3</sub>)<sub>0.25</sub>-MOF-5 and (OCH<sub>3</sub>)<sub>0.5</sub>-MOF-5 showed hydrogen uptake capacities similar to that of MOF-5. However, the incorporation of 75% methoxyterephthalate enhances the isosteric heat of hydrogen adsorption and leads to a higher hydrogen uptake capacity at 1 bar as compared to MOF-5. The presence of methoxy groups thus appears to have a favorable effect on the hydrogen uptake capability of MOF-5. With respect to OCH<sub>3</sub>-MOF-5, it showed a higher hydrogen uptake capacity than that of MOF-5 and (OCH<sub>3</sub>)<sub>x</sub>-MOF-5 (X=0.25 and 0.5) only in very low pressure range (below 0.1 bar) due to the improved isosteric heat of hydrogen adsorption. However, the poor structure results in the lowest hydrogen uptake capacity measured for OCH<sub>3</sub>-MOF-5 above 0.1 bar.

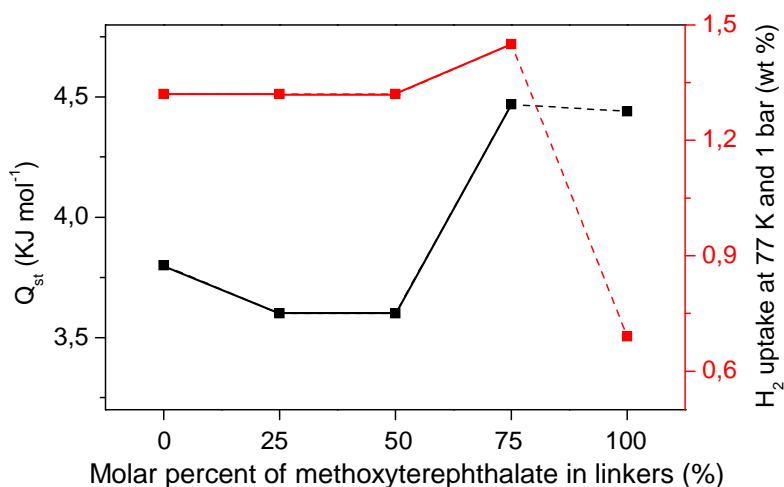


**Figure 3.7.** The isosteric heats of hydrogen adsorption (calculated at 0.5 wt% of hydrogen uptake capacity) and hydrogen uptake capacities of (OCH<sub>3</sub>)<sub>x</sub>-MOF-5 at 77 K and 1 bar (the x-axis represents the concentration of methoxyterephthalate (mol%). 0(MOF-5), 25((OCH<sub>3</sub>)<sub>0.25</sub>-MOF-5), 50((OCH<sub>3</sub>)<sub>0.5</sub>-MOF-5), 75((OCH<sub>3</sub>)<sub>0.75</sub>-MOF-5) and 100(OCH<sub>3</sub>-MOF-5)).

The high-pressure hydrogen adsorption isotherms of MOF-5 and the methoxy-modified MOF-5s are shown in Figure 3.8. (OCH<sub>3</sub>)<sub>0.25</sub>-MOF-5 and (OCH<sub>3</sub>)<sub>0.5</sub>-MOF-5 nearly

reached their saturated hydrogen uptake capacities of 5.9 wt% and 5.2 wt% at 50 bar, respectively, which are higher than that of MOF-5 (4.8 wt%).  $(\text{OCH}_3)_{0.75}$ -MOF-5 and  $\text{OCH}_3$ -MOF-5 showed lower excess hydrogen uptake capacities (4.2 wt% and 2.0 wt%) as compared to MOF-5. The excess hydrogen uptake capacities of the four MOFs follow the same trend as their surface areas, which is consistent with previous results.[11,19]

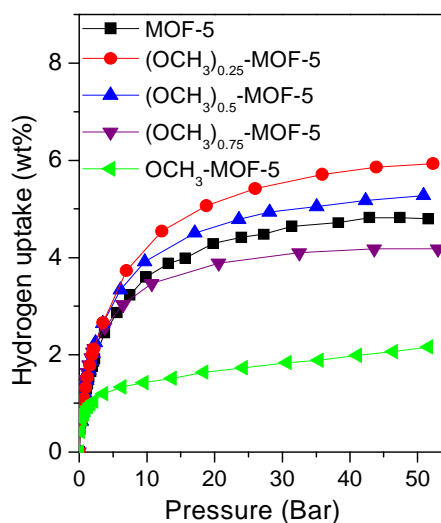


**Figure 3.8.** High-pressure excess hydrogen adsorption isotherms of MOF-5 and the methoxy-modified MOF-5s at 77 K.

### 3.4 Conclusions

A series of methoxy-modified MOF-5s,  $(\text{OCH}_3)_x$ -MOF-5 ( $x=0.25, 0.5$  and  $0.75$ ), has been synthesized via a mixed ligand approach. All methoxy-modified MOF-5s show the same crystal structure as the unsubstituted MOF-5 parent structure. The crystal quality, thermal stability, specific surface area and pore volume of MOF-5 can be retained when less than 75 mol% methoxyterephthalate is incorporated as the organic linker. However, the structure becomes compromised when the methoxyterephthalate concentration exceeds 75%. We found that the methoxy group enhances the isosteric heat of hydrogen adsorption for MOF-5 when the methoxyterephthalate content is larger than 75% ( $3.8 \text{ kJ mol}^{-1}$  for MOF-5 vs.  $4.5 \text{ kJ mol}^{-1}$  for  $(\text{OCH}_3)_{0.75}$ -MOF-5), giving rise to a hydrogen uptake capacity of 1.45 wt% for  $(\text{OCH}_3)_{0.75}$ -MOF-5 at 77 and 1 bar, which constitutes a 10% improvement over MOF-5 (1.32 wt%). In the high pressure range (50 bar and 77 K) an increase of 23% in hydrogen uptake capacity for  $(\text{OCH}_3)_{0.25}$ -MOF-5 was

observed. Due to the poor structure, OCH<sub>3</sub>-MOF-5 displays the lowest hydrogen uptake capacity near ambient pressure despite the strong affinity for hydrogen. Based on these results we conclude that it is worthwhile to search for the proper synthetic conditions towards preparing a stable MOF-5 solely build from methoxyterephthalate linkers as this will yield a MOF-5 structure with superior hydrogen storage capability over terephthalate-based MOF-5.

### 3.5 References

- [1] Rowsell, J.L.C.; Yaghi, O.M. *J. Am. Chem. Soc.* **2006**, *128*, 1304.
- [2] Collins, D.J.; Zhou, H.-C. *J. Mater. Chem.* **2007**, *17*, 3154.
- [3] Germain, J. Frechet, J. M. J.; Svec, F. *Small* **2009**, *5*, 1098.
- [4] Lochan, R.C.; Head-Gordon, M. *Phys. Chem. Chem. Phys.* **2006**, *8*, 1357.
- [5] Sagara, T.; Klassen, J.; Ortony, J.; Ganz, E.J. *Chem. Phys.* **2005**, *123*, 14701.
- [6] Zhao, Z.; Xia, Q.; Zhong, L. *Separation Science and Technology* **2011**, *46*, 1337.
- [7] Blanita, G.; Lupu, D.; Lazar, M.; Biris, A.R.; Pascalau, V.; Ardelean, O.; Coldea, I.; Misan, I.; Popeneciu, G.; Vlassa, M. *Journal of Physics: Conference Series* **2009**, *182*, 12047.
- [8] Chen, B.; Wang, X.; Zhang Q.; Xi, X.; Cai, J.; Qi, H.; Shi, S.; Wang, J.; Yuan, D.; Fang, M. *J. Mater. Chem.* **2010**, *20*, 3758.
- [9] Yang, S.J.; Cho, J.H.; Lee, K.; Kim, T.; Park, C.R. *Chem. Mater.* **2010**, *22*, 6138.
- [10] Kim, H.; Das, S.; Kim, M.G.; Dybtsev, D.N.; Kim, Y.; Kim, K. *Inorg. Chem.* **2011**, *50*, 3691.
- [11] Wong-Foy, A.G.; Matzger, A.J.; Yaghi, O.M. *J. Am. Chem. Soc.* **2006**, *128*, 3494.
- [12] Wu, T.J.; Shen, L.J.; Luebbers, M.; Hu, C.; Chen, Q.M.; Ni, Z.; Masel, R.I. *Chem. Commun.* **2010**, 6120.
- [13] Ni, Z.; Masel, R.I. *J. Am. Chem. Soc.* **2006**, *128*, 12394.
- [14] Yang, J.; Grzech, A.; Mulder, F.M.; Dingemans, T.J. *Chem. Commun.* **2011**, *47*, 5244.
- [15] Deng, H.; Doonan, C.J.; Furukawa, H.; Ferreira, R.B. Towne, J.; Knobler, C.B.; Wang, B. Yaghi, O. M. *Science* **2010**, *327*, 846.
- [16] Panella, B.; Hirscher, M.; Puetter, H.; Mueller, U. *Adv. Funct. Mater.* **2006**, *16*, 520.
- [17] (a) Hu, Y.; Zhang, L. *Adv. Mater.* **2010**, *22*, 117. (b) Murray, L.J.; Dinca, M.; J. R. Long, *Chem. Soc. Rev.* **2009**, *38*, 1294.
- [18] Mulder, F.M.; Dingemans, T.J.; Wagemaker, M.; Kearley, G.J. *Chem. Phys.* **2005**, *317*, 113.
- [19] Duren, T.; Bae, Y.-S.; Snurr, R.Q. *Chem. Soc. Rev.* **2009**, *38*, 1237.





# CHAPTER 4

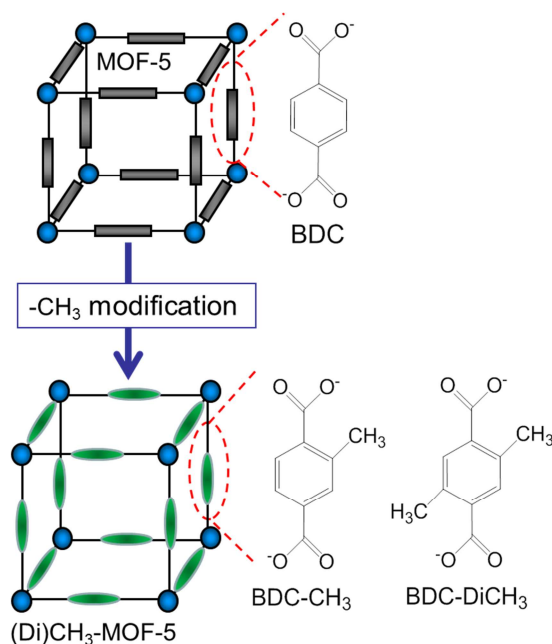
## **Methyl modified MOF-5: a water-stable hydrogen storage material**

---

In this chapter, water-stable methyl modified MOF-5 analogs will be discussed. Methyl- and 2,5-dimethyl-modified MOF-5s show the same topology and hydrogen uptake capability as that of unsubstituted MOF-5. The hydrogen uptake capacity of MOF-5 drops rapidly to ~0% when exposed to ambient air (relative humidity of 32-37%) for 1 day, whereas (di)methyl-modified hydrophobic MOF-5s maintain their hydrogen adsorption properties for 4 days. The hydrogen uptake capacity of methyl-modified MOF-5 (77 K and 1 bar) decreases from 1.42 wt% to 0.97 wt% after 4 days exposure to ambient air. Remarkably, dimethyl-modified MOF-5s displays an unaffected hydrogen uptake capacity (1.29 wt% vs. 1.25 wt%). Even after 8 days exposure to ambient air, ~65% of the hydrogen uptake capacity could be retained.

## 4.1 Introduction

Metal organic frameworks (MOFs) are crystalline materials consisting of metal ions (or metal clusters) and organic ligands, which are linked together to form extended porous frameworks. MOFs containing Zn, Mn, Cr, and Cu show outstanding hydrogen adsorption behaviour at 77 K and are among the most promising hydrogen storage materials.[1-3] Maybe the best known MOF to date is MOF-5. This three-dimensional network has a crystal structure where metal clusters  $[Zn_4O]^{6+}$  are joined to an octahedral array of benzene-1,4-dicarboxylate (BDC) groups to form a porous cubic  $Zn_4O(BDC)_3$  framework.[4] MOF-5 displays an excess hydrogen uptake capacity of 7.1 wt% at 77 K and 40 bar. At 100 bar, the total hydrogen uptake of MOF-5 can reach up to 10 wt%, corresponding to a record volumetric storage density of 66 g L<sup>-1</sup>. [2] However, most MOFs, in particular zinc-based MOFs, are moisture-sensitive because the relative weak metal-oxygen coordination allows for attack by water molecules, resulting in the phase transformation and decomposition of the framework.[5] Structural decomposition, caused by the presence of water, always leads to poor reproducibility and a decrease in gas sorption capacities of MOFs. Discrepancies in hydrogen uptake capacities have been found for MOF-5 and are thought to be due to the presence of water.[6-10] High quality MOF-5 can only be obtained when the exposure to water and ambient air was minimized.[2] Care must be taken to avoid the structural collapse of MOFs, since it will limit their potential commercial application. Therefore it is desirable to enhance the structural stability of MOFs towards moisture, but at the same time, the excellent hydrogen uptake capability of MOFs should remain unaffected. Very recently, researchers have demonstrated that it is possible to build water-stable MOF structures by introducing hydrophobic functional groups into the framework structures.[11,12] Yet, no results have been published on the hydrogen storage capability of such functionalized MOFs. In this chapter, the effect of moisture on the hydrogen storage capability of methyl (-CH<sub>3</sub>) and dimethyl (-DiCH<sub>3</sub>) modified MOF-5 will be discussed. The structures of methyl and 2,5-dimethyl-modified MOF-5s are shown in Scheme 4.1.



**Scheme 4.1.** Methyl and 2,5-dimethyl-modified MOF-5s.

## 4.2 Experimental

### 4.2.1 Materials

$\text{Zn}(\text{NO}_3)_2 \cdot 6\text{H}_2\text{O}$  (98%, Aldrich), 2,5-dimethylterephthalic acid (>97%, TCI) was recrystallized from 2-methyl-1-propanol. *N,N*-diethylformamide (DEF) (99%, Acros) and  $\text{CHCl}_3$  were dried over and distilled from  $\text{CaH}_2$  and  $\text{P}_2\text{O}_5$  before use, respectively. MOF-5 was synthesized according to a literature procedure.[13]

### 4.2.2 Synthesis of methyl modified MOF-5s

**Synthesis of  $\text{CH}_3$ -MOF-5.** 4 mL of a methylterephthalic acid solution in DEF (0.1 M) and 4 mL of a  $\text{Zn}(\text{NO}_3)_2 \cdot 6\text{H}_2\text{O}$  solution in DEF (0.3 M) were mixed in a 20 mL glass vial. The vial was sealed and heated in an oven at 100 °C for 49 h. When cooled to r.t. the supernatant was decanted and discarded. Cubic crystals were collected and immersed in DEF (3 mL) for 24 h (2×), followed by immersing the crystals in  $\text{CHCl}_3$  (4 mL) for 24 h (3×). The solvent-exchanged product was heated at 160 °C under vacuum for 24 h, and stored in a glove box (75 mg, 69% yield). Elemental analysis (EA): Calc. for

$\text{Zn}_4\text{O}(\text{C}_9\text{H}_6\text{O}_4)_3$ : C, 40.0%, H, 2.22%. Found C, 40.2%, H, 2.24%. FT-IR ( $\text{cm}^{-1}$ ): 2982, 1605, 1565, 1497, 1405, 1380, 1293, 1209, 1099, 911, 828, 788, 763.

**Synthesis of DiCH<sub>3</sub>-MOF-5.** DiCH<sub>3</sub>-MOF-5 was synthesized using a similar procedure as described for CH<sub>3</sub>-MOF-5. 4 mL of a 2,5-dimethylterephthalic acid solution in DEF (0.1 M) and 4 mL Zn(NO<sub>3</sub>)<sub>2</sub>·6H<sub>2</sub>O solution in DEF (0.3 M) were mixed in a 20 mL glass vial. The vial was sealed and heated in an oven at 100 °C for 29 h. A similar solvent exchange procedure was used as described for CH<sub>3</sub>-MOF-5. The solvent-exchanged product was heated at 160 °C under vacuum for 24 h, and stored in a glove box (40 mg, 35% yield). Elemental analysis (EA): Calc. for  $\text{Zn}_4\text{O}(\text{C}_{10}\text{H}_8\text{O}_4)_3$ : C, 42.2%; H, 2.81%. Found: C, 41.0%; H, 2.89%. FT-IR ( $\text{cm}^{-1}$ ): 2967, 2930, 1558, 1499, 1409, 1356, 1286, 1193, 1154, 1038, 910, 851, 795, 760.

### 4.2.3 Characterization

XRD patterns of all samples were recorded on an X'Pert X-ray diffractometer operated at 45 kV and 40 mA with monochromated Cu K $\alpha$  radiation within a 2-theta range of 5-60°. A sample was placed into an airtight sample-holder in order to limit exposure to air and moisture. IR spectra of the samples were collected on a PerkinElmer Spectrum 100 FT-IR Spectrometer. TGA curves of samples were obtained on a PerkinElmer Pyris Diamond Thermogravimetric Thermal Analyzer. Samples were investigated from room temperature to 600 °C with a heating rate of 10 °C min<sup>-1</sup> under a dry air flow (200 mL min<sup>-1</sup>). Elemental analyses were performed on a Thermo Scientific InterScience Flash 2000 Organic Elemental Analyzer. The pore textural properties, including BET surface area and pore volume, were recorded on a Micromeritics ASAP 2010 adsorption analyzer at 77 K. Prior to the adsorption measurements, the samples were degassed *in situ* using a vacuum at 135 °C. The dead volume of the sample cell was determined in a separate experiment. *In situ* pretreatment coupled to a separate dead volume measurement after the analysis was employed in order to avoid the helium entrapment phenomenon. The weight of the sample obtained after the pretreatment was used in the various calculations. BET surface areas were calculated in the adapted pressure range of  $P/P_0=0.01-0.1$ . Hydrogen storage measurements at different pressures were performed on a home-made Sievert's setup at 77 K. Samples were heated to 150 °C for 12 h. under high vacuum (10<sup>-6</sup> mbar) prior to each measurement. Hydrogen (ultra-high-purity grade, 99.999%) was additionally purified by passing it over a bed of zeolite spheres at 77 K before being loaded into the sample holder. The pressure change was monitored and recorded after the hydrogen reservoir was

connected to the sample holder. The samples were weighed in a glove box after the measurements.

## **4.3 Results and discussion**

### **4.3.1 Structures of methyl-modified MOF-5s**

The methyl-modified MOF-5s showed the same topology as that of MOF-5, which is supported by the high degree of correspondence between the PXRD patterns of methyl modified MOF-5 and MOF-5 (Figure 4.1). All MOF-5 samples were exposed to ambient air with a relative humidity of 32-37% and the structural stability was examined by PXRD under ambient conditions. With respect to MOF-5, our findings are in agreement with results reported in the literature.[4] When exposed to ambient air, with a relative humidity of 32-37%, an additional peak at  $2\theta = 8.8^\circ$  appeared after only 45 min. In addition, the intensity of the original peaks decreased dramatically with exposure time and after 1 day, the structure of MOF-5 completely transformed to  $\text{ZnBDC}\cdot\text{XH}_2\text{O}$  (Figure 4.2).[2,14] Interestingly, the PXRD pattern of  $\text{CH}_3\text{-MOF-5}$  remains unchanged even after 4 days exposure to ambient air ( $\text{CH}_3\text{-MOF-5-4d}$ ), as shown in Figure 4.3. Similar results were obtained for  $\text{DiCH}_3\text{-MOF-5}$  (Figure 4.4). Clearly, the structures of  $\text{CH}_3\text{-MOF-5}$  and  $\text{DiCH}_3\text{-MOF-5}$  remain stable up to 4 days after exposure to ambient air. Even after a total of 8 days exposure to ambient air, the original structures of  $\text{CH}_3\text{-MOF-5}$  and  $\text{DiCH}_3\text{-MOF-5}$  are still maintained according to the largely unchanged PXRD patterns (Figure 4.3 and 4.4). These results strongly imply that introducing hydrophobic methyl groups enhances the structural stability of MOF-5 type framework.

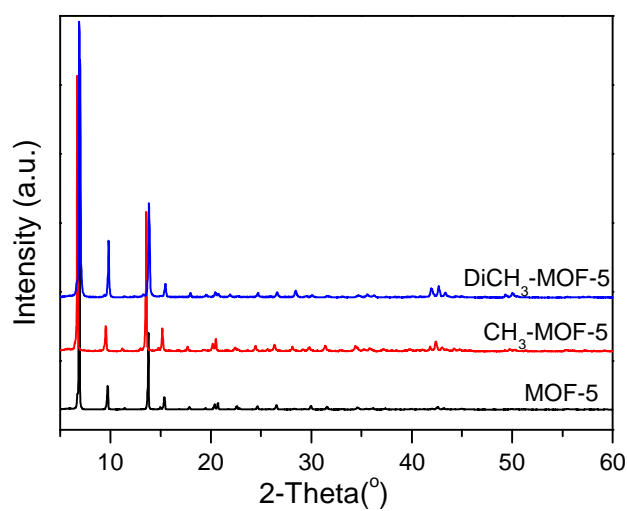


**Figure 4.1.** PXRD patterns of MOF-5 and methyl modified MOF-5s.

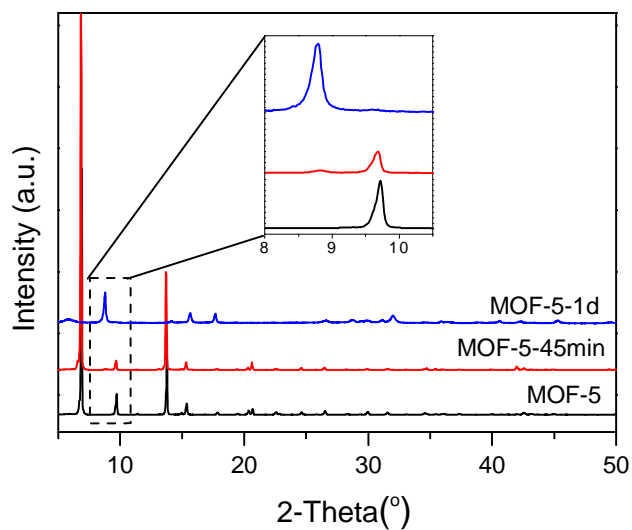


**Figure 4.2.** PXRD patterns of MOF-5 exposed to ambient air with a relative humidity of 32-37% for 45 min (MOF-5-45min) and 1 day (MOF-5-1d), respectively.

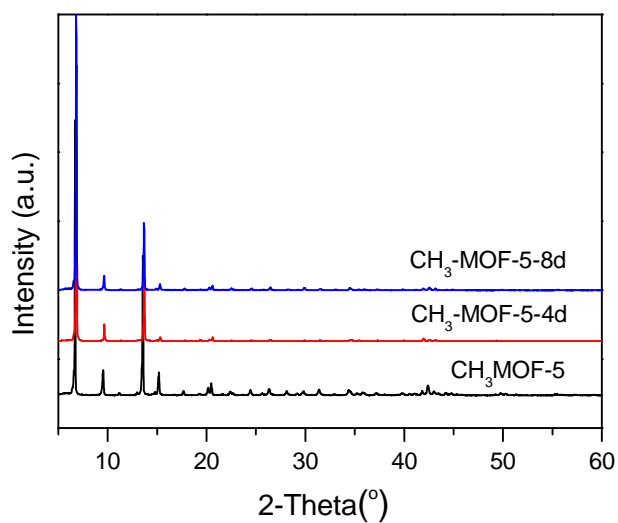


**Figure 4.3.** PXRD patterns of CH<sub>3</sub>-MOF-5s after 4 days (CH<sub>3</sub>-MOF-5-4d) and 8 days (CH<sub>3</sub>MOF--5-8d) exposure to ambient air with a relative humidity of 32-37%.

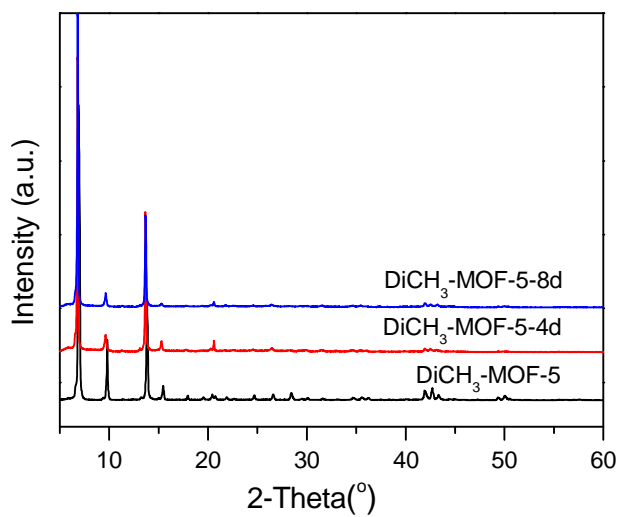


**Figure 4.4.** PXRD patterns of DiCH<sub>3</sub>-MOF-5s after 4 days (DiCH<sub>3</sub>-MOF-5-4d) and 8 days (DiCH<sub>3</sub>-MOF-5-8d) exposure to ambient air with a relative humidity of 32-37%.

### 4.3.2 Thermogravimetric analysis

TGA curves of CH<sub>3</sub>-MOF-5 and DiCH<sub>3</sub>-MOF-5 both exhibited weight loss events starting at ~400 °C, which is due to the decomposition of the organic linkers (Figure 4.5). Compared to the decomposition temperature of unsubstituted MOF-5, the decomposition temperatures for CH<sub>3</sub>-MOF-5 and DiCH<sub>3</sub>-MOF-5 are decreased by ~50 °C, suggesting that the thermal stability of MOF-5 is reduced somewhat by introducing methyl (CH<sub>3</sub>) groups on the terephthalic acid linker. A marginal difference in decomposition behaviour was observed between CH<sub>3</sub>-MOF-5 and DiCH<sub>3</sub>-MOF-5, implying that the thermal stability of the MOF-5 framework is insensitive to doubling the concentration of methyl groups present in the framework.

Compared to fresh samples, a weight loss of ~3% was observed for CH<sub>3</sub>-MOF-5-4d at about 100 °C (inset Figure 4.5), which is due to the removal of water. DiCH<sub>3</sub>-MOF-5-4d, on the other hand, showed a loss of water of ~0.25%, which is the result of the more hydrophobic character of this MOF. Both MOFs showed some outgassing above 100 °C, which appears to be *N,N*-diethylformamide (DEF). Both outgassing of water and DEF was confirmed by mass spectroscopy. According to molecular dynamics simulation results on the interaction of water and MOF-5, MOF-5 is only stable at a very low water content but unstable when exposed to more than 4 wt% water.[7] These results are in line with our findings: when the concentration of CH<sub>3</sub> functionalities increases (DiCH<sub>3</sub>-MOF-5-4d vs. CH<sub>3</sub>-MOF-5-4d) the water uptake decreases and the structures stay well below 4 wt%. After 8 days exposure to ambient air, compared to fresh samples, CH<sub>3</sub>-MOF-5-8d and DiCH<sub>3</sub>-MOF-5-8d showed ~1 wt% and ~3 wt% of water loss, respectively (Figure 4.6). A water uptake of < 4 wt% did not cause the structural collapse, as evidenced by the PXRD result. Therefore, introducing hydrophobic CH<sub>3</sub> groups is an effective approach towards the design of water-stable metal-organic frameworks.



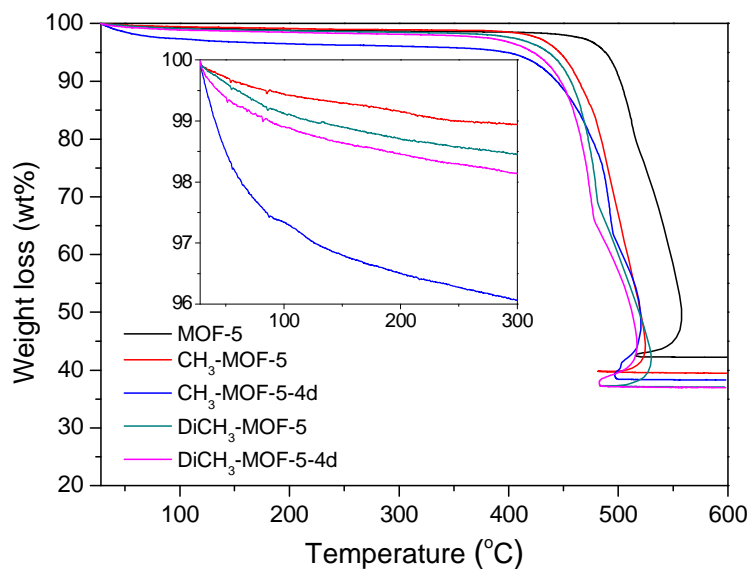


**Figure 4.5.** TGA curves of (Di)CH<sub>3</sub>-MOF-5 (before) after 4 days (4d) exposure to ambient air. MOF-5 is included for reference purposes.

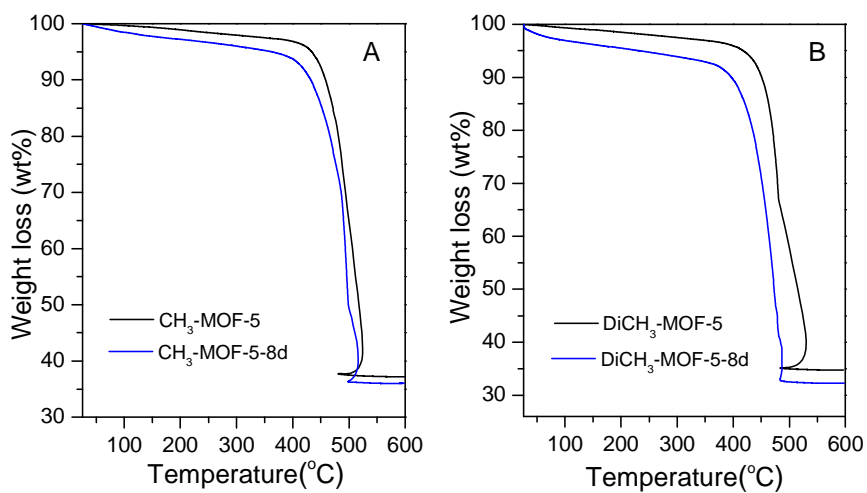


**Figure 4.6.** TGA curves of CH<sub>3</sub>-MOF-5 (A) and DiCH<sub>3</sub>-MOF-5 (B) (before) after 8 days (8d) exposure to ambient air.

### 4.3.3 Hydrogen storage properties

It was demonstrated by us that methyl modified MOF-5, very much like MOF-5, can load hydrogen within several minutes. CH<sub>3</sub>-MOF-5 showed almost the same hydrogen uptake capacity as that observed for MOF-5 in the studied pressure range (Figure 4.7). The hydrogen uptake capacities of CH<sub>3</sub>-MOF-5 and MOF-5 are 1.42 wt% and 1.44 wt% at 1 bar and 77 K, respectively. DiCH<sub>3</sub>-MOF-5 demonstrated a lower hydrogen uptake capacity of 1.29 wt% at 1 bar and 77 K. Compared to CH<sub>3</sub>-MOF-5 synthesized at 125 °C in Chapter 2, CH<sub>3</sub>-MOF-5 synthesized at 100 °C (this chapter) showed a lower hydrogen uptake capacity (1.48 wt% vs. 1.42 wt% at 77 K and 1 bar). This could be explained by a fraction of an interpenetrated structure that maybe present in CH<sub>3</sub>-MOF-5(125 °C). It is noteworthy, however, that the decrease in hydrogen uptake of DiCH<sub>3</sub>-MOF-5 compared to MOF-5 is relatively less than the lowering of surface area and pore volume. That may be related to the claim that although interpenetrated structures may limit the pore volume, they can also have a positive effect on the hydrogen uptake capability of MOFs when the interaction strength increases due to smaller pore sizes.[15]

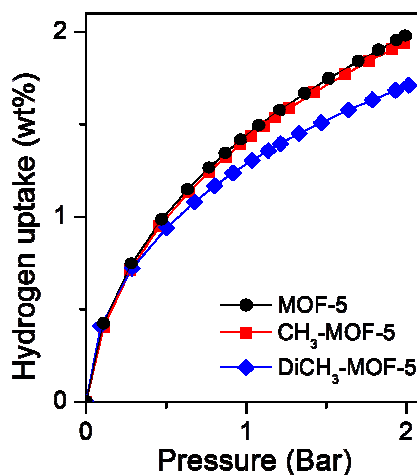


**Figure 4.7.** Low-pressure hydrogen adsorption isotherms of MOF-5 and (Di)CH<sub>3</sub>-MOF-5 at 77 K.

Of significant interest is the hydrogen storage uptake capability of the methyl and dimethyl modified MOF-5 after exposure to ambient air (Figure 4.8). MOF-5 completely loses its hydrogen storage capability after exposure to ambient air due to a total collapse of the framework structure within 1 day. This is in good agreement with

previous results.[2] The hydrogen uptake capacities of the methyl modified MOF-5s, on the other hand, can be recovered after exposure to ambient air with a relative humidity of 32-37%. Before each measurement, CH<sub>3</sub>-MOF-5-4d(8d) and DiCH<sub>3</sub>-MOF-5-4d(8d) were reactivated by heating the samples at 160 °C *in vacuo* for 24 h. The hydrogen uptake capacity of CH<sub>3</sub>-MOF-5 is reduced to 70% after 4 days exposure to ambient air, whereas the hydrogen uptake capacity of DiCH<sub>3</sub>-MOF-5-4d remained virtually the same. After a total of 8 days exposure to ambient air, CH<sub>3</sub>-MOF-5-8d showed the same hydrogen uptake capacity as that of CH<sub>3</sub>-MOF-5-4d. A reduced hydrogen uptake capacity by 35% was observed for DiCH<sub>3</sub>-MOF-5-8d as compared to DiCH<sub>3</sub>-MOF-5. These results, again, imply that methyl substituents can play an important role in designing water-stable MOFs without compromising the hydrogen uptake capacity.

According to the C and H elemental analysis results in Table 4.1, the H content in reactivated CH<sub>3</sub>-MOF-5-4d is higher than that of a fresh sample, which is due to the absorbed water and corresponds to a water content of about 3.2 wt%. This CH<sub>3</sub>-MOF-5, with strongly adsorbed water, showed a lower hydrogen uptake capacity as compared to a fresh sample. Although the structure of CH<sub>3</sub>-MOF-5 remains stable at low water concentrations, distortions in the framework structure might occur as reported in a simulated study for MOF-5.[7] Even 0.6 wt% of water in the structure may lead to the distortion of the ZnO<sub>4</sub> tetrahedron and this will result in a reduced hydrogen uptake capability. Introducing a second methyl group, as is the case for DiCH<sub>3</sub>-MOF-5, the water uptake is reduced even further, which can be concluded from the constant C and H contents found for DiCH<sub>3</sub>-MOF-5 and DiCH<sub>3</sub>-MOF-5-4d. This result confirms that incorporating hydrophobic methyl groups can indeed improve the water stability of MOF-5 without seriously compromising the hydrogen uptake capability. The significant reduction of surface area and pore volume (Table 4.1) indicate that the structure of DiCH<sub>3</sub>-MOF-5-8d becomes compromised and this could explain the reduced hydrogen uptake capacity. The structural integrity of DiCH<sub>3</sub>-MOF-5-8d might be reduced due to the high temperature (160 °C for 24 h) re-activation process after each exposure. Nevertheless, still about 65% of the original hydrogen uptake capacity of DiCH<sub>3</sub>-MOF-5 could be retained. This exciting result further demonstrates the potential of methyl modified MOF-5 as a hydrogen storage material.

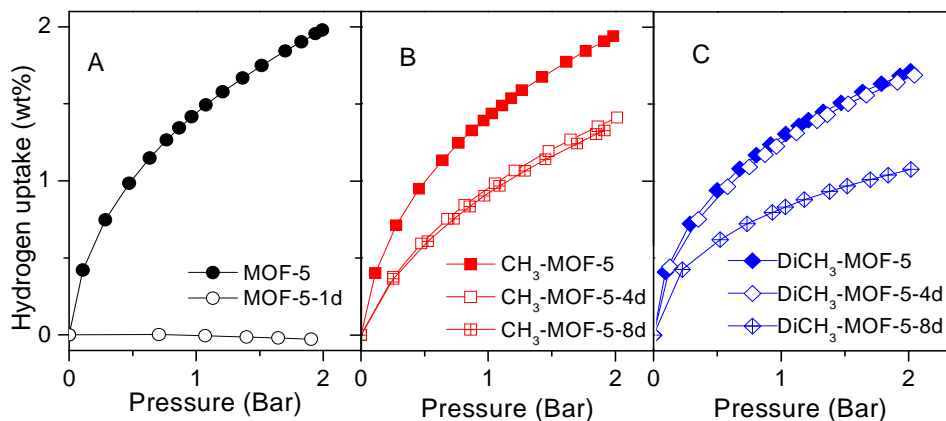


**Figure 4.8.** Low-pressure hydrogen adsorption isotherms of MOF-5 (A), CH<sub>3</sub>-MOF-5 (B) and DiCH<sub>3</sub>-MOF-5 (C) before and after exposed to ambient air with a relative humidity of 32-37% for 1 (1d), 4 (4d) or 8 days (8d).

**Table 4.1.** Elemental analysis results (calculated values in *italics*) and hydrogen uptake capacities.

| Sample                      | C (%)             | H (%)             | SSA <sub>BET</sub> (m <sup>2</sup> g <sup>-1</sup> ) | V <sub>ptotal</sub> (cm <sup>3</sup> g <sup>-1</sup> ) | H <sub>2</sub> uptake <sup>a</sup> (wt%) |
|-----------------------------|-------------------|-------------------|--|--|--|
| MOF-5                       | 37.6(37.5)        | 1.65(1.56)        | 2750   | 1.15   | 1.44                                     |
| CH <sub>3</sub> -MOF-5      | 40.2(40.0)        | 2.24(2.22)        | 2537   | 1.03   | 1.42                                     |
| CH <sub>3</sub> -MOF-5-4d   | 38.0 <sup>b</sup> | 2.47 <sup>b</sup> | n/a  | n/a  | 0.97                                     |
| CH <sub>3</sub> -MOF-5-8d   | n/a               | n/a               | 2145   | 0.88   | 0.93                                     |
| DiCH <sub>3</sub> -MOF-5    | 41.0(42.2)        | 2.89(2.81)        | 1927   | 0.82   | 1.29                                     |
| DiCH <sub>3</sub> -MOF-5-4d | 41.0 <sup>b</sup> | 2.93 <sup>b</sup> | n/a  | n/a  | 1.25                                     |
| DiCH <sub>3</sub> -MOF-5-8d | n/a               | n/a               | 987  | 0.45   | 0.82                                     |

<sup>a</sup> 77 K and 1 bar; <sup>b</sup> Values are for reactivated samples.

## 4.4 Conclusions

In summary, the crystal structure of MOF-5 is very sensitive to the presence of water and the hydrogen uptake capability becomes compromised, *i.e.* the hydrogen uptake capability of MOF-5 drops to zero after exposure to ambient air (RH of 32-37%) for 1 day. Here we have demonstrated that by simply introducing one or two hydrophobic methyl (-CH<sub>3</sub>) functionalities on the BDC moiety, the MOF-5 structure

becomes significantly less sensitive to water without impairing the hydrogen uptake capacity. CH<sub>3</sub>-MOF-5 and DiCH<sub>3</sub>-MOF-5 show hydrogen uptake capacities of 1.42 wt% and 1.29 wt%, respectively. Their hydrogen uptake capacities can recover after 4 days exposure to ambient air (0.97 wt% for CH<sub>3</sub>-MOF-5 and 1.25 wt% for DiCH<sub>3</sub>-MOF-5) and are only reduced by 35% after 8 days exposure to ambient air. Since 2-methylterephthalic acid and 2,5-dimethylterephthalic acid are readily available, this opens a route towards commercially available moisture-stable MOFs.

## 4.5 References

- [1] Wong-Foy, A.G.; Matzger, A.J.; Yaghi, O.M. *J. Am. Chem. Soc.* **2006**, *128*, 3494.
- [2] Kaye, S.S.; Dailly, A.; Yaghi, O.M.; Long, J.R. *J. Am. Chem. Soc.* **2007**, *129*, 14176.
- [3] Dinca, M.; Han, W.S.; Liu, Y.; Dailly, A.; Brown, C.M.; Long, J.R. *Angew. Chem. Int. Ed.* **2007**, *46*, 1419.
- [4] Dinca, M.; Long, J.R. *J. Am. Chem. Soc.* **2007**, *129*, 11172.
- [5] Kùsgens, P.; Rose, M.; Senkovska, I.; Fröde, H.; Henschel, A.; Siegle, S.; Kaskel, S. *Microporous Mesoporous Mater.* **2009**, *120*, 325.
- [6] Liang, Z.; Marshall, M.; Chaffee, A.L. *Energy Fuels* **2009**, *23*, 2785.
- [7] Greathouse, J.A.; Allendorf, M.D. *J. Am. Chem. Soc.* **2006**, *128*, 10678.
- [8] Schrock, K.; Schroder, F.; Heyden, M.; Fischer, R.A.; Havenith, M. *Phys. Chem. Chem. Phys.* **2008**, *10*, 4732.
- [9] Park, K.S.; Ni, Z.; Cote, A.P.; Choi, J.Y.; Huang, R.; Uribe-Romo, F.J.; Chae, H.K.; O'Keeffe, M.; Yaghi, O.M. *PNAS* **2006**, *103*, 10186;
- [10] Huang, L.M.; Wang, H.T.; Chen, J.X.; Wang, Z.B.; Sun, J.Y.; Zhao, D.Y.; Yan, Y.S. *Microporous mesoporous Mater.* **2003**, *58*, 105.
- [11] Wu, T.J.; Shen, L.J.; Luebbbers, M.; Hu, C.; Chen, Q.M.; Ni, Z.; Masel, R.I. *Chem. Commun.* **2010**, 6120.
- [12] Nguyen, J.G.; Cohen, S.M. *J. Am. Chem. Soc.* **2010**, *132*, 4560.
- [13] Panella, B.; Hirscher, M.; Puetter, H.; Mueller, U. *Adv. Funct. Mater.* **2006**, *16*, 520.
- [14] Chen, B.; Wang, X.; Zhang, Q.; Xi, X.; Cai, J.; Qi, H.; Shi, S.; Wang, J.; Yuan, D.; Fang, M. *J. Mater. Chem.* **2010**, *20*, 3758.
- [15] Ma, S.; Eckert, J.; Forster, P.M.; Yoon, J.W.; Hwang, Y.K.; Chang, J.-S.; Collier, C.D.; Parise, J.B.; Zhou, H.-C. *J. Am. Chem. Soc.* **2008**, *130*, 15896.



# CHAPTER 5

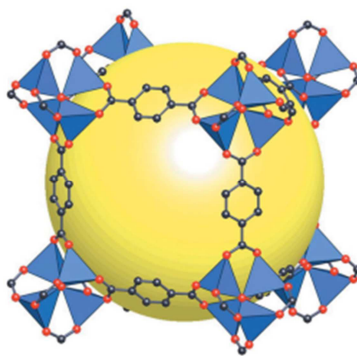
## **The metal-to-ligand ratio and the effect on the structure and hydrogen uptake capacity of MOF-5**

---

In this chapter, MOF-5 was synthesized using different zinc nitrate-to-terephthalic acid ratios. *N,N*-diethylformamide (DEF) was used as the solvent of choice and all samples were prepared at 100 °C. High quality MOF-5s with hydrogen uptake capacities of ~1.3 wt% were obtained when a zinc nitrate-to-terephthalic acid ratio of 2-4 was employed. Ratios below 2 give MOF-5s with a high level of impurities and a gradual drop in hydrogen uptake capacity was observed, whereas ratios above 4 give non-MOF-5 structures. In the latter case, the hydrogen uptake capacity drops instantaneously to 0.09 wt%.

## 5.1 Introduction

MOF-5, maybe one of the best-known metal organic frameworks, consists of  $\text{Zn}_4\text{O}$  clusters and 1,4-benzenedicarboxylate (BDC) linkers. Each  $\text{Zn}_4\text{O}$  cluster is attached to three BDC linkers to form a cubic repeating framework with a uniform  $\text{Zn}_4\text{O}(\text{BDC})_3$  composition. MOF-5, as shown in Scheme 5.1, is of interest because of its high porosity, outstanding thermal stability, and the ability to reversibly adsorb and desorb hydrogen (1.32 wt% at 1 bar [1]). This metal organic framework is attractive from a commercial point of view as well because it's easy to produce using cheap and readily available starting materials.[2-5]



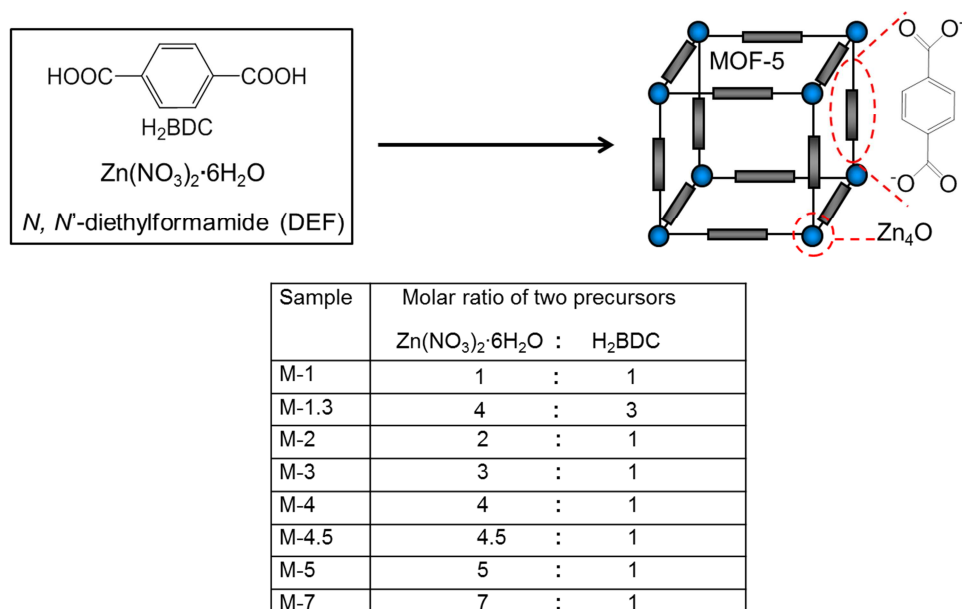
**Scheme 5.1.** The MOF-5 structure shown as  $\text{Zn}_4\text{O}_4$  tetrahedra (blue polyhedra) bridged by benzene dicarboxylate linkers (gray, C and red, O) to give an extended 3D cubic framework. The yellow sphere represents the largest sphere that can occupy the pores without penetrating the Van der Waals space of the framework. Reproduced from ref. [2b]. Copyright 2003, with permission from the American Association for the Advancement of Science.

MOF-5 can be prepared from zinc nitrate and terephthalic acid via various approaches, such as direct mixing, solvothermal, and sonochemical approaches. It is worth noting that different synthetic methods, and even within the same method, small changes in synthetic parameters affect the crystal quality, textural property and hydrogen adsorption capacity of MOF-5.[6-15] With respect to the conventional solvothermal method, the synthetic parameters, e.g. solvent, temperature, concentration and pH, could affect the structure of MOF-5 and hence the hydrogen adsorption characteristics.[12,16-22] Yang and co-workers found that a low terephthalic acid concentration ( $\leq 6 \text{ mmol L}^{-1}$ ) favors the formation of a non-interwoven MOF-5, where DMF was used as the sole solvent and the metal-ligand ratio was fixed at 3. While a high concentration ( $30\text{-}60 \text{ mmol L}^{-1}$ ) favors the interwoven MOF-5 form, resulting in an



enhancement in hydrogen uptake capacity over non-interwoven MOF-5 by ~70% due to the highly developed ultra-microporosity.[19] Kim and co-workers reported that a MOF-5 structure formed in DMF in the presence of melamine when the pH is 4.0-4.5. But at higher or lower pH ( $>5$  or  $\leq 3.5$ ), a non-MOF-5 structure resulted.[20] The water content during synthetic procedures has also been considered as a key factor. High quality MOF-5 could be obtained when the exposure to water and ambient air is minimized, which in turn results in a high hydrogen uptake capacity.[12] Therefore, in order to design MOFs with good hydrogen storage behavior, it is essential to understand how the synthetic variables affect crystal growth, crystal quality and the MOF porous structure.

MOF-5 can be synthesized in either *N,N*-dimethylformamide (DMF) or *N,N*-diethylformamide (DEF) as solvents via a solvothermal approach. Under similar conditions, the crystal quality of MOF-5 synthesized in DMF is lower than that of MOF-5 synthesized in DEF. It is known from the literature that most synthetic procedures call for an excess  $\text{Zn}^{2+}$  for the synthesis of MOF-5.[10] Chen and co-workers investigated the effect of the ratio of zinc nitrate-to-terephthalic acid on the formation of MOF-5 in DMF. The authors found that MOF-5 can be synthesized in DMF in the presence of water when the ratio of zinc nitrate-to-terephthalic acid is in the range of 1.3-2.7, whereas, lower ratios (0.7-1) result in a non-MOF-5 structure. The ratio of zinc nitrate-to-terephthalic acid employed in DEF is normally fixed at about 3 for the synthesis of MOF-5. To the best of our knowledge, the impact of the zinc nitrate-to-terephthalic acid ratio on the formation of MOF-5 in DEF has not been investigated before. In this chapter, we will discuss the synthesis of a MOF-5 series where we vary the zinc nitrate-to-terephthalic acid ratio in DEF, as shown in Scheme 5.2. The effect of the zinc nitrate-to-terephthalic acid ratio on the structure and hydrogen adsorption property of MOF-5 will be discussed.



**Scheme 5.2.** The synthesis of MOF-5 by varying the molar ratios of zinc nitrate-to-terephthalic acid.

## 5.2 Experimental

### 5.2.1 Materials

Zinc nitrate hexahydrate ( $\text{Zn}(\text{NO}_3)_2 \cdot 6\text{H}_2\text{O}$ , 98 %, Aldrich) and terephthalic acid ( $\text{H}_2\text{BDC}$ ) (>99%, BP Chembel) were used as received. *N,N*-diethylformamide (DEF, 99 %, Acros) and chloroform ( $\text{CHCl}_3$ ) were dried over and distilled from calcium hydride ( $\text{CaH}_2$ ) and phosphorus pentoxide ( $\text{P}_2\text{O}_5$ ), respectively, before use.

### 5.2.2 Synthesis of MOF-5 by varying the zinc nitrate-to-terephthalic acid ratio

A 100 mL flask charged with desired amounts of  $\text{Zn}(\text{NO}_3)_2 \cdot 6\text{H}_2\text{O}$ , terephthalic acid ( $\text{H}_2\text{BDC}$ ), and DEF was placed into a pre-heated oven at 100 °C for 48 h. The hot solution was decanted. The product was washed with DEF (10 mL) for 24 h (2×), followed by immersing the crystals in  $\text{CHCl}_3$  (20 mL) for 24 h (3×). The solvent-exchanged product was vacuum dried at 160 °C for 24 h and stored in a glove box. The amount of reagents and products are listed in Table 5.1. In all reaction mixtures, except

for the concentration of zinc nitrate hexahydrate, other synthetic parameters were kept constant, *i.e.* the pH value of solution (pH $\approx$ 4.9), temperature (100 °C), reaction time (48 h) and the concentration of terephthalic acid ( $33.5\times 10^{-3}$  M). The resulting products were labeled M-1, M-1.3, M-2, M-3, M-4, M-4.5, M-5 and M-7 according to the molar ratios of 1:1, 4:3, 2:1, 3:1, 4:1, 4.5:1, 5:1 and 7:1.

**Table 5.1.** Reagent ratios and product yields (after activation).

| Sample | Ratio | Concentration of<br>$\text{Zn}(\text{NO}_3)_2\cdot 6\text{H}_2\text{O}$<br>(mmol L <sup>-1</sup> ) | Concentration of<br>$\text{H}_2\text{BDC}$<br>(mmol L <sup>-1</sup> ) | Yield*<br>(g) |
|--------|-------|--|---|---------------|
| M-1    | 1:1   | 33.6   | 33.5  | 0.25          |
| M-1.3  | 4:3   | 44.8   | 33.4  | 0.26          |
| M-2    | 1:2   | 67.2   | 33.5  | 0.28(54%)*    |
| M-3    | 1:3   | 100.7  | 33.5  | 0.21(41%)*    |
| M-4    | 1:4   | 134.3  | 33.5  | 0.18(35%)*    |
| M-4.5  | 1:4.5 | 151.0  | 33.4  | 0.21          |
| M-5    | 1:5   | 168.2  | 33.5  | 0.21          |
| M-7    | 1:7   | 234.0  | 33.5  | 0.20          |

\* The values in brackets are yields calculated based on MOF-5 formula ( $\text{Zn}_4\text{O}(\text{C}_8\text{H}_4\text{O}_4)_3$ ). The yields in weight percentage of M-1, M-1.3, M-4.5, M-5 and M-7 could not be calculated due to their impure structures.

### 5.2.3 Characterization

XRD patterns of all samples were recorded on an X'Pert X-ray diffractometer operated at 45 kV and 40 mA with monochromated Cu K $\alpha$  radiation within a 2-theta range of 5-60°. The sample was placed into an air-tight sample holder in order to prevent air and moisture exposure. IR spectra of the samples were collected on a PerkinElmer Spectrum 100 FT-IR Spectrometer. TG curves of samples were obtained on a PerkinElmer Pyris Diamond Thermogravimetric Differential Thermal/Analyzer. Samples were investigated from room temperature to 600 °C with a heating rate of 10 °C min<sup>-1</sup> under a dry air flow. Elemental analyses were performed on a Thermo Scientific InterScience Flash 2000 Organic Elemental Analyzer. The textural properties, including BET surface area and pore volume, were recorded on a Micromeritics ASAP 2010 adsorption analyzer at 77 K. Prior to the adsorption measurements, the samples were

degassed *in-situ* in vacuum at 135 °C. The dead volume of the sample cell was determined in a separate experiment. *In situ* pretreatment coupled to a separate dead volume measurement after the analysis was employed in order to avoid the helium entrapment phenomenon. The weight of samples obtained after the pretreatment was used in calculations. BET surface areas were calculated in the adapted pressure range of  $P/P_0=0.01-0.1$ . Hydrogen storage measurements at different pressures were performed on a home-made Sievert's setup at 77 K. Samples were heated up to 150 °C overnight under high vacuum ( $10^{-6}$  mbar) prior to the measurements. Hydrogen (ultra-high-purity grade, 99.999%) was additionally purified by leading it over a bed of zeolite spheres at 77 K before being loaded in the sample holder. The pressure change was monitored and recorded after the hydrogen reservoir was connected to the sample holder. The samples were weighed in a glove box after the measurement for calculating the hydrogen uptake capacity. The amount of hydrogen stored in the dead volume was examined at low pressures (<2 bar) with sea sand as a reference.

## 5.3 Results and discussion

### 5.3.1 Structural and compositional characterization

**XRD patterns.** All samples were characterized by powder X-ray diffraction (PXRD) and the obtained PXRD patterns are shown in Figure 5.1. All peak positions in the PXRD patterns of M-1, M-1.3, M-2, M-3 and M-4 are consistent with the crystal structure of MOF-5.[23] Meanwhile, a significant variation in the peak intensity was observed. The peak intensities for M-2, M-3 and M-4, especially for the typical peaks at 6.9°, 9.7° and 13.7°, are higher than those of M-1 and M-1.3, suggesting that the qualities of the crystal structure for M-2, M-3 and M-4 are higher than that of M-1 and M-1.3. When the ratio was increased to 4.5, a poor and different PXRD pattern was obtained. The diffraction peak intensity decreased dramatically. Although the peaks at 6.9° and 13.7° are still visible, new peaks at 7.2° and 8.8° have appeared. The diffraction peaks at 7.2° and 8.8° can be assigned to  $\text{Zn}_5(\text{OH})_4(\text{BDC})_3$ . [22,24] This indicates that only a small fraction of MOF-5 structure is present in M-4.5. By increasing the ratio further to 5 or 7, the diffraction peaks at 6.9° and 13.7° have disappeared altogether and the peaks at 7.2° and 8.8° are still present, implying a non-MOF-5 structure. These results are a strong indication that the MOF-5 structure forms when the ratio of zinc nitrate-to-terephthalic acid is  $\leq 4$ . When a zinc nitrate-to-terephthalic acid ratio of 4.5 or higher was employed, the MOF-5 structure can no longer be formed. As reported by Rosi et al., addition of water to the reaction solution (DEF as a solvent) suppresses the formation of MOF-5.[25]

Therefore, we consider that the higher water content in the reaction mixture by increasing the amount of  $\text{Zn}(\text{NO}_3)_2 \cdot 6\text{H}_2\text{O}$  might be the reason why we observed non-MOF-5 structures for M-5 and M-7. In order to confirm this, we added a pre-calculated amount of water to a reaction mixture of M-4, resulting in a water content equal to that of the reaction mixture of M-7. As expected, the obtained structure is the same as M-7. This result confirms that a high water content has an adverse effect on the formation of MOF-5. Under the reaction conditions we applied, MOF-5 cannot be obtained when the water concentration is higher than  $0.9 \text{ mol L}^{-1}$ .

Subtle differences can be observed in the normalized PXRD patterns of M-1, M-1.3, M-2, M-3 and M-4 (Figure 5.2). A simulated PXRD pattern of MOF-5 is also included in Figure 5.2 for reference purposes. The ratios of the peak intensity ( $13.8^\circ/6.9^\circ$ ) for M-1, M-1.3, M-2, M-3 and M-4 are higher than the simulated data, indicating the presence of an interpenetrated structure.[10] A broad peak at  $\sim 10.1^\circ$  in very low intensity was observed for M-1 and M-1.3, which is absent in the patterns of M-2, M-3 and M-4. This peak was also observed in a PXRD pattern of a reported MOF-5 sample, which was synthesized under similar conditions, but the authors did not mention this diffraction peak.[10] Since we also found yellow needle-like crystals in M-1 and M-1.3 in addition to cubic crystals (M-2, M-3 and M-4 only form cubic crystals), this additional peak may be assigned to the yellow crystals. Moreover, a larger fraction of this yellow product was found for M-1 as compared with M-1.3. We isolated the yellow solid from M-1 and examined the structure by PXRD. The poor pattern, as shown in Figure 5.3, implies that the yellow solid is amorphous. The result reveals that a pure MOF-5 structure could not be achieved when low ratios of zinc nitrate-to- $\text{H}_2\text{BDC}$  were employed in the reaction mixture, *i.e.* 1 and 1.3. The yellow solid was difficult to isolate from the desired product, as indicated by the presence of the typical diffraction peak of MOF-5 ( $9.8^\circ$ ) in the PXRD pattern (Figure 5.3). Therefore, we could neither quantify the MOF-5/side product ratio nor determine the composition of the yellow solid.

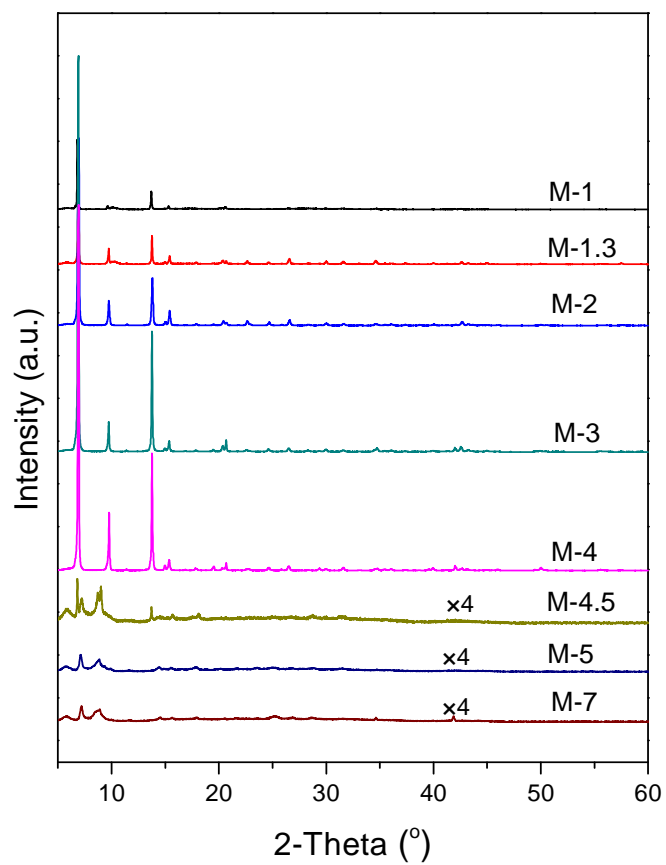


**Figure 5.1.** PXRD patterns of M-1, M-1.3, M-2, M-3, M-4, M-4.5, M-5 and M-7.

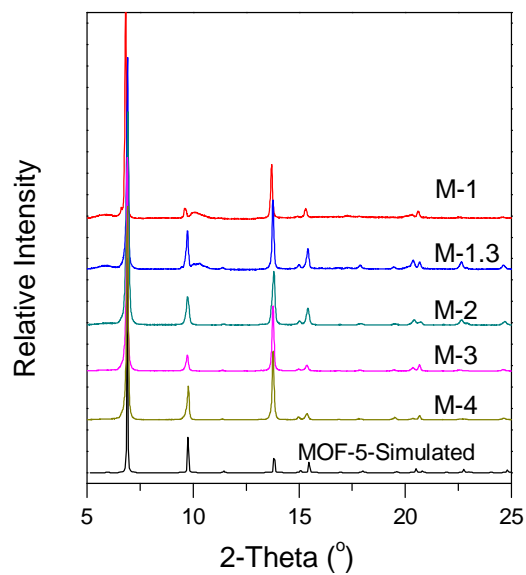


**Figure 5.2.** Normalized PXRD patterns of M-1, M-1.3, M-2, M-3 and M-4. The simulated MOF-5 PXRD pattern is shown for reference purposes.

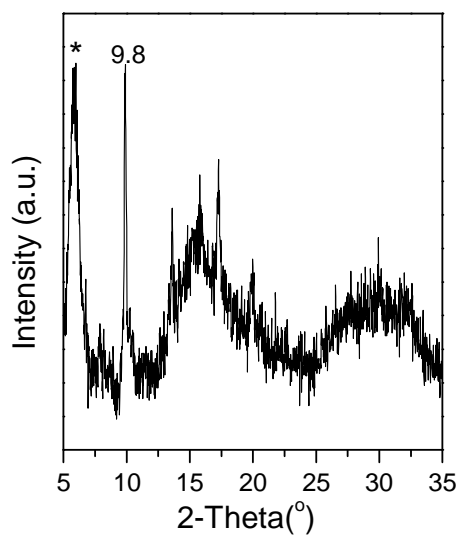


**Figure 5.3.** PXRD pattern of the yellow solid in M-1. The peak marked with an asterisk is from the sample holder.

**FT-IR spectra.** FT-IR spectra of all samples are shown in Figure 5.4. The absence of the absorption of protonated terephthalate (BDC) in the range of 1715-1680  $\text{cm}^{-1}$  for all samples confirms a complete deprotonation of  $\text{H}_2\text{BDC}$ . [17] The expected strong characteristic absorptions for the asymmetric and symmetric stretching vibrations of BDC (1611  $\text{cm}^{-1}$  and 1393  $\text{cm}^{-1}$ ) are present in the spectra of M-1, M-1.3, M-2, M-3 and M-4. Significant changes were found in the FT-IR spectra of M-4.5, M-5 and M-7 synthesized using the higher ratios of zinc nitrate-to-terephthalic acid ( $\geq 4.5$ ). The bands at 1611  $\text{cm}^{-1}$ , 1393  $\text{cm}^{-1}$  and the shoulder at 1435  $\text{cm}^{-1}$  disappeared. The band at 1557  $\text{cm}^{-1}$  became strong and a new band at 1377  $\text{cm}^{-1}$  related to  $\text{COO}^-$  appeared. These changes indicate the different coordination environment of  $\text{COO}^-$  for the samples prepared using the high ratios of zinc nitrate-to-terephthalic acid ( $\geq 4.5$ ). Moreover, the broad peak (3200-3500  $\text{cm}^{-1}$ ) suggests the existence of adsorbed water. Furthermore, a visible band at 3615  $\text{cm}^{-1}$  can be attributed to the hydroxyl vibration band of the strongly bond water. [17]

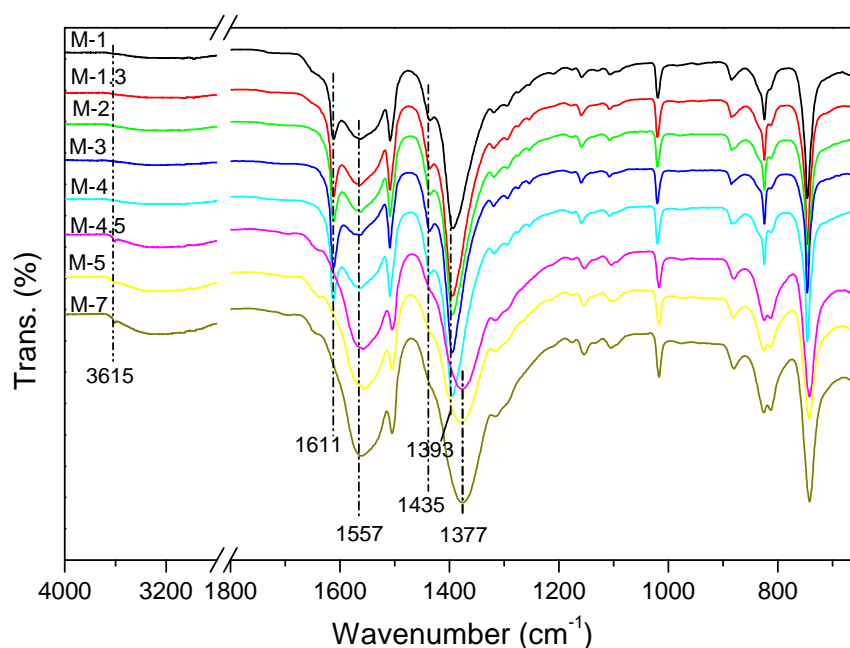


**Figure 5.4.** FT-IR spectra of M-1, M-1.3, M-2, M-3, M-4, M-4.5, M-5 and M-7.

**Thermogravimetric analysis.** All samples were examined by thermogravimetric analysis under a dry air flow (Figure 5.5). No pronounced weight loss



step was observed below 350 °C in the thermograms of M-2, M-3 and M-4, implying an effective activation. This can also be corroborated by the absence of nitrogen (N) (elemental analysis results; Table 5.2). The release of water and DEF were observed (6-7 wt%) for M-4.5, M-5 and M-7. M-1 and M-1.3 showed pronounced weight loss steps (~9% and ~6%) in the range of 150 °C to 350 °C, which are related to DEF removal. Supposing that the N content (1.63% for M-1 and 1.20% for M-1.3) obtained from elemental analysis is only attributed to DEF, M-1 and M-1.3 should contain 12% and 7% of DEF. However, the values are 3% and 1% higher than the values obtained from the TGA curves. This indicates that the side product (yellow solid) also contributes to the N content in addition to DEF.

Based on the TGA curves, we estimated the weight loss attributed to the decomposition of the organic linkers. The weight loss for M-2, M-3 and M-4 (58.4%, 57.6% and 57.9%) are consistent with the theoretical value (57.8%) calculated from the MOF-5 formula ( $\text{Zn}_4\text{C}_{24}\text{H}_{12}\text{O}_{13}$ ). The weight loss for M-1, M-1.3, M-4.5, M-5 and M-7 are 61.3%, 60.2%, 54.9%, 55.6% and 55.6%, which are inconsistent with the theoretical values for these five samples. This result indicates the presence of a side product (yellow solid) in M-1 and M-1.3 and non-MOF-5 structures for M-4.5, M-5 and M-7, which can also be supported by the discrepancies between the experimental and theoretical elemental analysis results, as shown in Table 5.2. The lower carbon (C) contents and higher hydrogen (H) contents of M-2, M-3 and M-4 as compared to the theoretical values of MOF-5 are the result of water adsorbed from ambient air during elemental analyses.

**Specific surface area and pore volume.** M-2, M-3 and M-4 showed almost identical specific surface areas and pore volumes (~3050 m<sup>2</sup> g<sup>-1</sup> and 1.29 cm<sup>3</sup> g<sup>-1</sup>), which is significantly higher than that of the other samples examined. The specific surface area and pore volume of M-1.3 is about three times higher than that of M-1 (1697 m<sup>2</sup> g<sup>-1</sup> vs. 477 m<sup>2</sup> g<sup>-1</sup> and 0.71 cm<sup>3</sup> g<sup>-1</sup> vs. 0.21 cm<sup>3</sup> g<sup>-1</sup>), which can be explained by a larger fraction of MOF-5 structure in M-1.3. Very low surface areas (7~35 m<sup>2</sup> g<sup>-1</sup>) and pore volumes (0.01~0.02 cm<sup>3</sup> g<sup>-1</sup>) were found for M-4.5, M-5 and M-7, indicating their poor porous structures.

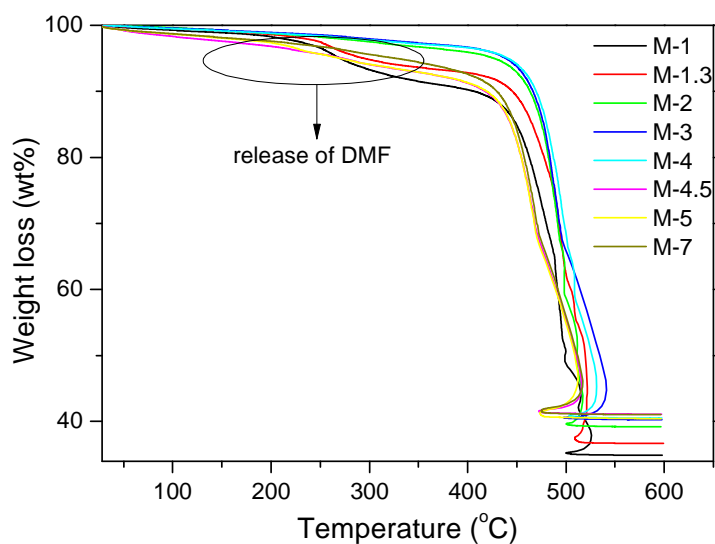


**Figure 5.5.** TGA curves of M-1, M-1.3, M-2, M-3, M-4, M-4.5, M-5 and M-7 analysed under a dry air flow.

**Table 5.2.** Elemental results and textural properties of all samples (MOF-5 is included for reference purposes).

| Sample | C (%) | H (%) | N (%) | $S_{\text{bet}}$ ( $\text{m}^2 \text{g}^{-1}$ ) | $V_{\text{ptotal}}$ ( $\text{cm}^3 \text{g}^{-1}$ ) |
|--------|-------|-------|-------|---|---|
| MOF-5  | 37.5  | 1.56  | 0     | 2885*   | 1.18*   |
| M-1    | 41.6  | 3.45  | 1.63  | 477   | 0.21  |
| M-1.3  | 40.8  | 2.80  | 1.20  | 1697  | 0.71  |
| M-2    | 36.1  | 1.91  | 0     | 3059  | 1.29  |
| M-3    | 35.0  | 1.98  | 0.01  | 3039  | 1.29  |
| M-4    | 37.2  | 1.80  | 0     | 3070  | 1.29  |
| M-4.5  | 34.2  | 2.35  | 0.25  | 34  | 0.02  |
| M-5    | 34.2  | 2.30  | 0.35  | 26  | 0.02  |
| M-7    | 34.5  | 2.37  | 0.27  | ~7  | 0.01  |

\* The values are reported in ref.[26].

### 5.3.2 Hydrogen storage property

The hydrogen uptake capacities of all samples in the low-pressure range (0-2 bar) are shown in Figure 5.6. M-2, M-3 and M-4 displayed similar hydrogen uptake capacities at 77 K and 1 bar (in the range of 1.24-1.31 wt%), which is in agreement with reported values.[1] Moreover, their hydrogen uptake capacities are higher than that of other samples in the whole pressure range studied. M-1, M-1.3, M-4.5, M-5 and M-7 gave hydrogen uptake capacities of 0.44 wt%, 0.74 wt%, 0.21 wt%, 0.20 wt% and 0.09 wt% at 77 K and 1 bar, respectively. The hydrogen uptake capacities of all samples showed the same trend as the purity of the MOF-5 phase, *i.e.*  $M-2 \approx M-3 \approx M-4 > M-1.3 > M-1 > M-4.5 \approx M-5 > M-7$ . The high hydrogen uptake capacities of M-2, M-3 and M-4 can be attributed to the pure MOF-5 structure. The lower hydrogen uptake capacities of M-1.3 and M-1 can be explained by the presence of a yellow amorphous side product, which does not contribute to the hydrogen adsorption. A larger fraction of the amorphous phase in M-1 results in a lower hydrogen uptake capacity as compared to M-1.3. Hydrogen uptake capacities for M-4.5, M-5 and M-7 (0.09-0.21 wt%) are the result of their non-MOF-5 structure with very poor porosity.

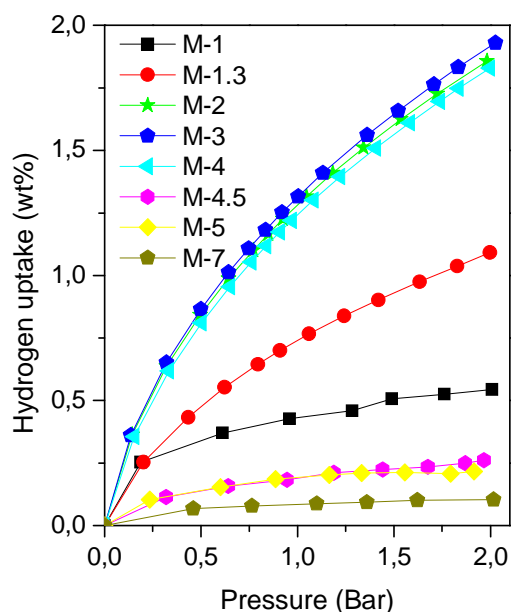


**Figure 5.6.** Low-pressure hydrogen adsorption isotherms of M-1, M-1.3, M-2, M-3, M-4, M-4.5, M-5 and M-7.

To explore the effect of the ratio of zinc nitrate-to-terephthalic acid on the formation of MOF-5 in *N,N*-diethylformamide (DEF), we synthesized MOF-5 by varying the concentration of  $\text{Zn}(\text{NO}_3)_2 \cdot 6\text{H}_2\text{O}$  in the starting DEF solution while fixing other parameters, *i.e.* the pH value of solution ( $\text{pH} \approx 4.9$ ), temperature ( $100^\circ\text{C}$ ), reaction time (48 h) and the concentration of terephthalic acid ( $33.5 \times 10^{-3} \text{ M}$ ). The results reveal that the ratio of  $\text{Zn}(\text{NO}_3)_2 \cdot 6\text{H}_2\text{O}$ -to-terephthalic acid does affect the formation of a MOF-5 structure and hence the hydrogen adsorption capability. MOF-5 formed along with the formation of a yellow amorphous side product when the ratios are 1 and 1.3. The presence of the impurity leads to lower surface areas, lower pore volumes and lower hydrogen uptake capacities. When the ratio is in the range of 2-4, a high quality MOF-5 can be obtained which showed a high surface area, high pore volume and maximum hydrogen uptake capacity. However, a non-MOF-5 structure formed when the ratio exceeds 4, and low surface areas and poor hydrogen uptake capacities were found for the obtained products (Figure 5.7). It is conceivable that a high water concentration ( $>0.9 \text{ mol L}^{-1}$ ), which is from a large amount of  $\text{Zn}(\text{NO}_3)_2 \cdot 6\text{H}_2\text{O}$  employed, suppresses the formation of MOF-5. Based on our results, the optimal ratio of zinc nitrate-to-terephthalic acid is in the range of 2 to 4 for synthesizing MOF-5 in DEF.

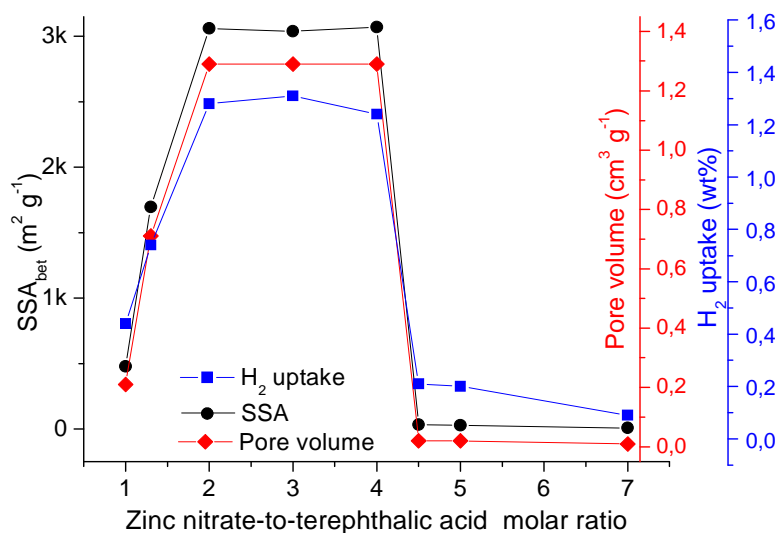


**Figure 5.7.** Surface areas, pore volumes and hydrogen adsorption capacities (77 K and 1 bar) of M-1, M-1.3, M-2, M-3, M-4, M-4.5, M-5 and M-7.

## 5.4 Conclusions

A MOF-5 series was prepared by varying the zinc nitrate ( $\text{Zn}(\text{NO}_3)_2 \cdot 6\text{H}_2\text{O}$ )-to-terephthalic acid ( $\text{H}_2\text{BDC}$ ) ratio in the starting reaction mixture. The crystal structure development and related properties such as specific surface area, pore volume and hydrogen uptake capacity were investigated. When low ratios ( $<2$ ) were applied, MOF-5 compounds were obtained with a high concentration of impurities, which resulted in a reduced hydrogen uptake capacity. High quality MOF-5 could be obtained by employing a zinc nitrate-to-terephthalic acid ratio of 2 to 4. In this range, all MOFs exhibited a high specific surface area, high pore volume and a maximum hydrogen storage capacity (1.24–1.31 wt%). However, MOF-5 did not form when the zinc nitrate-to-terephthalic acid ratio exceeds 4.5. Our results show unambiguously that the zinc nitrate-to-terephthalic acid ratio is in fact not very critical when MOF-5 is synthesized in DEF via a solvothermal approach (at 100 °C for 48 hrs).

## 5.5 References

- [1] Rowsell, J.L.C.; Millward, A.R.; Park, K.S.; Yaghi, O.M. *J. Am. Chem. Soc.* **2004**, *126*, 5666.
- [2] (a) Li, H.; Eddaoudi, M.; O'Keeffe, M.; Yaghi, O.M. *Nature* **1999**, *402*, 276. (b) Rosi, N.L.; Eckert, J.; Eddaoudi, M.; Vodak, D.T.; Kim, J.; O'Keeffe, M.; Yaghi, O.M. *Science* **2003**, *300*, 1127.
- [3] Czaja, A.U.; Trukhan, N.; Muller, U. *Chem. Soc. Rev.* **2009**, *38*, 1284.
- [4] Murray, L.J.; Dinca, M.; Long, J.R. *Chem. Soc. Rev.* **2009**, *38*, 1294.
- [5] Tranchemontagne, D.J.; Hunt, J.R.; Yaghi, O.M. *Tetrahedron* **2008**, *64*, 8553.
- [6] Dailly, A.; Vajo, J.J.; Ahn, C.C. *J. Phy. Chem. B* **2006**, *110*, 1099.
- [7] Panella, B.; Hischer, M. *Adv. Mater.* **2005**, *17*, 538.
- [8] Wong-Foy, A.G.; Matzger, A.J.; Yaghi, O.M. *J. Am. Chem. Soc.* **2006**, *128*, 3494.
- [9] Dybtsev, D.N.; Chun, H.; Kim, K. *Angew. Chem. Int. Ed.* **2004**, *43*, 5033.
- [10] Chen, B.; Wang, X.; Zhang, Q.; Xi, X.; Cai, J.; Qi, H.; Shi, S.; Wang, J.; Yuan, D.; Fang, M. *J. Mater. Chem.* **2010**, *20*, 3758.
- [11] Buso, D.; Nairn, K.M.; Gimona, M.; Hill, A.J.; Falcaro, P. *Chem. Mater.* **2011**, *23*, 929.
- [12] Kaye, S.S.; Dailly, A.; Yaghi, O.M.; Long, J.R. *J. Am. Chem. Soc.* **2007**, *129*, 14176.
- [13] Xin, Z.; Bai, J.; Pan, Y.; Zaworotko, M.J. *Chem. Eur. J.* **2010**, *16*, 13049.
- [14] Lu, C.-M.; Liu, J.; Xiao, K.; Harris, A.T. *Chem. Eng. J.* **2010**, *156*, 465.
- [15] Son, W.-J.; Kim, J.; Kim, J.; Ahn, W.-S. *Chem. Commun.* **2008**, 6336.
- [16] Saha, D.; Deng, S.; Yang, Z. *J. Porous Mater.* **2009**, *16*, 141.

- [17] Huang, L.; Wang, H.; Chen, J.; Wang, Z.; Sun, J.; Zhao, D.; Yan, Y. *Microporous Mesoporous Mater.* **2003**, *58*, 105.
- [18] Zhao, Z.; Xia, Q.; Li, Z. *Separation Science and Technology* **2011**, *46*, 1337.
- [19] Yang, S.J.; Cho, J.H.; Lee, K.; Kim, T.; Park, C.R. *Chem. Mater.* **2010**, *22*, 6138.
- [20] Kim, H.; Das, S.; Kim, M.G.; Dybtsev, D.N.; Kim, Y.; Kim, K. *Inorg. Chem.* **2011**, *50*, 3691.
- [21] Blanita, G.; Lupu, D.; Lazar, M.; Biris, A.R.; Pascalau, V.; Ardelean, O.; Coldea, I.; Misan, I.; Popeneciu, G.; Vlassa, M. *Journal of Physics: Conference Series* **2009**, *182*, 12047.
- [22] Liao J.-H.; Lee, T.-J.; Su, C.-T. *Inorg. Chem. Commun.* **2006**, *9*, 201.
- [23] Panella, B.; Hirscher, M.; Puetter, H.; Mueller, U. *Adv. Funct. Mater.* **2006**, *16*, 520.
- [24] Hausdorf, S.; Wagler, J.; Mossig, R.; Mertens, F.O.R.L. *J. Phys. Chem. A* **2008**, *112*, 7567.
- [25] Rosi, N.L.; Kim, J.; Eddaoudi, M.; Chen, B.; O'Keeffe, M.; Yaghi, O.M. *J. Am. Chem. Soc.* **2005**, *127*, 1504.

# CHAPTER 6

## **Synthesis and characterization of MOFs comprised of short organic linkers**

---

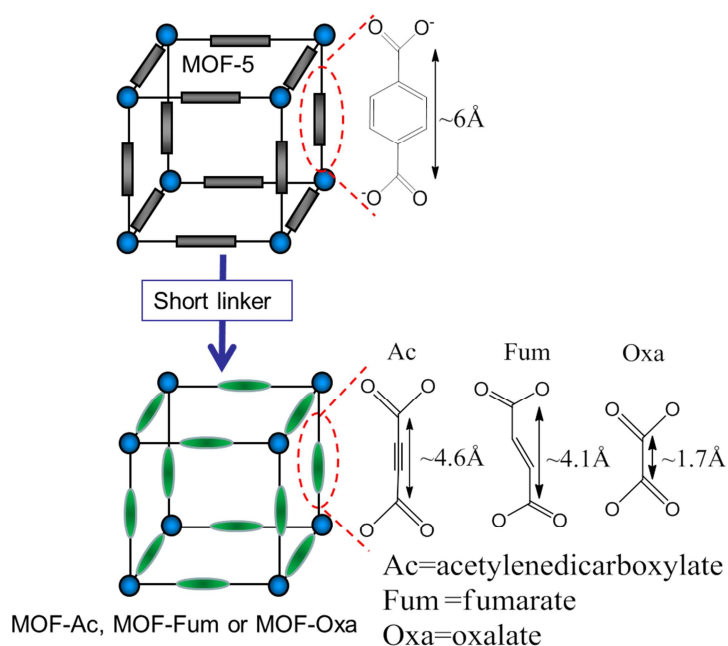
In this chapter we present the synthesis and hydrogen adsorption properties of MOFs constructed from three short linkers, *i.e.* acetylenedicarboxylate (Ac), fumarate (Fum) and oxalate (Oxa). The MOF constructed from fumarate shows the same topology as MOF-5 and exhibits a hydrogen uptake capacity of 0.93 wt% at 77 K and 1 bar. The MOF built from acetylenedicarboxylate displays a MOF-5 type structure but shows no hydrogen uptake due to the blocked pores. We were unsuccessful in obtaining a metal organic framework by reacting oxalic acid with  $\text{Zn}^{2+}$ .

## 6.1 Introduction

Metal organic frameworks (MOFs) have attracted much research attention because of their potential use in gas sorption, catalysis and gas separation applications. With respect to hydrogen storage, MOFs have been considered as promising candidates due to their fast kinetics, complete reversibility and functionality. A large number of porous MOFs have been designed and synthesized over the past decade.[1-7] Meanwhile, increasing effort has also been made in understanding the relationship between hydrogen molecules and the MOF structures because it is crucial towards the design of novel MOFs with high hydrogen uptake capacities.

The adsorption sites of hydrogen molecules in MOF-5 have been intensively investigated experimentally and theoretically.[8-11] Previous studies have confirmed that the  $\text{Zn}_4\text{O}$  cluster in MOF-5 is responsible for most of the hydrogen adsorption, and the organic linker plays a secondary role.[12,13] Therefore, it would be reasonable to assume that increasing the density of  $\text{Zn}_4\text{O}$  clusters per unit volume will enhance the interaction strength. When the  $\text{Zn}_4\text{O}$  clusters become close enough, an adsorbed hydrogen molecule is expected to interact with more neighboring  $\text{Zn}_4\text{O}$  clusters, leading to an increased interaction strength and improved hydrogen adsorption capacity.[14] Several strategies can be used to increase the  $\text{Zn}_4\text{O}$  cluster density, such as achieving interpenetrated structures and employing short rod-like ligands. Generally, an interpenetrated structure can be achieved when long and flexible ligands are used. The degree of interpenetration, however, is difficult to control. In this chapter, we will describe our attempt to synthesize MOF-5 analogs (iso-reticular MOFs, IRMOFs) with a high  $\text{Zn}_4\text{O}$  cluster density using three short diacid moieties, as shown in Scheme 6.1. The spacer length in MOF-5 is typically 6 Å, and by replacing the benzene ring with acetylene, ethylene or by using oxalate, the spacer length is reduced to 4.6, 4.1 and 1.7 Å, respectively. Doing so constitutes an increase in  $\text{Zn}_4\text{O}$  cluster concentration (weight percentage) of 24, 25 and 42% (*i.e.* 50%, 57% and 140% increase in the  $\text{Zn}_4\text{O}$  cluster density per unit volume) as compared to MOF-5. Whether a high  $\text{Zn}_4\text{O}$  cluster density can be realized and in addition is favorable with respect to the hydrogen storage capability will be investigated.





**Scheme 6.1.** Structures of IRMOFs with three short organic linkers, *i.e.* acetylenedicarboxylate (Ac), fumarate (Fum) and oxalate (Oxa).

## 6.2 Experimental

### 6.2.1 Materials

Zinc nitrate hexahydrate ( $\text{Zn}(\text{NO}_3)_2 \cdot 6\text{H}_2\text{O}$ , 98%, Aldrich), zinc acetate dehydrate ( $\text{Zn}(\text{C}_2\text{O}_2\text{H}_3)_2 \cdot 2\text{H}_2\text{O}$ , Sigma), zinc oxide (ZnO, Sigma), oxalic acid ( $\text{C}_2\text{H}_2\text{O}_4$ , Sigma), fumaric acid ( $\text{C}_4\text{H}_4\text{O}_4$ , Sigma), acetylenedicarboxylic acid ( $\text{C}_4\text{H}_2\text{O}_4$ , Sigma), sodium metasilicate pentahydrate (>97%, Sigma), and triethylamine (TEA, Aldrich) were purchased from commercial sources and used without further purification. *N,N*-diethylformamide (DEF, Acros) and *N,N*-dimethylformamide (DMF, Acros) were dried over and distilled from calcium hydride ( $\text{CaH}_2$ ). Dichloromethane ( $\text{CH}_2\text{Cl}_2$ ) and chloroform ( $\text{CHCl}_3$ ) were dried over and distilled from phosphorus pentoxide ( $\text{P}_2\text{O}_5$ ) prior to use.

### 6.2.2 Synthesis of MOFs using short ligands

**Synthesis of MOF constructed from acetylenedicarboxylate (MOF-Ac).** 0.093 g (0.88 mmol) of acetylenedicarboxylic acid and 0.121 g (0.41 mmol) of  $\text{Zn}(\text{NO}_3)_2 \cdot 6\text{H}_2\text{O}$  were dissolved in 10 mL of ethanol. The acetylenedicarboxylic acid

solution was added carefully to a 20 mL vial charged with the  $\text{Zn}(\text{NO}_3)_2 \cdot 6\text{H}_2\text{O}$  solution. The vial was further placed into a 40 mL vial containing triethylamine/ethanol (0.2 mL/4.0 mL). The larger vial was sealed and the smaller vial was kept open. The vials were left undisturbed at room temperature for 15 days, after which a white precipitate formed in the 20 mL vial. The precipitate was washed with ethanol (10 mL $\times$ 2) and  $\text{CHCl}_3$  (10 mL), and evacuated at 55 °C overnight. The resulting product (0.12 g) was stored in a glove box and labeled as MOF-Ac. Elemental analysis (EA): Calc. for  $\text{Zn}_4\text{O}(\text{C}_4\text{O}_4)_4(\text{Et}_3\text{N})_6$ : C, 46.9%, H, 6.77%, N, 6.30%. Found C, 47.3%, H, 6.47%, N, 5.13%. FT-IR ( $\text{cm}^{-1}$ ): 3060, 2983, 1601, 1463, 1312, 1166, 1055, 1010, 843, 775, 673.

**Synthesis of MOF constructed from fumarate (MOF-Fum).** 3.09 g (10.4 mmol) of  $\text{Zn}(\text{NO}_3)_2 \cdot 6\text{H}_2\text{O}$ , 0.37 g (3.12 mmol) of fumaric acid and 50 mL of *N,N*-dimethylformamide (DMF) were added to a two-neck flask equipped with a condenser. The clear solution was heated at 115 °C for 24 h. The white precipitate was washed with DMF (30 mL $\times$ 3) and  $\text{CHCl}_3$  (30 mL $\times$ 3), and vacuum dried at 70 °C overnight. The product (0.93 g) was stored in a glove box and labeled as MOF-Fum-DMF. FT-IR ( $\text{cm}^{-1}$ ): 3092, 3873, 1536, 1456, 1409, 1376, 1237, 984, 798, 718.

We also synthesized a MOF constructed from fumarate by following a reported procedure.[15]  $\text{Zn}(\text{NO}_3)_2 \cdot 6\text{H}_2\text{O}$  (0.286 g, 0.96 mmol), fumaric acid (0.116 g, 1.0 mmol) and 100 mL of DEF were added to a 500 mL flask. The flask was placed into a pre-heated oven at 100 °C for 24 h, after which the hot mother liquid was decanted. Yellow crystals were washed with DEF (40 mL $\times$ 3) and followed by immersing the crystals in  $\text{CH}_2\text{Cl}_2$  (40 mL) for 24 h (3 $\times$ ). The product was dried at 130 °C under vacuum for 24 h. The resulting sample was labeled as MOF-Fum-DEF and stored in a glove box (50 mg, 24% yield). Elemental analysis (EA): Calc. for  $\text{Zn}_4\text{O}(\text{C}_4\text{H}_2\text{O}_4)_3$ : C, 23.3%, H, 0.1%. Found C, 22.7%, H, 2.03%, N, 0.27%. FT-IR ( $\text{cm}^{-1}$ ): 3252, 1614, 1550, 1389, 1210, 1110, 977, 898, 797, 685.

**Synthesis of MOF constructed from oxalate (MOF-Oxa).** MOF-Oxa was approached using four different synthetic procedures:

**Procedure I.**  $\text{Zn}(\text{NO}_3)_2 \cdot 6\text{H}_2\text{O}$  (1.380 g, 4.6 mmol), oxalic acid (0.14 g, 1.5 mmol) and 40 mL of DMF were added to a two-neck flask equipped with a condenser. A white precipitation formed rapidly and the mixture was heated at 70 °C for 21 h. The product was collected and washed with DMF (30 mL $\times$ 3) and  $\text{CHCl}_3$  (30 mL $\times$ 3), and dried at 50 °C overnight under a nitrogen flow. The sample (0.21 g, 92 % yield, based on  $\text{Zn}(\text{C}_2\text{O}_4)$ ) was labeled as MOF-Oxa-DMF.

**Procedure II.**  $\text{Zn}(\text{NO}_3)_2 \cdot 6\text{H}_2\text{O}$  (0.595 g, 2.0 mmol) and oxalic acid (0.090 g, 0.96 mmol) were dissolved in DEF/1,4-dioxane (10 mL/4 mL). The solution was transferred

to a 40 mL autoclave. The autoclave was sealed and placed into an oven at 120 °C for 80 h. The product was washed with DEF (10 mL×2) and CHCl<sub>3</sub> (10 mL ×3), and dried at 50 °C overnight under a nitrogen flow. The sample was denoted as MOF-Oxa-DD. FT-IR (cm<sup>-1</sup>): 3389, 2943, 2815, 1622, 1468, 1364, 1317, 1258, 1124, 1066, 1022, 798.

**Procedure III.** An aqueous solution of 0.2 M sodium metasilicate (16 mL) was poured into a glass vial, which was charged with 20 mL of a 0.2 M oxalic acid solution. The glass vial was sealed, and kept undisturbed overnight at room temperature to allow the formation of a gel. An aqueous solution of 0.75 M Zn(NO<sub>3</sub>)<sub>2</sub>·6H<sub>2</sub>O (12 mL) was carefully placed on the gel, avoiding damaging the gel surface. The vial was kept at 30 °C for 6 days. The product was washed with H<sub>2</sub>O (20 mL×3) and ethanol (30 mL×3), followed by drying at 50 °C overnight under a nitrogen flow. The sample was labeled as MOF-Oxa-Gel. FT-IR (cm<sup>-1</sup>): 3360, 2962, 1623, 1361, 1315, 1260, 1090, 1019, 895, 798.

**Procedure IV.** ZnO powder was pressed into tablets with a diameter of about 2 cm. Four ZnO tablets (~1.5 g) were immersed into a 2M HNO<sub>3</sub> solution for 1 min, and then dried at 60 °C for 10 min in air. The pre-treated ZnO tablets were placed into an autoclave containing oxalic acid (0.32 g, 4.57 mmol) and 30 mL of DMF. The autoclave was placed into a pre-heated oven at 100 °C for 4 days. A white solid formed on the surface of the ZnO tablets. This solid was carefully removed from the surface of the tablets, washed with DMF (10 mL×3) and immersed in 10 mL of CHCl<sub>3</sub> for 12h (3×). The product was dried at 80 °C under vacuum for 12 h and labeled as MOF-Oxa-ZnO. Elemental analysis (EA): Found C, 19.2%, H, 2.65%, N, 4.00%. FT-IR (cm<sup>-1</sup>): 3432, 3126, 2967, 2803, 2496, 1611, 1466, 1363, 1321, 1010, 799.

### 6.2.3 Characterization

XRD patterns of all samples were recorded on an X'Pert X-ray diffractometer operated at 45 kV and 40 mA with monochromated Cu K $\alpha$  radiation within a 2-theta range of 5-60°. Samples were placed into an air-tight sample-holder in order to prevent air and moisture exposure. IR spectra of the samples were collected on a PerkinElmer Spectrum 100 FT-IR Spectrometer. Elemental Analyses were performed on a Thermo Scientific InterScience Flash 2000 Organic Elemental Analyzer. TG curves of samples were obtained on a PerkinElmer Pyris Diamond Thermogravimetric Differential Thermal/Analyzer. Samples were investigated from room temperature to 600 °C with a heating rate of 10 °C min<sup>-1</sup> under a nitrogen flow or dry air flow. Hydrogen storage measurements at different pressures were performed on a home-made Sievert's setup at 77 K. Samples were heated to 120 °C for 2 days under high vacuum (10<sup>-6</sup> mbar) prior to

each measurement (MOF-Ac was heated at 75 °C for 3 days). Hydrogen (ultra-high-purity grade, 99.999%) was additionally purified by passing it over a bed of zeolite spheres at 77 K before being loaded into the sample holder. The pressure change was monitored and recorded after the hydrogen reservoir was connected to the sample holder. The samples were weighed in a glove box after the measurements.

## 6.3 Results and discussion

### 6.3.1 Characterization of MOF-Ac

The PXRD pattern of MOF-Ac is shown in Figure 6.1. When we were in the process of synthesizing the IRMOF using acetylenedicarboxylic acid as the ligand, this material was reported and labeled as IRMOF-0 by Tranchemontagne and co-workers.[16] The authors synthesized IRMOF-0 via a different route, *i.e.* by stirring a DEF solution containing  $\text{Zn}(\text{OAc})_2$  and acetylenedicarboxylic acid at room temperature in the presence of triethylamine. Compared with the PXRD pattern of IRMOF-0, our MOF-Ac showed the same PXRD pattern, with very well resolved diffraction peaks, suggesting that MOF-Ac has the same crystal structure as IRMOF-0 (and the same topology as MOF-5). The  $\text{Zn}_4\text{O}$  clusters are bridged by rod-like acetylenedicarboxylate linkers and form an extended two-fold interpenetrated structure, as shown in Figure 6.2 (right). Computational results have shown that the pore size is  $\sim 7.8$  Å in diameter for the non-interpenetrated structure. In the two-fold interpenetrated structure, the distance between two interpenetrating frameworks is  $\sim 5.5$  Å (measured between the center of two opposite alkynes) and the largest sphere that can fit between the alkynes where they intersect is  $\sim 4.4$  Å in diameter.[16]

The thermal stability of MOF-Ac was investigated using thermogravimetric analysis. Figure 6.2 shows the TGA curve of MOF-Ac. No obvious weight loss was observed below 100 °C. A significant weight loss in the range of 130 °C-600 °C was observed and is attributed to the release of solvents and the decomposition of the acetylenedicarboxylate linker. The low decomposition temperature infers a very poor thermal stability of the framework. The presence of the solvent ( $\text{NEt}_3$ ) was confirmed by the high N content (5.13%) according to the elemental analysis results, which corresponds to 37 wt% of  $\text{NEt}_3$ . The TGA data is in good agreement with TGA results reported by Tranchemontagne *et al.*

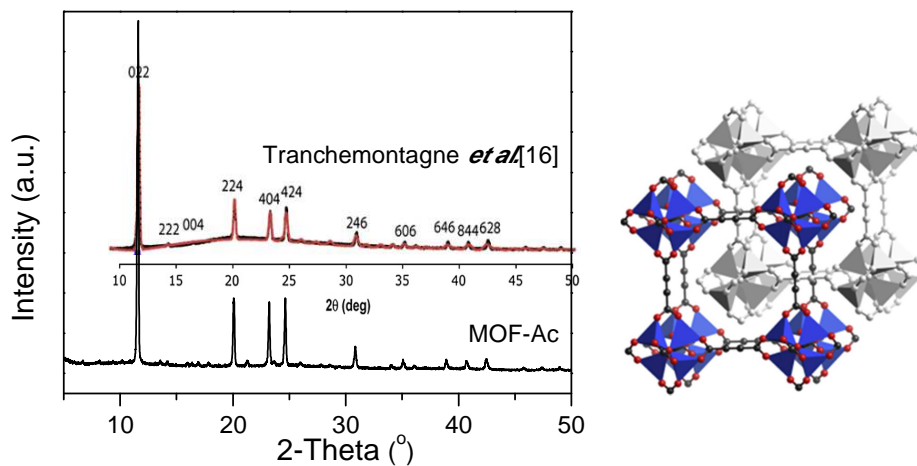


**Figure 6.1.** PXRD patterns of MOF-Ac and IRMOF-0 (left) and the two-fold interpenetrated structure of IRMOF-0(right). Reproduced from ref. [16]. Copyright 2008, with permission from Elsevier.

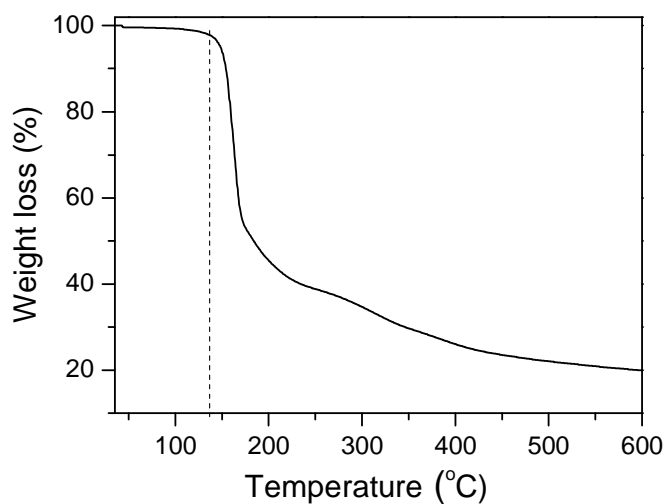


**Figure 6.2.** TGA curve of MOF-Ac measured using a heating rate of 10 °C min<sup>-1</sup> under a nitrogen flow.

To understand why MOF-Ac exhibits such poor thermal stability, we heated MOF-Ac at 150 °C for 0.5 h in an argon filled glove box. MOF-Ac changed from light yellow to dark yellow during heating. In the IR spectra of MOF-Ac before and after the heat treatment, it is clear that the chemical composition has changed (Figure 6.3). A new band at 2091  $\text{cm}^{-1}$  was observed for the heated sample. This band could be assigned to the stretching vibration of  $\text{C}\equiv\text{C}$ , which is invisible in the spectrum of MOF-Ac because it is symmetry forbidden. The appearance of this band implies that the symmetry was broken, possibly due to bond cleavage between the carboxyl carbon atom and  $\text{C}\equiv\text{C}$  group. At the same time, the band at 1720  $\text{cm}^{-1}$  corresponding to the asymmetric stretching vibration of uncoordinated carboxyl groups appeared after heat treatment. The strong band at 1604  $\text{cm}^{-1}$  related to the stretching vibration of carboxyl groups coordinated with  $\text{Zn}^{2+}$  is still present in the spectrum of MOF-Ac after heat treatment. These observations indicate that most carboxyl groups are still coordinated with  $\text{Zn}^{2+}$ , but a fraction has been disrupted. As expected, the PXRD pattern of MOF-Ac after heating at 150 °C for 0.5 h is very poor (Figure 6.4), which suggests that the structure has collapsed. These results reveal that the weak stability of the  $\text{C}_{\text{C}\equiv\text{C}}\text{-COO}^-$  and  $\text{Zn-O(OC)}$  bond is the reason of the poor thermal stability of MOF-Ac. In contrast, the  $\text{Zn-O(OC)}$  bond appears to be stable up to 250 °C in many other MOFs.[18]

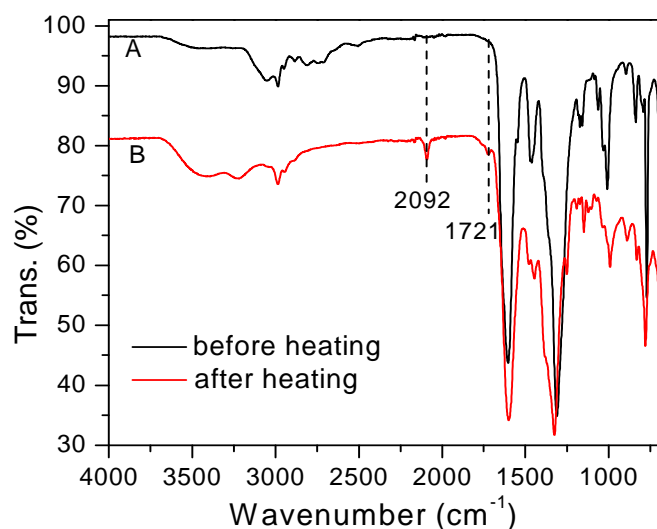


**Figure 6.3.** FT-IR spectra of MOF-Ac before (A) and after (B) heat treatment (150 °C for 0.5 h under an argon atmosphere).

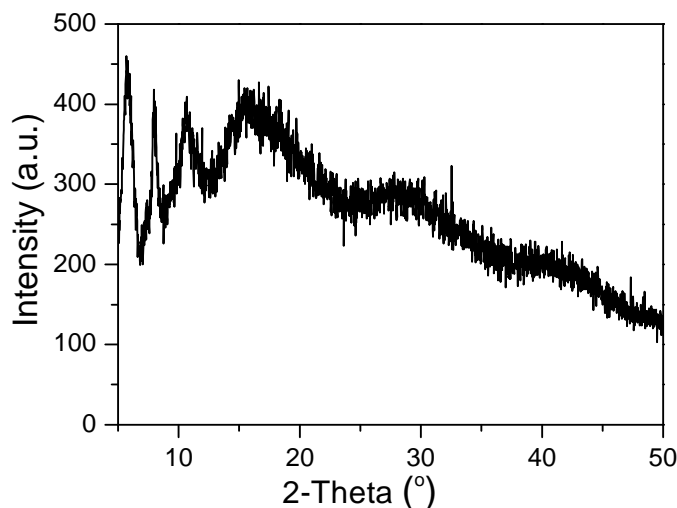


**Figure 6.4.** PXRD pattern of MOF-Ac after heating at 150 °C for 0.5 h under an argon atmosphere.

### 6.3.2 Characterization of MOF-Fum

Figure 6.5 shows the PXRD pattern of MOF-Fum-DMF, the fumarate-based MOF prepared in DMF. A reported XRD pattern of the zinc fumarate is displayed as well for comparison.[17] In addition to the peaks at 15.6°, 27.2° and 40.4° assigned to the zinc fumarate, additional strong peaks are also present in the PXRD pattern of MOF-Fum-DMF, *i.e.* 11.8°, 18.6°, 22.6° and 24.2°. These findings suggest that MOF-Fum-DMF was formed together with zinc fumarate and some other undefined structures. Two weight loss steps can be observed in the TGA curve of MOF-Fum-DMF (Figure 6.6). The first weight loss step started at ~250 °C, which is in agreement with the decomposition temperature of zinc fumarate.[17] The second weight loss event can be attributed to the combined decomposition of the unknown side products and zinc fumarate.

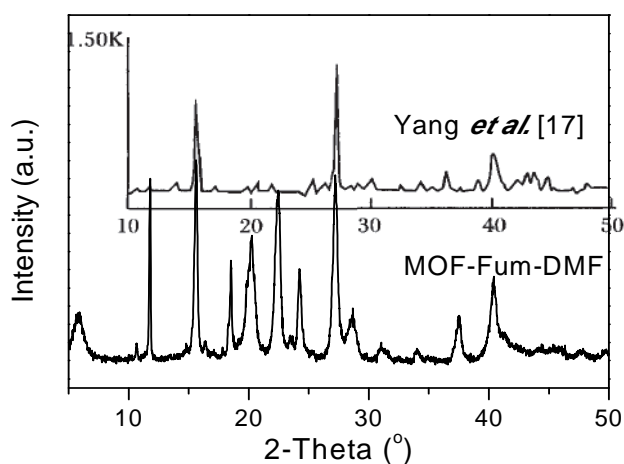


**Figure 6.5.** PXRD patterns of MOF-Fum-DMF and zinc fumarate (inserted for comparison).

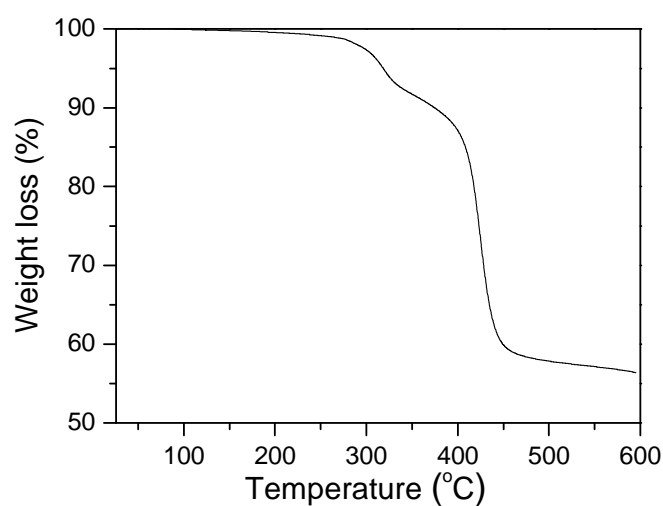


**Figure 6.6.** TGA curve of MOF-Fum-DMF measured using a heating rate of 10 °C min<sup>-1</sup> under a dry N<sub>2</sub> flow.

Since the synthesis method above yielded less pure samples, we also synthesized a sample denoted as MOF-Fum-DEF by following a procedure as reported by Xue et al.[15] The PXRD pattern of MOF-Fum-DEF, as shown in Figure 6.7, is in close agreement with the reported PXRD pattern by Xue et al., indicating that MOF-Fum-DEF has the same topology as MOF-5. The structure has intersecting pores of ca. 6.8×6.8 Å. In



comparison with the reaction conditions used to prepare MOF-Fum-DMF, a highly diluted solution and lower ratio of  $\text{Zn}(\text{NO}_3)_2 \cdot 6\text{H}_2\text{O}$  to fumaric acid was used for the synthesis of MOF-Fum-DEF. This implies that the formation of IRMOFs constructed from fumarate is strongly affected by the concentration of the precursors. The latter approach seems to result in a better quality MOF-Fum. After activation, a small amount of DEF is present in MOF-Fum-DEF, as confirmed by a N content of 0.27% ( $\sim 2$  wt% DEF) obtained from elemental analysis. The thermal stability of MOF-Fum-DEF was determined using TGA under a dry air flow and the results are shown in Figure 6.8. The thermogram shows  $\sim 3$  wt% of weight loss below  $250^\circ\text{C}$ , which is attributed to the release of water and DEF. Between  $250^\circ\text{C}$  and  $450^\circ\text{C}$  the framework decomposed and the weight loss of 47% is in close agreement with the calculated value (47.6%) based on the formula of  $\text{Zn}_4\text{O}(\text{C}_4\text{H}_2\text{O}_4)_3$ . MOF-Fum-DEF showed a high BET surface area of  $1808\text{ m}^2\text{ g}^{-1}$  and a pore volume of  $0.73\text{ cm}^3\text{ g}^{-1}$ . Its BET surface area is significantly higher than that of  $\text{Zn}_4\text{O}(\text{FMA})_3$  reported by Xue and co-workers ( $1120\text{ m}^2\text{ g}^{-1}$ ). Also the PXRD pattern shows more well resolved peaks belonging to the structure  $\text{Zn}_4\text{O}(\text{C}_4\text{H}_2\text{O}_4)_3$ .

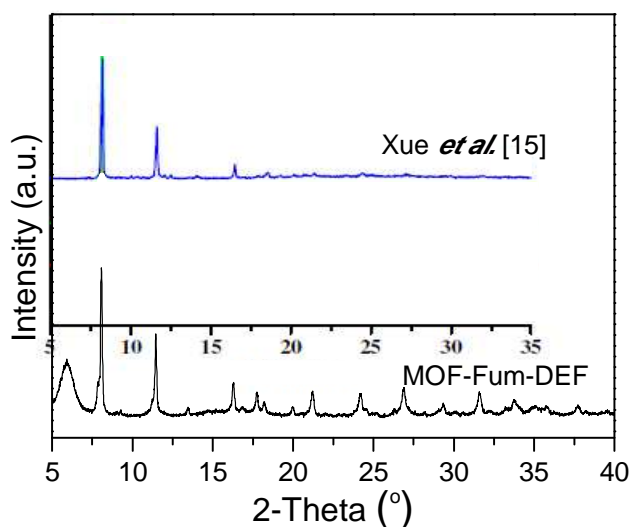


**Figure 6.7.** PXRD pattern of MOF-Fum-DEF and the reported PXRD pattern [15] of IRMOF constructed by fumarate. The peak at  $5.9^\circ$  stems from the sample holder.

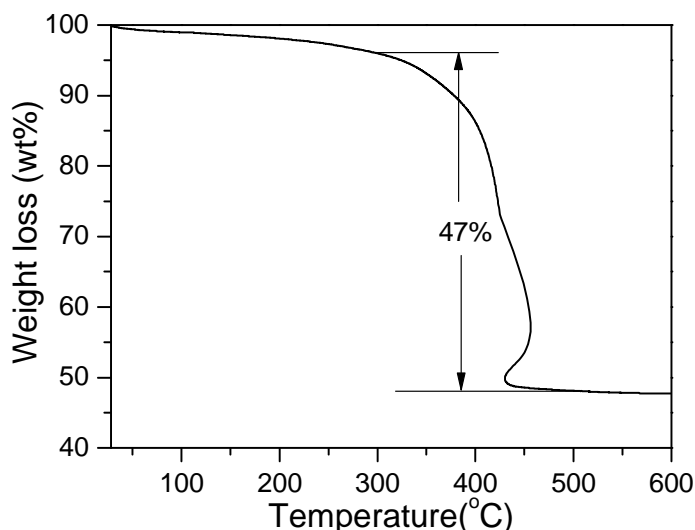


**Figure 6.8.** TGA curve of MOF-Fum-DEF measured using a heating rate of  $10\text{ }^{\circ}\text{C min}^{-1}$  under a dry air flow.

### 6.3.3 Characterization of MOF-Oxa

We explored four different routes towards the synthesis of an oxalate-based MOF, where it may be noted that this is the shortest di-acid linker. Since there was no literature precedence we started with a classic solvothermal approach. We investigated two different solvent systems, *i.e.* DMF and a mixture of DEF/1,4-dioxane (DD). During the synthesis of MOF-Oxa-DMF and MOF-Oxa-DD, a precipitate formed almost immediately after oxalic acid was added to the zinc nitrate solution, which is not favorable to the formation of MOFs. This method was abandoned and we attempted to avoid premature precipitation by using a gel method (MOF-Oxa-Gel) and by growing MOF crystals on ZnO tablets (MOF-Oxa-ZnO). The PXRD patterns of MOF-Oxa-DMF, MOF-Oxa-DD and MOF-Oxa-Gel are shown in Figure 6.9. For comparison, the PXRD pattern of zinc oxalate is also included. The PXRD pattern of MOF-Oxa-DMF is almost identical to that of zinc oxalate, which means we were unsuccessful in obtaining a MOF-like structure via this synthetic route. Changing the solvent to a DEF/1,4-dioxane mixture does not have much of an effect on the outcome either. Again, the diffraction pattern of MOF-Oxa-DD is to a large extent similar to that of zinc oxalate, but this time the appearance of additional diffraction peaks at  $24.0^{\circ}$ ,  $31.8^{\circ}$ ,  $34.5^{\circ}$  and  $36.4^{\circ}$  has to be

noted, which indicates the presence of unknown compounds. Although the gel method is effective in slowing down precipitation, this method also results in the formation of zinc oxalate as the main product as indicated by their similar PXRD patterns. It should be noted that MOF-Oxa-ZnO gave a totally different PXRD pattern, which resembles neither zinc oxalate nor the predicted MOF structure (Figure 6.10). The three diffraction peaks at  $8.7^\circ$ ,  $11.7^\circ$  and  $13.2^\circ$  suggest that MOF-Oxa-ZnO has a larger lattice parameter compared to zinc oxalate. The obtained PXRD pattern of MOF-Oxa-ZnO is not consistent with the simulated PXRD pattern of an IRMOF constructed from oxalate linkers, implying a new non-IRMOF like structure has been obtained. The obtained product formed hexagonal crystals with a diameter of  $\sim 50\ \mu\text{m}$ . No large crystals ( $>100\ \mu\text{m}$ ) could be obtained; therefore, structural determination by single crystal XRD technique was not possible. The thermal stability of MOF-Oxa-ZnO was investigated using TGA and the thermogram shows three very distinct weight loss steps (Figure 6.11), *i.e.* 8% below  $150\ ^\circ\text{C}$  and 30% in the range of  $150\ ^\circ\text{C}$ - $350\ ^\circ\text{C}$ , are attributed to the release of water and DMF, respectively (confirmed by Mass Spectroscopy). The last weight loss step is assigned to the decomposition of the linker ( $-\text{C}_2\text{O}_4-$ ) indicating that unknown MOF structure appears to be stable up to  $350\ ^\circ\text{C}$ .

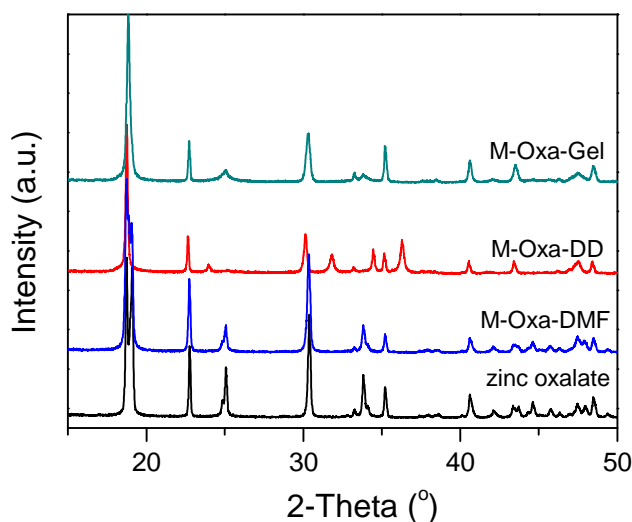


**Figure 6.9.** PXRD patterns of zinc oxalate, MOF-Oxa-DMF, MOF-Oxa-DD and MOF-Oxa-Gel.

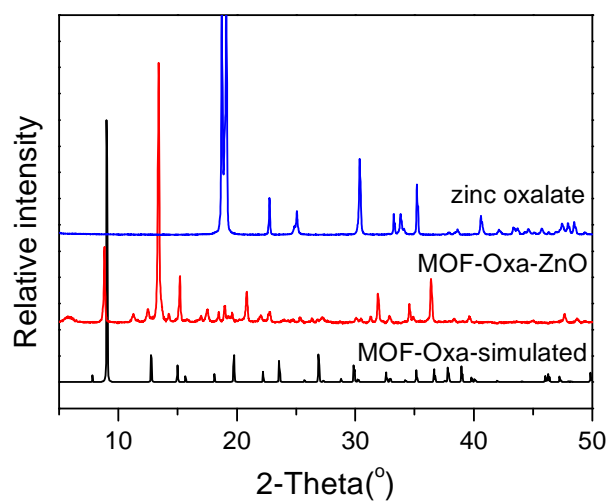


**Figure 6.10.** PXRD patterns of zinc oxalate, MOF-Oxa-ZnO and the simulated pattern of an IRMOF constructed from oxalate-based linkers.

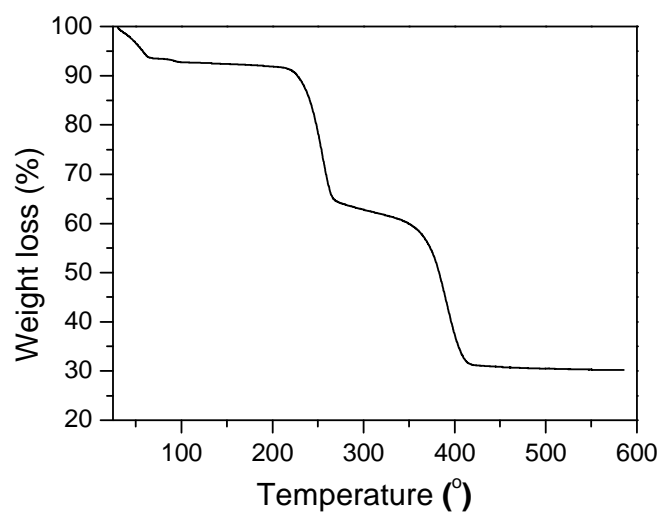


**Figure 6.11.** TGA curve of MOF-Oxa-ZnO measured using a heating rate of  $10\text{ }^{\circ}\text{C min}^{-1}$  under a  $\text{N}_2$  flow.

### 6.3.4 Hydrogen storage property

Because MOF-Fum-DMF, MOF-Oxa-DMF, MOF-Oxa-DD and MOF-Oxa-Gel are non-porous zinc salts, their hydrogen storage properties were not investigated. The hydrogen uptake capacities of MOF-Fum-DEF, MOF-Ac, and MOF-Oxa-ZnO were measured using a Sievert's setup at 77 K and low pressures (<1.4 bar). MOF-Fum-DEF demonstrated a type-I adsorption isotherm and 0.93 wt% of hydrogen uptake capacity at 77 K and 1 bar, which is slightly lower than the value (1.16 wt%) reported by Xue *et al.* MOF-Ac and MOF-Oxa-ZnO, however, showed negligible hydrogen uptake capacities (below 0.05 wt%) over the pressure range studied (<1.4 bar) (Figure 6.12).

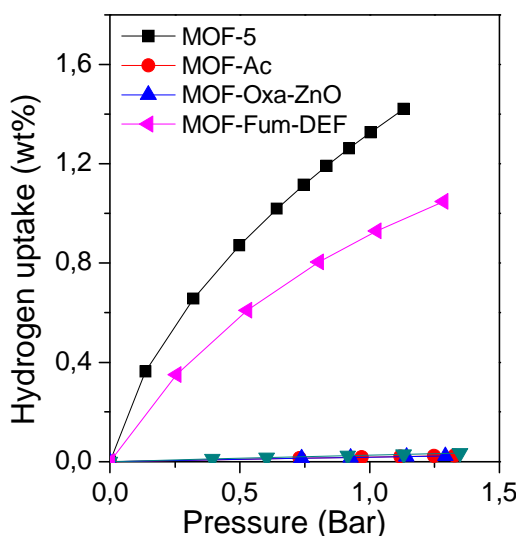


**Figure 6.12.** Low-pressure hydrogen adsorption isotherms of MOF-5, MOF-Fum-DEF, MOF-Ac and MOF-Oxa-ZnO at 77 K.

It has been well documented that a reduced pore size and high concentration of metal site per unit volume will enhance the interaction between hydrogen and MOF-5 type frameworks.[14,19] In order to achieve a high gravimetric hydrogen uptake capacity, we attempted to synthesize MOFs with a high Zn<sub>4</sub>O density by using three short ligands, *i.e.* acetylenedicarboxylate, fumarate and oxalate. For all samples prepared, only MOF-Fum-DEF and MOF-Ac showed the same topology as MOF-5 but they exhibited smaller pore size diameters, *i.e.* 6.8 Å for MOF-Fum-DEF and 4.4 Å for MOF-Ac vs. 9.2 Å for MOF-5. The exact structure of MOF-Oxa-ZnO remains unknown for the time being.

Compared to the hydrogen uptake capacity of MOF-5, MOF-Fum-DEF showed a lower hydrogen uptake capacity over the whole pressure range studied (<1.4 bar). Xue and co-workers also reported that the hydrogen adsorption enthalpy in  $\text{Zn}_4\text{O}(\text{FMA})_3$  ( $4.2 \text{ kJ mol}^{-1}$ ) is comparable to that of MOF-5 ( $3.5\text{-}5.2 \text{ kJ mol}^{-1}$  [20]), indicating no specific strong binding sites for hydrogen adsorption in  $\text{Zn}_4\text{O}(\text{FMA})_3$ . It seems that the smaller pore size and higher  $\text{Zn}_4\text{O}$  density in MOF-Fum-DEF/ $\text{Zn}_4\text{O}(\text{FMA})_3$  could not result in an improvement in the hydrogen adsorption capacity. We consider that the lack of aromaticity might be a reason why we did not observe an improvement in hydrogen uptake capacity by replacing phenyl with ethylene. Previous studies have revealed that increasing the aromaticity of organic linkers plays a positive effect on hydrogen uptake capacity of MOF series incorporating the same metal cluster or metal ion.[21] Therefore, it is reasonable to claim that organic linkers play a more critical role in hydrogen adsorption capability than previously understood. With respect to MOF-Ac, the small apertures resulted from the interpenetration may prevent the solvent molecules from escaping from the pores during the activation process, resulting in a non-porous structure. This could explain why MOF-Ac, which has the same topology as MOF-5, is unable to adsorb hydrogen. Since the structure of MOF-Oxa-ZnO could not be determined, we cannot speculate on the reason why MOF-Oxa-ZnO did not show hydrogen adsorption behavior.

## 6.4 Conclusions

Three short ligands, acetylenedicarboxylic acid (Ac), fumaric acid (Fum) and oxalic acid (Oxa), have been employed to synthesize IRMOFs labeled as MOF-Ac, MOF-Fum and MOF-Oxa, respectively. Except for oxalic acid, acetylenedicarboxylic acid and fumaric acid reacted with  $\text{Zn}(\text{II})$  and formed the same primitive cubic topology as MOF-5. MOF-Ac shows a very poor thermal stability (<140 °C) due to unstable  $\text{C}\equiv\text{C}-\text{COO}^-$  and  $\text{Zn}-\text{O}(\text{OC})$  bonds. In addition, the two-fold interpenetrated structure of MOF-Ac results in small pore windows, which prevents the removal of solvent molecules from the pores during the MOF activation process. Therefore, MOF-Ac is nonporous and not capable of adsorbing hydrogen. MOF-Fum-DEF displays a non-interpenetrated structure and a hydrogen storage capacity of 0.93 wt% at 77 K and 1 bar, which is lower than that of MOF-5 (1.32 wt%). This may be explained by the lack of 'linker aromaticity'. In the absence of aromatic moieties, a reduced pore size (6.8 Å for MOF-Fum-DEF vs. 9.2 Å for MOF-5) and increased  $\text{Zn}_4\text{O}$  cluster concentration (25% higher than that of MOF-5) by replacing phenyl with ethylene does not necessarily result in a MOF-5 structure with an

increased hydrogen adsorption capacity. Our results suggest that the aromatic nature of the organic linkers also play an important role in hydrogen adsorption behavior of MOFs.

## 6.5 References

- [1] Carne, A.; Carbonell, C.; Imaz, I.; Maspoch, D. *Chem. Soc. Rev.* **2011**, *40*, 291.
- [2] Czaja, A.U.; Trukhan, N.; Muller, U. *Chem. Soc. Rev.* **2009**, *38*, 1284.
- [3] Ferey, G. *Struct. Bonding* **2009**, *132*, 87.
- [4] Horike, S.; Shimomura, S.; Kitagawa, S. *Nat. Chem.* **2009**, *1*, 695.
- [5] Kuppler, R.J.; Timmons, D.J.; Fang, Q. R.; Li, J.R.; Makal, T.A.; Young, M.D.; Yuan, D.Q.; Zhao, D.; Zhuang, W.J.; Zhou, H.-C. *Coord. Chem. Rev.* **2009**, *253*, 3042.
- [6] Meek, S.T.; Greathouse, J.A.; Allendorf, M.D. *Adv. Mater.* **2011**, *23*, 249.
- [7] Yaghi, O.M.; Li, Q.W. *MRS Bull.* **2009**, *34*, 682.
- [8] Mulder, F.M.; Dingemans, T.J.; Wagemaker, M.; Kearley, G.J. *Chem. Phys.* **2005**, *317*, 113.
- [9] Yildirim, T.; Hartman, M.R. *Phys. Rev. Lett.* **2005**, *95*, 215504.
- [10] Mulder, F.M.; Dingemans, T.J.; Schimmel, H.G.; Ramirez-Cuesta, A.J.; Kearley, G.J. *Chem. Phys.* **2008**, *351*, 72.
- [11] Yang, S.J.; Choi, J.Y.; Chae, H.K.; Cho, J.H.; Nahm, K.S.; Park, C.R. *Chem. Mater.* **2009**, *21*, 1893.
- [12] Han, S.S.; Goddard, W.A. *J. Am. Soc. Chem.* **2007**, *129*, 8422.
- [13] Collins, D.J.; Zhou, H.-C. *J. Chem. Mater.* **2007**, *17*, 3154.
- [14] Ryan, P.; Broadbelt, L.J.; Snurr, R.Q. *Chem. Commun.* **2008**, 4132.
- [15] Xue, M.; Liu, Y.; Schaffino, R.M.; Xiang, S.; Zhao, X.; Zhu, G.-S.; Qiu, S.-L.; Chen, B. *Inorg. Chem.* **2009**, *48*, 4649.
- [16] Tranchemontagne, D.J.; Hunt, J.R.; Yaghi, O.M. *Tetrahedron* **2008**, *64*, 8553.
- [17] Yang, X. *Applied Chemical Industry* **2005**, *34*, 560.
- [18] (a) Farha, O.K.; Spokoyny, A.M.; Mulfort, K.L.; Hawthorne, C.; Mirkin, C.A.; Hupp, J.T. *J. Am. Soc. Chem.* **2007**, *129*, 12680. (b) Sun, D.; Ma, S.; Ke, Y.; Petersen, T. M.; Zhou, H.-C. *Chem. Commun.* **2005**, 2663.
- [19] Ma, S. *Pure Appl. Chem.* **2009**, *81*, 2235.
- [20] Sillar, K.; Hofmann, A.; Sauer, J. *J. Am. Chem. Soc.* **2009**, *131*, 4143.
- [21] (a) Han, S.S.; Goddard III. W. A. *J. Am. Chem. Soc.* **2007**, *129*, 8422. (b) Rowsell, J.L.C.; Millward, A.R.; Park, K.S.; Yaghi, O.M. *J. Am. Chem. Soc.* **2004**, *126*, 5666.





# CHAPTER 7

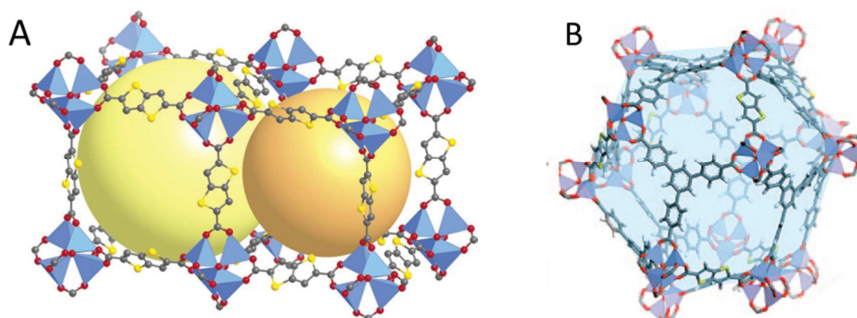
## **Cu(II) coordination polymers comprised of thiophene-2,5-dicarboxylate and furan-2,5-dicarboxylate**

---

Self-assembled copper (II) coordination polymers have been synthesized from thiophene-2,5-dicarboxylic acid (Cu-TDC) and furan-2,5-dicarboxylic acid (Cu-FDC) via a solvothermal method. Both coordination polymers were characterized by single crystal X-ray diffraction, FT-IR and thermogravimetric techniques. Structural analysis reveals that Cu-TDC and Cu-FDC show a similar 2-D layered structure but are stacked in different fashions. Activated Cu-TDC and Cu-FDC exhibit hydrogen adsorption capacities of 0.75 wt% and 0.64 wt% at 77 K and 1 bar, respectively. The hydrogen storage capability is rather high considering the low surface area ( $\sim 300 \text{ m}^2 \text{ g}^{-1}$ ), which is attributed to their high heats of hydrogen adsorption, *i.e.*  $9.2 \text{ kJ mol}^{-1}$  for Cu-TDC and  $7.5 \text{ kJ mol}^{-1}$  for Cu-FDC.

## 7.1 Introduction

Metal organic coordination polymers are receiving attention because they are potentially interesting materials for hydrogen storage, gas separation and optoelectronic applications. In these materials, polyfunctional organic ligands can form coordination bonds with multiple metal atoms, which may extend in one-, two-, or three-dimensional polymeric structures.[1,2] Polycarboxylic acids ligands, such as benzenecarboxylic acids and nitrogen-based heterocyclic carboxylic acids, have been well documented as useful building blocks for the construction of a wide variety of coordination polymers because of their various coordination modes. Many metal organic coordination polymers constructed from such ligands show promising hydrogen adsorption properties.[3] So far, research on the hydrogen adsorption capabilities of metal organic coordination polymers incorporating other heterocyclic carboxylic acids, e.g. sulfur- and oxygen-based heterocyclic carboxylic acids, has been limited. It was reported that IRMOF-20 and UMCM-2 built from thieno[3,2-b]thiophene-1,5-dicarboxylate (Scheme 7.1) display hydrogen storage capacities of 1.35 wt% and 1.28 wt% at 77 K and 1 bar, respectively.[4]

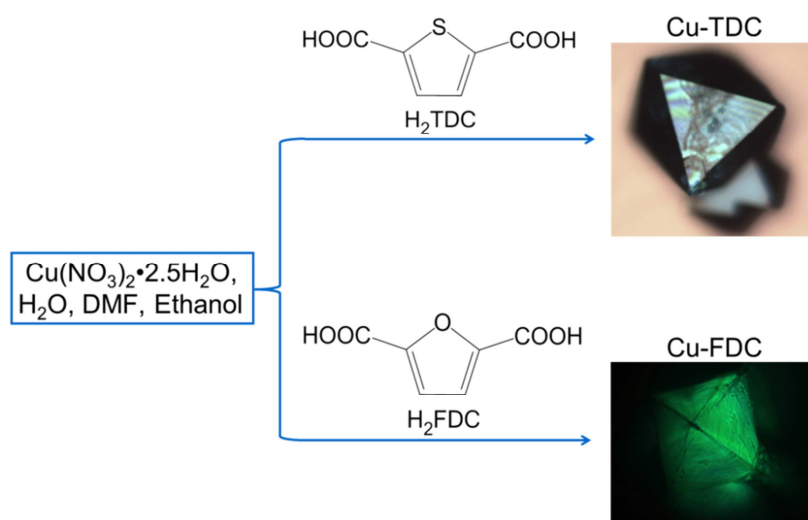


**Scheme 7.1.** The structures of IRMOF-20 constructed by thieno[3,2-b]thiophene-1,5-dicarboxylate (A) and UMCM-2 composed of thieno[3,2-b]thiophene-1,5-dicarboxylate and benzene-1,3,5-tricarboxylate (B). Reproduced from ref. [4]. Copyright 2006 and 2009, American Chemical society.

Thiophene-2,5-dicarboxylic acid ( $\text{H}_2\text{TDC}$ ) and furan-2,5-dicarboxylic acid ( $\text{H}_2\text{FDC}$ ) are the most basic representatives of the heterocyclic dicarboxylic acid family. The thiophene ring possesses unique physical and chemical properties. Owing to the larger radius of the S atom as compared to C, N, and O, its lone pair of electrons can easily delocalize over the heterocyclic ring, and as a ligand  $\text{H}_2\text{TDC}$  exhibits good a charge-transfer ability. Furan-2,5-dicarboxylic acid, on the other hand, is of interest for

similar reasons but in particular because it is considered to be a bio-renewable building block in the formation of polymers from biomass. It is therefore of special interest because of its potential to replace terephthalic, isophthalic and adipic acids in MOF syntheses. Some coordination polymers containing thiophene-2,5-dicarboxylate have been reported.[5-7] However, to the best of our knowledge, the hydrogen adsorption properties of such materials have not been reported. In addition, no research on a coordination polymer constructed from furan-2,5-dicarboxylate has been reported before.

In this chapter we will present the synthesis of two novel Cu-based coordination polymers (Cu-TDC and Cu-FDC) derived from thiophene-2,5-dicarboxylic acid and furan-2,5-dicarboxylic acid, as shown in Scheme 7.2. The structural characteristics and the hydrogen adsorption properties of Cu-TDC and Cu-FDC will be investigated.



**Scheme 7.2.** The synthesis of two novel Cu-based coordination polymers (Cu-TDC and Cu-FDC) derived from thiophene-2,5-dicarboxylic acid and furan-2,5-dicarboxylic acid, respectively.

## 7.2 Experimental

### 7.2.1 Materials

$\text{Cu}(\text{NO}_3)_2 \cdot 2.5\text{H}_2\text{O}$  (Acros, 97%), thiophene-2,5-dicarboxylic acid ( $\text{H}_2\text{TDC}$ , George Uh4 Co., Inc.), furan-2,5-dicarboxylic acid ( $\text{H}_2\text{FDC}$ , TCI, 98%), *N,N*-dimethylformamide (DMF, Acros) chloroform ( $\text{CHCl}_3$ ), ethanol (EtOH), and benzene were used as received.

### 7.2.2 Synthesis of Cu-TDC and Cu-FDC

**Synthesis of Cu-TDC.** In a 20 mL vial, 23.7 mg (0.080 mmol) of  $\text{Cu}(\text{NO}_3)_2 \cdot 2.5\text{H}_2\text{O}$  and 23.0 mg (0.16 mmol) of thiophene-2,5-dicarboxylic acid were dissolved in DMF/ $\text{H}_2\text{O}$ /EtOH (1.5 mL/0.25 mL/0.5 mL). The vial was placed into a preheated oven and kept at 80 °C for 24 h. Blue crystals were collected and washed with DMF and EtOH, then vacuum dried overnight at 25 °C. The product was labeled Cu-TDC and stored in a glove box (23.5 mg, 55% yield).

**Synthesis of Cu-FDC.** In a 20 mL vial, 22.3 mg (0.076 mmol) of  $\text{Cu}(\text{NO}_3)_2 \cdot 2.5\text{H}_2\text{O}$  and 21.4 mg (0.15 mmol) of furan-2,5-dicarboxylic acid were dissolved in DMF/ $\text{H}_2\text{O}$ /EtOH (1.5 mL/0.5 mL/0.5 mL). The vial was placed into a preheated oven and kept at 80 °C for 24 h. Blue crystals were filtered and washed with DMF and EtOH, then vacuum dried overnight at 25 °C. The product was labeled Cu-FDC and stored in a glove box (25 mg, 76% yield).

**Activation.** Samples were activated using the following two methods. **(A1)**  $\text{CHCl}_3$ -exchange: under an inert atmosphere, the sample was extracted three times with fresh  $\text{CHCl}_3$  (2 mL×15 h, 2 mL×9 h, 2 mL×15 h), and dried under vacuum at room temperature overnight and at 60 °C for 3 days. The activated samples were denoted as Cu-TDC-A1 and Cu-FDC-A1. **(A2)** Freeze-drying: about 400 mg of a fresh sample was placed in a Schlenk tube and washed with  $\text{CH}_2\text{Cl}_2$  (10 mL×3) and benzene (8 mL×2), followed by immersing in 10 mL of benzene overnight. The tube was placed into an ice-water bath (0 °C). After three freeze-thaw cycles, the sample was evacuated in an ice-water bath for 1 day. The sample was kept under vacuum at room temperature for 1 day and at 60 °C for 1 day. The samples activated via this freeze-drying process were labeled CuTDC-A2 and CuFDC-A2.

### 7.2.3 Characterization

**Single-crystal X-ray diffraction analysis of Cu-TDC:**  $\text{C}_9\text{H}_9\text{CuNO}_5\text{S}$  + disordered solvent, Fw = 306.77[\*] ([\*] derived values do not contain the contribution of the disordered solvent). Sample appearance and dimensions: blue block, 0.41 x 0.39 x 0.26 mm<sup>3</sup>. Trigonal, R(-3)c (no. 167), a = b = 20.0402(6), c = 41.6541(13) Å,  $\alpha = \beta = 90^\circ$ ,  $\gamma = 120^\circ$ , V = 14487.5(8) Å<sup>3</sup>, Z = 36,  $D_x = 1.266 \text{ g cm}^{-3}$  [\*],  $\mu = 1.49 \text{ mm}^{-1}$  [\*]. 62951 reflections were measured on a Bruker Kappa ApexII diffractometer with sealed tube and Triumph monochromator ( $\lambda = 0.71073 \text{ Å}$ ) up to a resolution of  $(\sin\theta/\lambda)_{\text{max}} = 0.65 \text{ Å}^{-1}$  at a temperature of 150(2) K. Intensity data were integrated with the Saint software.[9]

Absorption correction and scaling were performed based on multiple measured reflections with SADABS (0.65-0.75 correction range).[10] 3715 reflections were unique ( $R_{\text{int}} = 0.026$ ), of which 2649 were observed [ $I > 2\sigma(I)$ ]. The structure was solved with Direct Methods using the program SHELXS-97 and refined with SHELXL-97 against  $F^2$  of all reflections.[11] Non hydrogen atoms were refined with anisotropic displacement parameters. Hydrogen atoms were introduced in calculated positions and refined with a riding model. The crystal structure contains solvent accessible voids (5441 Å<sup>3</sup> per unit cell) filled with disordered solvent molecules. Their contribution to the structure factors was secured by back-Fourier transformation using the SQUEEZE routine of PLATON resulting in 1482 electrons per unit cell.[12] The *N,N*-dimethylformamide ligand was refined with a disorder model. 182 parameters were refined with 54 restraints (concerning the disordered DMF).  $R1/wR2$  [ $I > 2\sigma(I)$ ]: 0.0367/0.1204.  $R1/wR2$ : 0.0473/0.1281.  $S = 1.141$ . Residual electron density is between -0.47 and 0.49 e Å<sup>-3</sup>. [9-15] Geometry calculations and checking for higher symmetry were performed with the PLATON program.[12]

**Single-crystal X-ray diffraction analysis of Cu-FDC:**  $C_{18}H_{12}Cu_3O_{18}$  + disordered solvent,  $F_w = 706.90$  [°]. Sample appearance and dimensions: blue needle,  $0.40 \times 0.15 \times 0.14$  mm<sup>3</sup>. Monoclinic,  $C2/m$  (no. 12),  $a = 18.9198(11)$ ,  $b = 18.8335(14)$ ,  $c = 12.6671(8)$  Å,  $\beta = 92.396(3)^\circ$ ,  $V = 4509.7(5)$  Å<sup>3</sup>,  $Z = 4$ ,  $D_x = 1.041$  g cm<sup>-3</sup> [°],  $\mu = 1.45$  mm<sup>-1</sup> [°]. 75193 reflections were measured on a Bruker Kappa ApexII diffractometer with sealed tube and Triumph monochromator ( $\lambda = 0.71073$  Å) up to a resolution of  $(\sin \theta/\lambda)_{\text{max}} = 0.65$  Å<sup>-1</sup> at a temperature of 150(2) K. The crystal was non-merohedrally twinned with a twofold rotation about  $uvw = [-1, -1, 2]$  as twin operation. Intensity data were integrated with the Eval14 software [13] taking the twin relation into account. Absorption correction, scaling, and de-twinning were performed based on multiple measured reflections with TWINABS [10] (0.65-0.75 correction range). 5351 reflections were unique ( $R_{\text{int}} = 0.040$ ), of which 4804 were observed [ $I > 2\sigma(I)$ ]. The structure was solved with Direct Methods using the program SHELXS-97 and refined with SHELXL-97 against  $F^2$  of all reflections.[11] Non hydrogen atoms were refined with anisotropic displacement parameters. Hydrogen atoms were introduced in calculated positions and refined with a riding model. The crystal structure contains solvent accessible voids (2650 Å<sup>3</sup> per unit cell) filled with disordered solvent molecules. Their contribution to the structure factors was secured by back-Fourier transformation using the SQUEEZE routine of PLATON resulting in 838 electrons per unit cell.[12] 181 parameters were refined with no restraints.  $R1/wR2$  [ $I > 2\sigma(I)$ ]: 0.0320/0.0835.  $R1/wR2$ : 0.0354/0.0850.  $S = 1.040$ . [9-15] Residual electron density is between -0.50 and 2.39 e Å<sup>-3</sup>. Geometry

calculations and checking for higher symmetry were performed with the PLATON program. [12]

PXRD patterns of all samples were recorded on an X'Pert X-ray diffractometer operated at 45 kV and 40 mA with monochromatic Cu  $K\alpha$  radiation within a 2-theta range of 5-60°. IR spectra were collected on a PerkinElmer Spectrum 100 FT-IR Spectrometer. Elemental analyses were performed on a Thermo Scientific InterScience Flash 2000 Organic Elemental Analyzer. TGA curves were obtained on a PerkinElmer Pyris Diamond Thermogravimetric Differential Thermal/Analyzer. Samples were heated from room temperature to 600 °C with a heating rate of 10 °C min<sup>-1</sup> under a dry air flow. The pore textural properties, including BET surface area and pore volume, were recorded on a Micromeritics ASAP 2010 adsorption analyzer at 77 K. Prior to the adsorption measurements, the samples were degassed *in situ* under vacuum at 80 °C overnight. The dead volume of the sample cell was determined in a separate experiment. *In situ* pretreatment coupled to a separate dead volume measurement after the analysis was employed in order to avoid the helium entrapment phenomenon. The weight of a sample obtained after the pretreatment was used in various calculations. BET surface areas were calculated in the adapted pressure range of  $P/P_0 = 0.01-0.1$ . Hydrogen storage measurements in the low-pressure range (< 2 bar) were performed on a Sievert's setup at 77 K. Prior to the measurement, the samples activated by CHCl<sub>3</sub>-exchange were pretreated under high vacuum (10<sup>-6</sup> mbar) at 25 °C for 1 day; the samples activated by freeze-drying were pretreated under high vacuum (10<sup>-6</sup> mbar) at 80 °C for 1 day. Hydrogen (ultra-high-purity grade, 99.999%) was additionally purified by leading it over a bed of zeolite spheres at 77 K before being loaded onto the samples. The pressure change was monitored and recorded after the hydrogen reservoir was connected to the sample holder. The samples were weighed in a glove box after the measurements for calculating the hydrogen uptake capacities. The amount of hydrogen stored in the dead volume was examined using sea sand as a reference. The hydrogen uptake capacities of all samples were obtained by subtracting the amount of hydrogen in the dead volume from the total amount of hydrogen released from the reservoir.

## 7.3 Results and discussion

### 7.3.1 Structures of Cu-TDC and Cu-FDC

The structures of Cu-TDC and Cu-FDC were characterized by single crystal X-ray diffraction.

**Cu-TDC.** The study reveals that Cu-TDC crystallizes in the trigonal space group  $R\bar{3}c$  (no. 167). Compared with a Cu-based MOF constructed from 2,5-thiophene dicarboxylate (MOF-110) reported by Eddaoudi *et al.*, [8] Cu-TDC shows a different space group ( $R\bar{3}c$  for Cu-TDC vs.  $R\bar{3}m$  for MOF-110) and a larger  $c$  value (unit cell dimension, 41.7 Å vs. 20.7 Å). We found that the discrepancy is resulted from different reflections applied and Cu-TDC and MOF-110 have similar structure. In Cu-TDC, the asymmetric unit contains one  $\text{Cu}^{2+}$  ion, one 2,5-thiophenedicarboxylate (TDC) ligand and one DMF molecule (Figure 7.1). Both carboxylate groups of the TDC ligand are deprotonated resulting in a dianion. A pair of Cu atoms are bridged by four *syn, syn*- $\mu$ -carboxylato- $O,O'$  groups of  $\text{TDA}^{2-}$  and form a paddle-wheel  $\text{Cu}_2(\text{OOCR})_4$  cluster. The  $\text{Cu1-Cu1}^i$  distance is 2.6471(5) Å ( $i: 1-x, 1-y, 1-z$ ). In addition to the Cu-Cu contact and the four carboxylate oxygen atoms, the coordination environment of Cu1 is completed by O5 from a coordinated *N,N*-dimethylformamide molecule. As expected, the neutral oxygen O5 has a longer Cu-O distance than the negatively charged carboxylate oxygen atoms. The environment of Cu1 is best described as a distorted octahedron. Selected bond distances and angles are listed in Table 1 in Appendix.

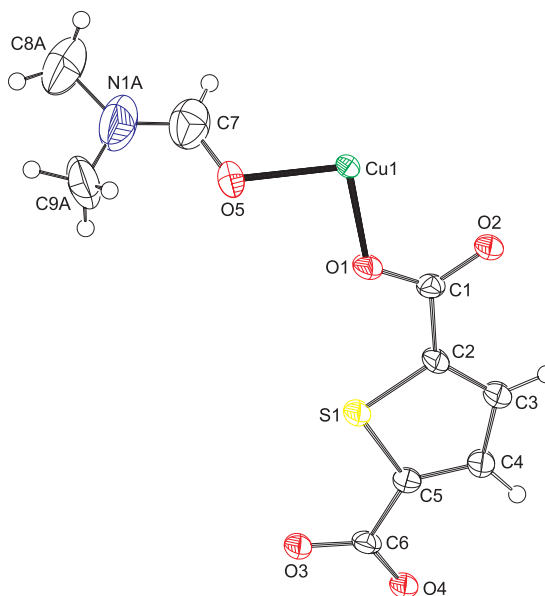


**Figure 7.1.** Asymmetric unit of the Cu-TDC crystal structure. Viewed along the crystallographic  $a$ -axis. Displacement ellipsoids are drawn at the 50% probability level. Only the major form of the disordered *N,N*-dimethylformamide (DMF) is shown. Non-coordinated solvent molecules are treated as diffuse electron density (see Experimental section) and are omitted in the drawing.

The Cu<sub>2</sub> dimers are further inter-linked via bridging of *syn, syn, syn, syn*-tetradentate thiophene-2,5-dicarboxylate to form an infinite two-dimensional network in the crystallographic a,b-plane (Figure 7.2A). Due to the space group symmetry, the Cu ions occupy the corners of a triangle. The Cu1...Cu1<sup>ii</sup> and Cu1...Cu1<sup>iv</sup> distances between the corners are 9.2917(5) Å (*ii*: 1-x+y, 1-x, z; *iv*: 1-y, x-y, z). The two-dimensional coordination layers are stacked on top of each other in the direction of the c-axis. They are connected by weak intermolecular C-H...O hydrogen bonds (Figure 7.3). Hereby, the thiophene carbon atoms C3 and C4 act as hydrogen bond donors and the carboxylate oxygen atoms O2 and O4 act as acceptors (Table 2 in Appendix). The layer stacking offers open triangular- and hexagonal-shaped channels along the c-axis (Figure 7.2B). Overall, the unit cell contains approximately 36% solvent accessible voids, as determined with the PLATON software.



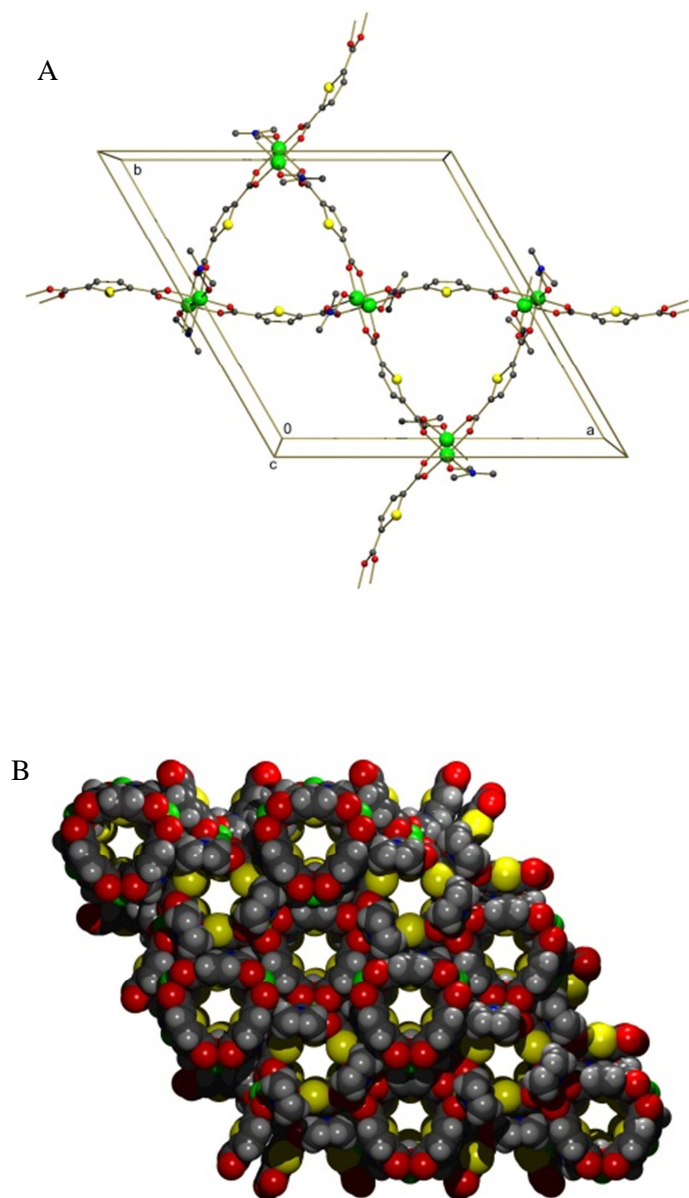


**Figure 7.2.** (A) Infinite two-dimensional coordination layer in the crystal structure of Cu-TDC. Hydrogen atoms are omitted for clarity. Only the major disordered form of *N,N*-dimethylformamide (DMF) is shown. (B) Space filling plot of the crystal structure of Cu-TDC. Viewed along the crystallographic *c*-axis. Green: Cu, red: O, Grey: C, yellow: S, blue: N.

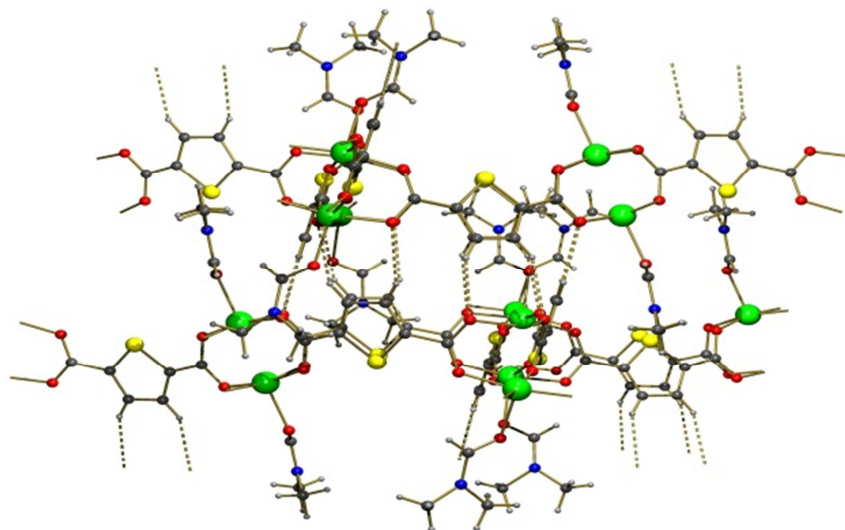


**Figure 7.3.** Weak C-H...O hydrogen bonding in the crystal structure of Cu-TDC. Viewed along the crystallographic a-axis. The two-dimensional coordination planes are shown horizontally. Hydrogen bonds are shown as dashed lines. Only the major disordered form of *N,N*-dimethylformamide (DMF) is shown.

**Cu-FDC.** Cu-FDC is in monoclinic space group  $C2/m$ . The asymmetric unit contains 1.5  $\text{Cu}^{2+}$  ions, 1.5 FDC ligands and 1.5 coordinated  $\text{H}_2\text{O}$  molecules (Figure 7.4). Cu1 and water oxygen O1 are located on the mirror plane ( $x, 0.5, z$ ) and oxygen O5 of a FDC ligand is located on the mirror plane ( $x, 0, z$ ). Because of the lower symmetry there are two independent Cu-Cu distances of 2.6518(6) and 2.6782(5) Å, respectively. In the axial positions of the  $\text{Cu}_2$  dimer, two water molecules are coordinated to each Cu ion. The Cu-O distances of the water ligands are longer than the carboxylate distances. Both independent Cu centers are in distorted octahedral environments. Selected bond distances and angles are listed in Table 3 in Appendix. Similar to the layers in Cu-TDC, each  $\text{Cu}_2$  dimer is further inter-linked via bridging of *syn, syn, syn, syn*-tetradentate furan-2,5-dicarboxylate to form an infinite two-dimensional network in the crystallographic (2,0,1) plane and the Cu ions occupy the corners of triangles (Figure 7.5A). The Cu...Cu distances between the corners vary between 8.2732(7) for  $\text{Cu2}...\text{Cu1}^i$  and 10.5170(8) Å for  $\text{Cu2}...\text{Cu2}^v$  ( $i: -x, y, 1-z$ ;  $v: x, -y, z$ ).

Cu-FDC contains coordinated water molecules, which can act as hydrogen bond donors. The acceptors for these hydrogen bonds are not a part of the framework structure but are located in the solvent area. In the framework there is only one weak C-H...O hydrogen bond linking the stacked 2D layers (Figure 7.6). Furan carbon atom C32 is the donor of the hydrogen bond and carboxylate oxygen O11 is the acceptor (Table 4 in Appendix). The layer stacking generates tetragonal- and cylindrical-shaped channels in the directions of the *a*- and *c*-axis, respectively. A PLATON program analysis suggests that ~58% of the crystal volume is accessible to the solvents. The solvent channels are displayed in Figure 7.5B.

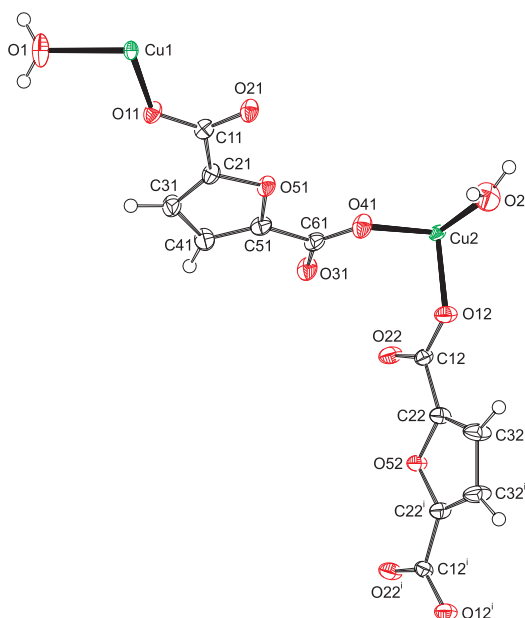


**Figure 7.4.** Asymmetric unit of Cu-FDC crystal structure. Viewed along the crystallographic *c*-axis. Displacement ellipsoids are drawn at the 50% probability level. Non-coordinated solvent molecules are treated as diffuse electron density (see Experimental Section) and are omitted in the drawing. Symmetry operation *i*: *x*, -*y*, *z*.

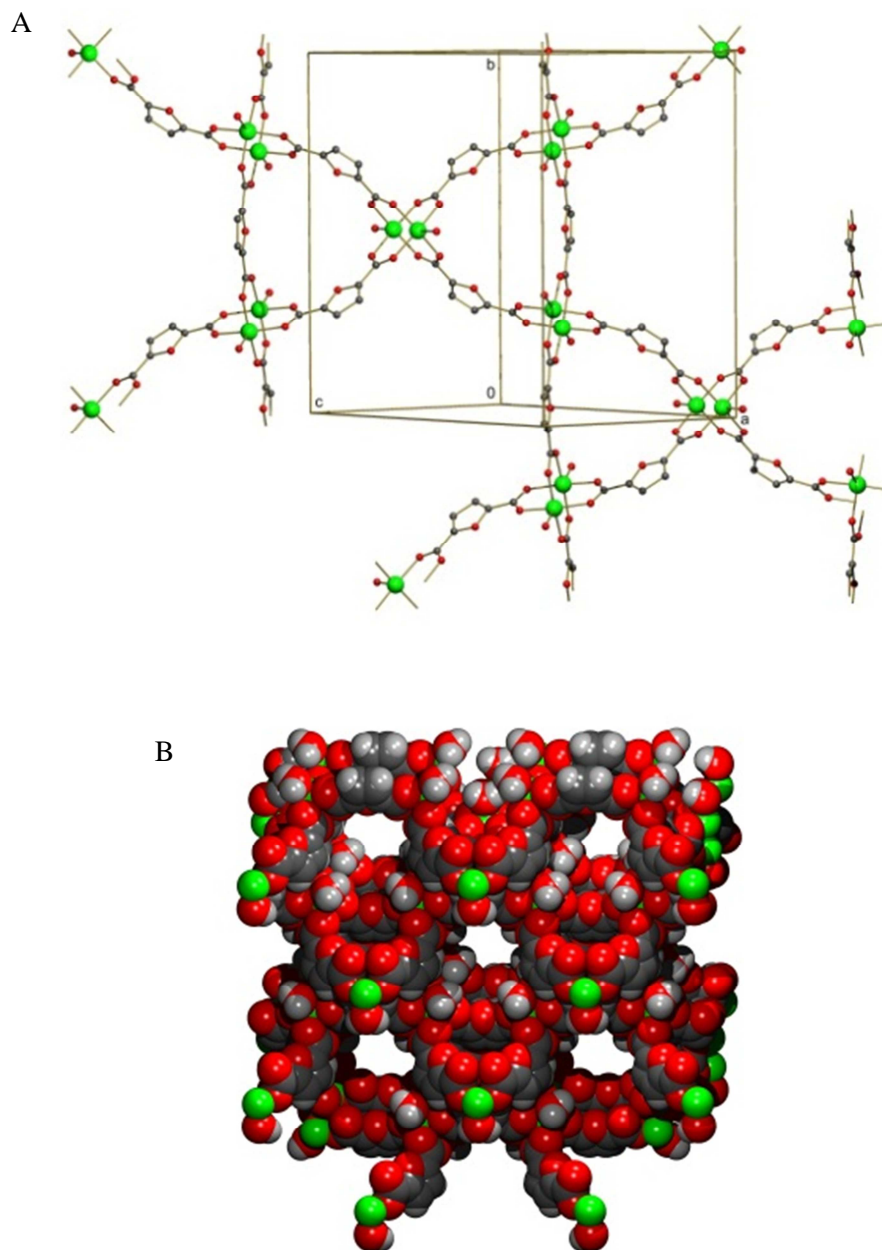


**Figure 7.5.** (A) Infinite two-dimensional coordination layer in the crystal structure of Cu-FDC. Hydrogen atoms are omitted for clarity. (B) Space filling plot of the crystal structure of Cu-FDC. Viewed along the crystallographic a-axis. Green: Cu, red: O, Grey: C.

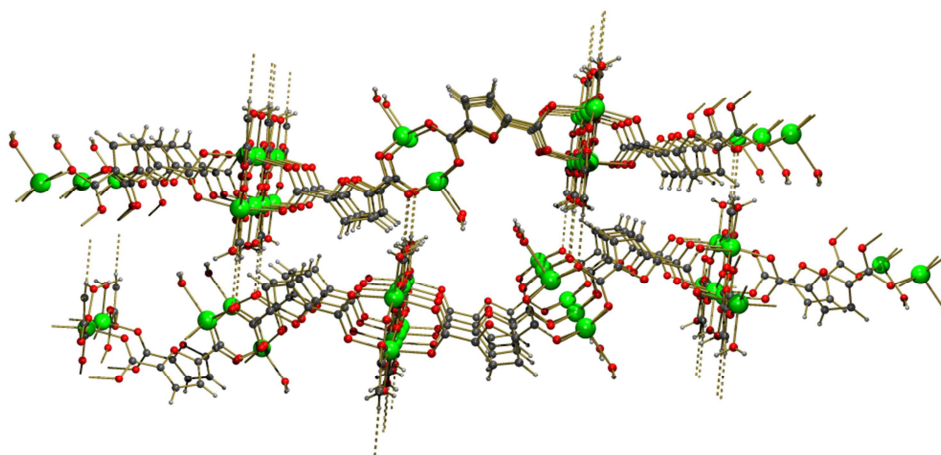


**Figure 7.6.** Weak C-H...O hydrogen bonding in the crystal structure of Cu-FDC. View along the crystallographic b-axis. Two-dimensional coordination planes are shown horizontally. Hydrogen bonds are shown as dashed lines.

In both structures, the  $\text{Cu}_2$  dimers are connected with each other via *syn, syn, syn, syn*-tetradentate thiophene-2,5-dicarboxylate or furan-2,5-dicarboxylate, forming similar 2-dimensional layers despite their different exocyclic bond angles ( $148^\circ$  for thiophene-2,5-dicarboxylic acid and  $125^\circ$  for furan-2,5-dicarboxylic acid, respectively). It seems that the exocyclic bond angle does not play a major role in the coordination geometry of the copper ion and the bridging mode of  $\text{TDC}^{2+}$  and  $\text{FDC}^{2+}$ . Interestingly, the similar layers are stacked on top of each other via hydrogen bonds and form two different three-dimensional frameworks. This may be explained by the effect of the amount of hydrogen bonds (C-H...O) on the self-assembly of the layers. Only one of the  $\beta$ -hydrogen atoms of the furan ring has a hydrogen bond interaction with a carboxyl oxygen atom in Cu-FDC. This is slightly different for Cu-TDC, where both  $\beta$ -hydrogen atoms of the thiophene ring participate in hydrogen bond formation. In the latter case a stronger interaction between the layers is the result. It was reported that end-capping ligands play an important role in the construction of coordination polymers. For instance, in manganese (II) complexes with 2,5-thiophene dicarboxylate, different structures were found for complexes containing water, pyridine and 2,2'-dipyridine as end-capping ligands.[6] The same role was also observed in manganese (II) complexes constructed from terephthalate.[14] Therefore, an alternative explanation of different structure of Cu-TDC and Cu-FDC could be the end-capping ligands coordinated with the Cu ions in the axial position, *i.e.* DMF for Cu-TDC and  $\text{H}_2\text{O}$  for Cu-FDC.

**SEM Analysis.** SEM images demonstrate that the size of Cu-TDC and Cu-FDC crystals are in the range of 50-300  $\mu\text{m}$ . Most Cu-TDC and Cu-FDC crystals are octahedral and showed smooth triangular surfaces. However, the Cu-FDC crystals showed a strong tendency to aggregate. Both Cu-TDC and Cu-FDC crystals grew layer by layer, as can be seen in Figure 7.7B and 7.7D.

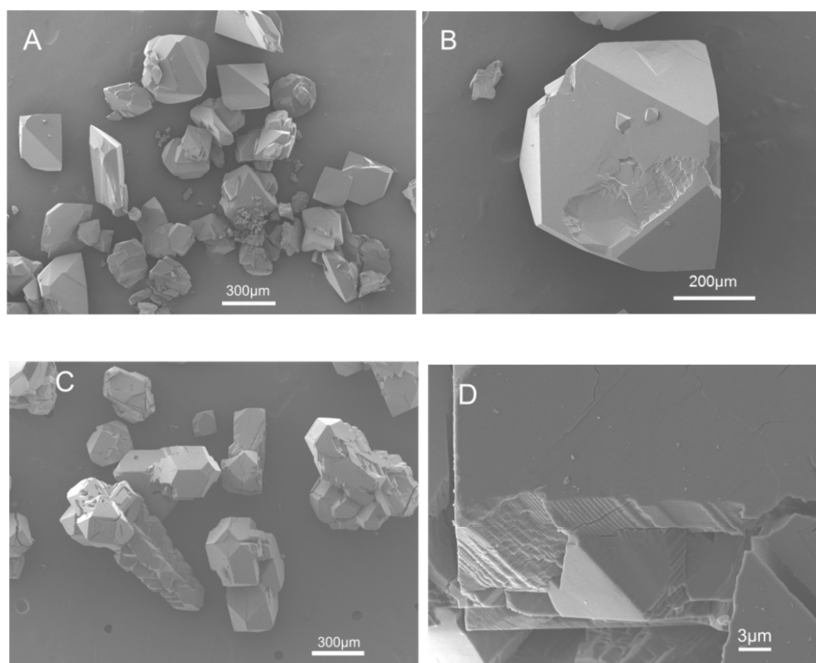


**Figure 7.7.** SEM images of Cu-TDC (A and B) and Cu-FDC (C and D) showing the distinct different morphologies.

### 7.3.2 Thermogravimetric analysis

Figure 7.8 shows the TGA curves of as-synthesized Cu-TDC and Cu-FDC. There are three distinct weight loss steps in the thermogram of Cu-TDC. The weight loss below 230  $^{\circ}\text{C}$  ( $\sim 33$  wt%) can be attributed to solvent loss (water, ethanol and DMF). The last weight loss event starting at  $\sim 250$   $^{\circ}\text{C}$  can be assigned to the thermal decomposition of the organic linker, *i.e.* thiophene-2,5-dicarboxylate ( $-\text{C}_6\text{H}_2\text{O}_4\text{S}-$ ). Cu-FDC showed a more continuous weight loss from room temperature to about 300  $^{\circ}\text{C}$ .

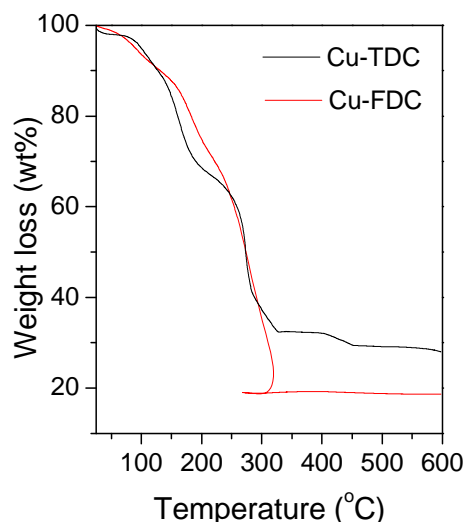


**Figure 7.8.** TGA curves of as-synthesized Cu-TDC and Cu-FDC using a heating rate of 10 °C min<sup>-1</sup> under a dry air atmosphere.

### 7.3.3 Structural stability of Cu-TDC and Cu-FDC

The structural stability of Cu-TDC and Cu-FDC was also investigated at elevated temperatures using X-ray diffraction. Figure 7.9 and 7.10 show the PXRD patterns of Cu-TDC and Cu-FDC as a function of temperature. In comparison with as-synthesized Cu-TDC, similar PXRD patterns can be observed when Cu-TDC was heated at 90 °C and 120 °C, which is an indication that the structure of Cu-TDC can be retained at 120 °C. When the temperature was increased to 150 °C, the typical diffraction peaks disappeared and new peaks emerged, implying a phase transformation (the structure of the new phase is unknown). Finally, at temperatures close to 270 °C, the peak at 36.3° has appeared, indicating that Cu-TDC started to transfer to Cu<sub>2</sub>O.[16] With respect to Cu-FDC, with the increase in temperature, the peaks at 11.7° and 11.9° overlapped at 90 °C, the peaks at 6.8° and 13.5° split into two peaks at 120 °C. These findings imply that the lattice parameters of Cu-FDC have changed due to the release of solvent molecules upon heating. A significant decrease in the peak intensities at 180 °C indicates the presence of a compromised structure. Similar to Cu-TDC, at 270 °C, Cu-FDC started to convert to Cu<sub>2</sub>O.

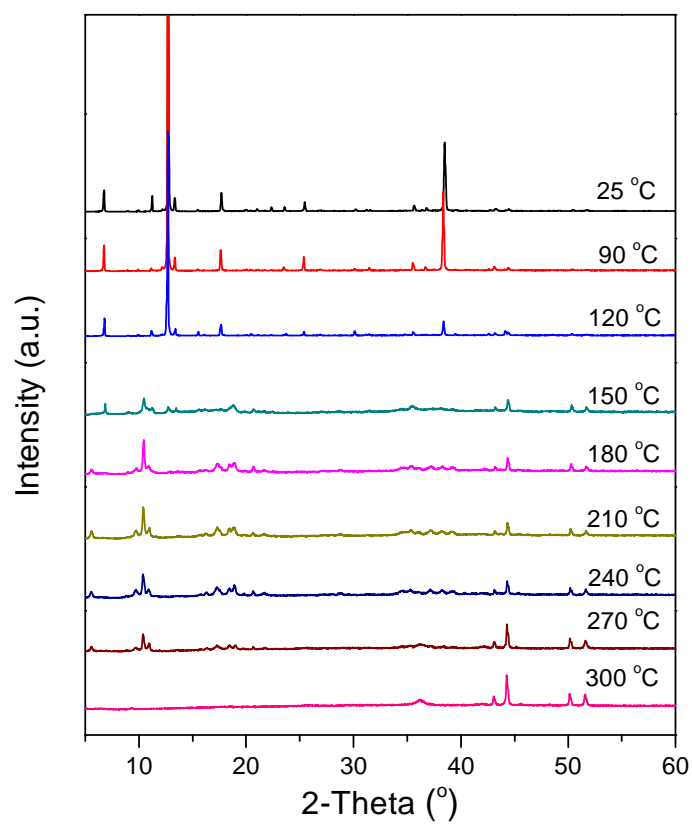


**Figure 7.9.** PXRD patterns of Cu-TDC as a function of temperature.



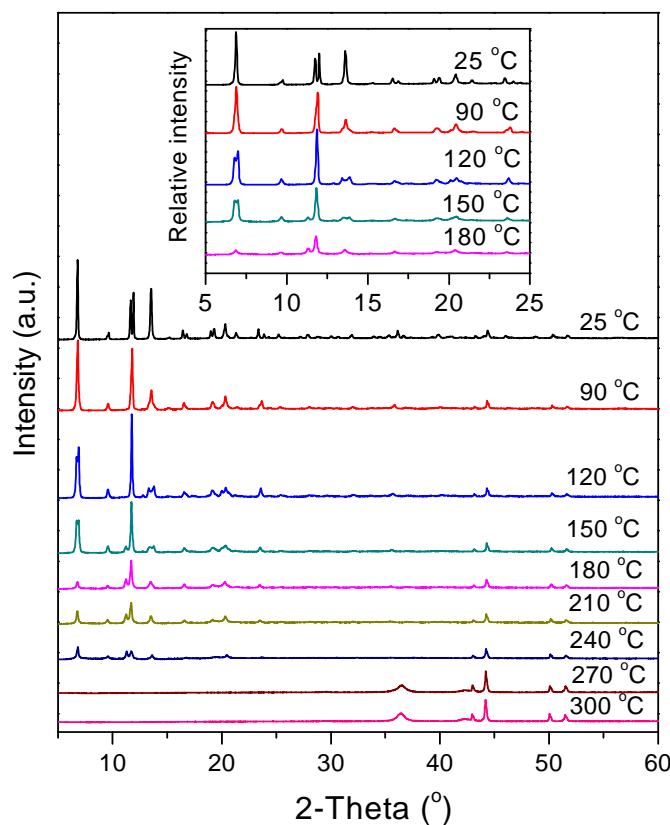


**Figure 7.10.** PXRD patterns of Cu-FDC as a function of temperature.

### 7.3.4 Structure and composition of Cu-TDC-A and Cu-FDC-A

In order to activate the as-synthesized coordination polymers, entrapped reagents and solvents have to be removed via a process generally referred to as activation. This process is rather delicate and care has to be taken to avoid the collapse of the crystalline framework.[15,17] Figure 7.11 shows the PXRD patterns of activated Cu-TDC and Cu-FDC. The peak intensities in the PXRD pattern of Cu-TDC-A1 decreased significantly as compared to untreated Cu-TDC, which suggests that the structure of Cu-TDC has become compromised after  $\text{CHCl}_3$ -exchange. Activated Cu-FDC-A1, on the other hand, displayed a very poor PXRD pattern compared to that of untreated Cu-FDC,

implying complete destruction of the framework. In contrast, the structures of Cu-TDC and Cu-FDC both remain intact after freeze-drying as indicated by the largely unaffected PXRD patterns of Cu-TDC-A2 and Cu-FDC-A2. Similar to the PXRD pattern of Cu-FDC heated at 120 °C, the peak splitting ( $2\text{-}\theta = 6.8^\circ$  and  $13.5^\circ$ ) was also found for Cu-FDC-A2, suggesting a small change of the lattice parameters for Cu-FDC after freeze-drying. We can conclude that the structures of Cu-TDC and Cu-FDC are retained after freeze-drying, but  $\text{CHCl}_3$ -exchange destabilizes the Cu-TDC structure and destroys the structure of Cu-FDC.

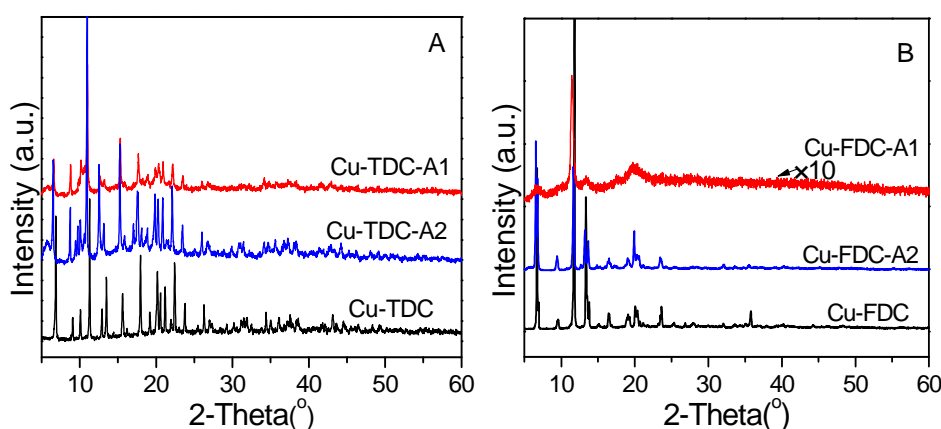


**Figure 7.11.** The PXRD patterns of Cu-TDC (A) and Cu-FDC (B) after activation by  $\text{CHCl}_3$ -exchange (A1, red) and freeze-drying (A2, blue). The PXRD patterns of untreated Cu-TDC and Cu-FDC are shown (black) for comparison.

The TGA curves of activated Cu-TDC and Cu-FDC are shown in Figure 7.12. In comparison to the untreated samples, activated Cu-TDC and Cu-FDC both showed less weight loss between 150 °C and 230 °C, suggesting that both activation procedures have been successful in terms of removing guest molecules from the respective frameworks. The removal of DMF, for example, could be confirmed by elemental analysis. Based on the N content, we calculated the DMF content in all samples and the values are summarized in Table 7.1. The theoretical values calculated from the formulas obtained from single-crystal XRD are also shown. The DMF contents of untreated Cu-TDC and Cu-FDC are 34.1% and 31.0%, respectively. Compared to the theoretical values (23.8% for Cu-TDC and 0% for Cu-FDC), it is clear that  $\sim 10\%$  and  $\sim 31\%$  of free DMF molecules are present in Cu-TDC and Cu-FDC, respectively. After activation, Cu-TDC-A1 and Cu-TDC-A2 displayed a similar DMF content ( $\sim 21\%$ ), which is in close agreement with the theoretical value and suggests that both activation methods work equally well for

removal of free DMF molecules. The DMF content for Cu-FDC-A1 and Cu-FDC-A2 appears to be quite different. Cu-FDC-A1 showed a DMF content of 1.7%, whereas a DMF content of 21.9% was found for Cu-FDC-A2. This implies that  $\text{CHCl}_3$ -exchange removes DMF molecules more efficiently from Cu-FDC. Subtracting the contribution of DMF to the hydrogen (H) content, the hydrogen content for Cu-FDC-A2 is higher than the theoretical value, which indicates the presence of free  $\text{H}_2\text{O}$ . On the other hand, the structure of Cu-FDC became compromised after  $\text{CHCl}_3$ -exchange, which may be due to the weaker interaction between the adjacent layers in Cu-FDC as compared to Cu-TDC.

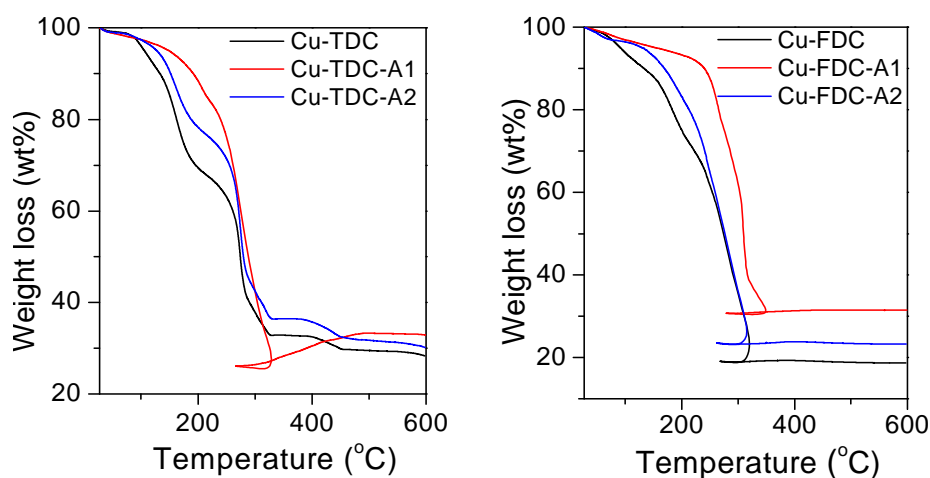


**Figure 7.12.** TGA curves of Cu-TDC and Cu-FDC (untreated and activated) measured using a heating rate of  $10\text{ }^{\circ}\text{C min}^{-1}$  under a dry air flow. A1 = solvent activated and A2 = activation via freeze-drying.

**Table 7.1.** Chemical composition of Cu-TDC and Cu-FDC before and after activation (theoretical values from single crystal X-ray diffraction measurements are shown in brackets).

| Sample    | N (%)      | H(%)       | DMF (%)    |
|-----------|------------|------------|------------|
| Cu-TDC    | 6.53(4.56) | 4.10(2.94) | 34.1(23.8) |
| Cu-TDC-A1 | 3.94       | 3.06       | 20.5       |
| Cu-TDC-A2 | 4.10       | 3.10       | 21.4       |
| Cu-FDC    | 5.95(0)    | 4.61(1.69) | 31.0(0)    |
| Cu-FDC-A1 | 0.32       | 2.00       | 1.7        |
| Cu-FDC-A2 | 4.19       | 3.63       | 21.9       |

### 7.3.5 Hydrogen adsorption properties of activated Cu-TDC and Cu-FDC

The hydrogen storage properties of activated Cu-TDC and Cu-FDC were measured using a Sievert's setup at 77 K and the low-pressure adsorption isotherms are shown in Figure 7.13. Activated Cu-TDC and Cu-FDC both showed hydrogen storage capability. The hydrogen uptake capacity of activated Cu-TDC is somewhat higher than that of activated Cu-FDC. Cu-TDC-A1 and Cu-TDC-A2 showed hydrogen storage capacities of 0.73 wt% and 0.75 wt% at 77 K and 1 bar, respectively. The hydrogen storage capacity of Cu-FDC-A1 is much lower than Cu-FDC-A2 over the whole pressure range studied (<2 bar). Cu-FDC-A1 and Cu-FDC-A2 gave hydrogen storage capacities of 0.37 wt% and 0.64 wt% at 77 K and 1 bar, respectively.

The two activation methods, *i.e.* CHCl<sub>3</sub>-exchange and freeze-drying, have been employed in our work to activate Cu-TDC and Cu-FDC. The two methods resulted in comparable hydrogen uptake capacities for Cu-TDC-A1 and Cu-TDC-A2. However, the hydrogen uptake results are different for the furan-based system Cu-FDC. The structure of Cu-FDC remains intact after freeze-drying, but does not survive the CHCl<sub>3</sub>-exchange process. As a result, Cu-FDC-A1 gave a lower hydrogen uptake capacity than that of Cu-FDC-A2.

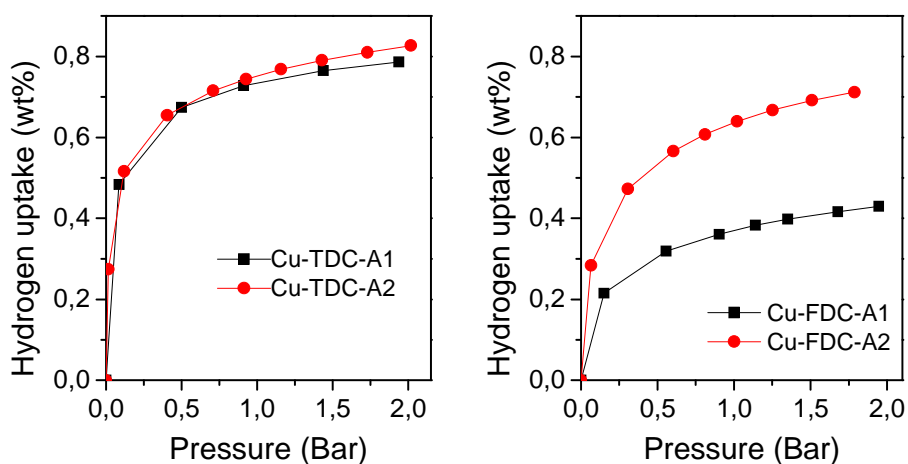


**Figure 7.13.** Low-pressure hydrogen adsorption isotherms of activated Cu-TDC and Cu-FDC.

Cu-TDC-A2 and Cu-FDC-A2 showed similar textural properties. Cu-TDC-A2 has a BET surface area of 308 m<sup>2</sup> g<sup>-1</sup> and a pore volume of 0.16 cm<sup>3</sup> g<sup>-1</sup>. The BET surface area

and pore volume of Cu-FDC-A2 are  $310 \text{ m}^2 \text{ g}^{-1}$  and  $0.21 \text{ cm}^3 \text{ g}^{-1}$ , respectively. A BET surface area of  $308 \text{ m}^2 \text{ g}^{-1}$  has to be considered very low as compared to most other physisorbent materials used for hydrogen storage, and indicates a poor porous structure. Compared with MOF-5, which has a BET surface area of  $3039 \text{ m}^2 \text{ g}^{-1}$  (M-3 in *Chapter 5*), the BET surface areas of Cu-TDC-A2 and Cu-FDC-A2 are only one tenth of what is observed for MOF-5, whereas the hydrogen uptake capacities of Cu-TDC-A2 and Cu-FDC-A2 at 77 K and 1 bar are half of that of MOF-5. Moreover, a rapid increase in the hydrogen uptake capacities of activated Cu-TDC and Cu-FDC at low pressures ( $<0.5 \text{ bar}$ ) indicates a strong interaction between hydrogen molecules and the framework. Therefore we calculated the heats of hydrogen adsorption for Cu-TDC and Cu-FDC from the Clausius-Clapeyron equation at 0.2 wt% of hydrogen uptake capacity. As expected, Cu-TDC-A2 and Cu-FDC-A2 showed high heats of hydrogen adsorption, *i.e.* 9.2 and  $7.5 \text{ kJ mol}^{-1}$ , respectively, which is much higher than that of MOF-5 ( $3\text{--}5 \text{ kJ mol}^{-1}$ ). It has been documented that the presence of open metal sites can enhance the interaction between hydrogen molecules and the framework structures. Unfortunately, we did not find evidence for the presence of open copper sites in Cu-TDC and Cu-FDC. The elemental analysis results suggest that the solvent molecules (DMF for Cu-TDC and  $\text{H}_2\text{O}$  for Cu-FDC), which are coordinated with copper ions, were not removed by activation (Table 7.1). So we have to consider the possibility that the polarizability of the thiophene ring and furan ring plays a critical role in improving the heat of hydrogen adsorption in this class of metal organic frameworks. A similar explanation was proposed by the Yaghi group for IRMOF-20, constructed from a linear thieno[3,2-*b*]thiophene-1,5-dicarboxylate moiety, and by Barman and co-workers for a MOF comprised of 1,3-azulenedicarboxylate.[4,18] Our findings suggest that even with a much more limited specific surface area (about 5 times smaller than for MOF-5) MOFs with high hydrogen uptake capacities at low pressures can be designed due to the larger local hydrogen adsorption interaction. Finding MOFs based on heterocyclic moieties that could form stable frameworks with high specific surface areas is therefore a research topic that should be pursued.

## 7.4 Conclusion

We have synthesized and characterized two coordination polymers, namely,  $[\text{Cu}(\text{TDC})(\text{DMF})]_n$  (Cu-TDC) and  $[\text{Cu}(\text{FDC})(\text{H}_2\text{O})]_n$  (Cu-FDC). Each structure consists of dicopper paddlewheel clusters and organic linkers. The dicopper paddlewheel clusters are bridged by thiophene-2,5-dicarboxylate or furan-2,5-dicarboxylate to form two-dimensional layers. These layers are assembled into different porous 3-D frameworks

via hydrogen bonds between the  $\beta$ -hydrogen atom(s) of the heterocycle system, *i.e.* thiophene or furan, and the oxygen atom of the carboxylate group. Cu-TDC displays hexagonal and triangular channels, which are both parallel to the *c*-axis. Cu-FDC shows a tetragonal channel along the *x*-axis and a cylindrical channel along the *c*-axis. After freeze-drying, Cu-TDC and Cu-FDC show hydrogen uptake capacities of 0.75 wt% and 0.64 wt% at 77 K and 1 bar, respectively, regardless of their low BET surface areas of  $\sim 300 \text{ m}^2 \text{ g}^{-1}$ . Their relatively high hydrogen uptake capacities at 77 K and 1 bar originate from their high heats of hydrogen adsorption ( $9.2 \text{ kJ mol}^{-1}$  for Cu-TDC and  $7.5 \text{ kJ mol}^{-1}$  for Cu-FDC).

## 7.5 References

- [1] (a) Kitagawa, S.; Kitaura, R.; Noro, S. *Angew. Chem. Int. Ed.* **2004**, *43*, 2334. (b) Ferey, G. *Chem. Soc. Rev.* **2008**, *37*, 191.
- [2] Eddaoudi, M.; Moler, D.B.; Li, H.; Chen, B.; Reineke, T.M.; O'Keeffe, M.; O.; Yaghi, O.M. *Acc. Chem. Res.* **2001**, *34*, 319.
- [3] Murray, L.J.; Dinca, M.; Long, J.R. *Chem. Soc. Rev.* **2009**, *38*, 1294.
- [4] (a) Rowsell, J.L.C.; Yaghi, O.M. *J. Am. Chem. Soc.* **2006**, *128*, 1304. (b) Koh, K.; Wong-Foy, A.G.; Matzger, A.J. *J. Am. Chem. Soc.* **2009**, *131*, 4184.
- [5] (a) Yesilel, O.Z.; Ilker, I.; Buyukgungor, O. *Polyhedron* **2009**, *28*, 3010. (b) Gong, Y.; Li, J.; Qin, J.; Wu, T.; Cao, R.; Li, J. *Cryst. Growth Des.* **2011**, *11*, 1662.
- [6] Chen, B.-L.; Mok, K.-F.; Ng, S.-C.; Drew, M.G.B. *New J. Chem.* **1999**, *23*, 877. (b) Zou, H.-H.; He, Y.-P.; Gui, L.-C.; Liang, F.-P.; *CrystEngComm* **2011**, *13*, 3325.
- [7] (a) Huang, W.; Wu, D.; Zhou, P.; Yan, W.; Guo, D.; Duan, C.; Meng, Q. *Cryst. Growth Des.* **2009**, *9*, 1361. (b) Zhan, C. H.; Wang, F.; Kang, Y.; Zhang, J. *Inorg. Chem.* **2012**, *51*, 523.
- [8] Eddaoudi, M.; Kim, J.; Vodak, D.; Suidik, A.; Wachael, J.; O'Keeffe, Yaghi, O.M. *PNAS*, **2002**, *99*, 4900.
- [9] Bruker. SAINT-Plus. Bruker AXS Inc., Madison, Wisconsin, **2001**, USA.
- [10] Sheldrick, G. M. SADABS and TWINABS: Area-Detector Absorption Correction, v2.10, Universität Göttingen, **1999**, Germany.
- [11] Sheldrick, G.M. *Acta Cryst.* **2008**, *64*, 112.
- [12] Spek, A.L. *Acta Cryst.* **2009**, *65*, 148.
- [13] Duisenberg, A.J.M.; Kroon-Batenburg, L.M.J.; Schreurs, A.M.M. *J. Appl. Cryst.* **2003**, *36*, 220.
- [14] (a) Hong, C.S.; Do, Y. *Inorg. Chem.* **1997**, *36*, 5684; (b) Hong, C.S.; Do, Y. *Inorg. Chem.* **1998**, *37*, 4470.

- [15] Eddaoudi, M.; Kim, J.; Rosi, N.L.; Vodak, D.T.; Wocher, J.; O’Keeffe, M.; Yaghi, O.M. *Science* **2002**, 295, 469.
- [16] (a) Grzech, A.; Yang, J.; Dingemans, T.J.; Srinivasan, S. Magusin, P.C.M.M.; Mulder, F.M. *J. Phys. Chem. C* **2011**, 115, 21521. (b) Schlichte, K.; Kratzke, T.; Kaskel, S. *Microporous Mesoporous Mater.* **2004**, 73, 81.
- [17] Barman, S.; Furukawa, H.; Blacque, O.; Venkatesan, K.; Yaghi, O.M.; Berke, H. *Chem. Commun.* **2010**, 46, 7981.





## Appendix

### Selected bond distances, angles and hydrogen bonds for the crystal structures of Cu-TDC and Cu-FDC

**Table 1.** Selected bond distances [ $\text{\AA}$ ] and angles [ $^\circ$ ] for the crystal structure of Cu-TDC.

|   |            |   |           |
|---|------------|---|-----------|
| Cu1-O1                                  | 1.9592(16) | O4 <sup>iii</sup> -Cu1-O2 <sup>i</sup>  | 88.57(8)  |
| Cu1-O3 <sup>ii</sup>                    | 1.9631(17) | O1-Cu1-O5                               | 96.81(7)  |
| Cu1-O4 <sup>iii</sup>                   | 1.9656(16) | O3 <sup>ii</sup> -Cu1-O5                | 92.18(7)  |
| Cu1-O2 <sup>i</sup>                     | 1.9730(16) | O4 <sup>iii</sup> -Cu1-O5               | 99.43(7)  |
| Cu1-O5                                  | 2.1310(18) | O2 <sup>i</sup> -Cu1-O5                 | 94.72(7)  |
| Cu1-Cu1 <sup>i</sup>                    | 2.6471(5)  | O1-Cu1-Cu1 <sup>i</sup>                 | 84.68(5)  |
| O1-Cu1-O3 <sup>ii</sup>                 | 88.74(9)   | O3 <sup>ii</sup> -Cu1-Cu1 <sup>i</sup>  | 83.24(5)  |
| O1-Cu1-O4 <sup>iii</sup>                | 90.45(8)   | O4 <sup>iii</sup> -Cu1-Cu1 <sup>i</sup> | 85.14(5)  |
| O3 <sup>ii</sup> -Cu1-O4 <sup>iii</sup> | 168.38(7)  | O2 <sup>i</sup> -Cu1-Cu1 <sup>i</sup>   | 83.75(5)  |
| O1-Cu1-O2 <sup>i</sup>                  | 168.43(7)  | O5-Cu1-Cu1 <sup>i</sup>                 | 175.16(5) |
| O3 <sup>ii</sup> -Cu1-O2 <sup>i</sup>   | 89.91(8)   |   |           |

Symmetry operations, i: 1-x, 1-y, 1-z; ii: 1-x+y, 1-x, z; iii: x-y, x, 1-z.

**Table 2.** Weak C-H...O hydrogen bonds in the crystal structure of Cu-TDC.

| D-H...A                  | D-H [ $\text{\AA}$ ] | H...A [ $\text{\AA}$ ] | D...A [ $\text{\AA}$ ] | D-H...A [ $^\circ$ ] |
|--------------------------|----------------------|------------------------|------------------------|----------------------|
| C3-H3...O2 <sup>v</sup>  | 0.95                 | 2.57                   | 3.417(3)               | 148                  |
| C4-H4...O4 <sup>vi</sup> | 0.95                 | 2.53                   | 3.393(3)               | 151                  |

Symmetry operations, v: 1/3+x-y, 2/3-y, 7/6-z; vi: 1/3+y, x-1/3, 7/6-z.

**Table 3.** Selected bond distances [ $\text{\AA}$ ] and angles [ $^\circ$ ] for the crystal structure of Cu-FDC.

|                       |            |  |           |
|-----------------------|------------|--|-----------|
| Cu1-O21 <sup>i</sup>  | 1.9628(14) | O21 <sup>iii</sup> -Cu1-O21 <sup>i</sup> | 88.88(9)  |
| Cu1-O11               | 1.9740(14) | O21 <sup>iii</sup> -Cu1-O11              | 168.28(6) |
| Cu1-O1                | 2.124(2)   | O1-Cu1-Cu1 <sup>i</sup>                  | 178.27(7) |
| Cu1-Cu1 <sup>i</sup>  | 2.6518(6)  | O22 <sup>ii</sup> -Cu2-O12               | 167.72(6) |
| Cu2-O22 <sup>ii</sup> | 1.9583(15) | O12-Cu2-O31 <sup>ii</sup>                | 89.00(7)  |
| Cu2-O12               | 1.9626(15) | O12-Cu2-O41                              | 91.09(7)  |
| Cu2-O31 <sup>ii</sup> | 1.9721(14) | O31 <sup>ii</sup> -Cu2-O41               | 167.54(6) |
| Cu2-O41               | 1.9762(15) | O31 <sup>ii</sup> -Cu2-O2                | 97.35(7)  |
| Cu2-O2                | 2.1201(17) | O41-Cu2-Cu2 <sup>ii</sup>                | 82.92(5)  |
| Cu2-Cu2 <sup>ii</sup> | 2.6782(5)  | O2-Cu2-Cu2 <sup>ii</sup>                 | 177.25(6) |

Symmetry operations, *i*: -x, y, 1-z; *ii*:  $\frac{1}{2}$ -x,  $\frac{1}{2}$ -y, -z; *iii*: -x, 1-y, 1-z.

**Table 4.** Weak C-H...O hydrogen bond in the crystal structure of Cu-FDC.

| D-H...A                     | D-H [ $\text{\AA}$ ] | H...A [ $\text{\AA}$ ] | D...A [ $\text{\AA}$ ] | D-H...A [ $^\circ$ ] |
|-----------------------------|----------------------|------------------------|------------------------|----------------------|
| C32-H32...O11 <sup>iv</sup> | 0.95                 | 2.38                   | 3.211(3)               | 146                  |

Symmetry operations, *iv*:  $x+\frac{1}{2}$ ,  $\frac{1}{2}$ -y, -z.

# Curriculum Vitae

---

## Jie Yang

Dorn on 07 Jun 1976  
in Tianjin, China

**Sept. 2000-Jul. 2003:**

Master of Organic Chemistry, Department of Chemistry, Shaanxi Normal University,  
Xi'an, China

**Jul. 2003-May 2007:**

Assistant Professor in State Key Laboratory of Catalysis, Dalian Institute of Chemical  
Physics, Chinese Academy of Sciences, Dalian, China

**Oct. 2007-May 2008:**

Visiting research fellow in Department of Chemical Engineering and Chemistry,  
Eindhoven University of Technology, Eindhoven, The Netherlands

**Jun. 2008-present:**

PhD candidate in Novel Aerospace Materials group, Faculty of Aerospace Engineering,  
Delft University of Technology, Delft, The Netherlands



## List of publications

---

- Yang, J.; Grzech, A.; Mulder, F.M.; Dingemans, T.J. Mono-substituted MOF-5 derivatives: an experimental and computational approach, *Microporous Mesoporous Mater.* **2012**, to be submitted.
- Yang, J.; Grzech, A.; Mulder, F.M.; Dingemans, T.J. Methoxy-modified MOF-5: a new MOF-5 framework prepared via a mixed ligand approach, *J. Mater. Chem.* **2012**, to be submitted.
- Yang, J.; Grzech, A.; Mulder, F.M.; Dingemans, T.J. The metal-to-ligand ratio and the effect on the structure and hydrogen uptake capacity of MOF-5, *J. porous materials* **2012**, to be submitted.
- Yang, J.; Grzech, A.; Lutz, M.; Mulder, F.M.; Dingemans, T.J. Hydrogen storage in Cu(II) coordination polymers comprised of thiophene-2,5-dicarboxylate and furan-2,5-dicarboxylate, in preparation.
- Yang, J.; Grzech, A.; Mulder, F.M.; Dingemans, T.J. Methyl modified MOF-5: a water-stable hydrogen storage material, *Chem. Commun.* **2011**, 47, 5244.